Abstract

Title of Dissertation: THE GATING OF THE BACTERIAL MECHANOSENSITIVE CHANNEL MSCS REFLECTS ITS FUNCTION AS A SENSOR OF BOTH CROWDING AND LATERAL PRESSURE AS WELL AS ITS ROLE IN OSMOREGULATION

Ian Donald Rowe, Doctor of Philosophy, 2014

Directed By: Professor Sergei Sukharev
Department of Biology

The mechanosensitive channel MscS is a ubiquitous bacterial membrane valve that opens by increased tension in the event of osmotic down-shock, releasing small internal osmolytes and thus preventing the cell from excessive hydration and possible lysis. This osmolyte release is accompanied by a reduction of osmotic pressure and volume of the cell, which simultaneously increases crowding. The large catalogue of MscS homologs in both prokaryotes and eukaryotes makes the study of this channel enticing to the field of physical biochemistry.

Here are the results of three different studies, two of which focus on the gating of MscS in the presence of large osmolytes and amphipathic compounds and a third which describes the first electrophysiological examination of the inner membrane of the facultative pathogen *Vibrio cholerae*. The first study in Chapter 2 describes the sensitivity of gating transitions in MscS to large intracellular macromolecules. This

sensitivity originates at the cytoplasmic cage domain and the perceived crowding alters the rate of opening, closing and inactivation. Chapter 3 details the utilization of MscS as a sensor for changes in the lateral pressure profile of native bilayers and how this technique can be used to resolve the potential of antibacterial agents to partition into the membrane. The third and final study describes our development of a procedure to generate giant spheroplasts of *Vibrio cholerae* and the subsequent characterization of its two major mechanosensitive channels in terms of gating, inactivation, conductivity, and compatible osmolyte sensitivity as well as the durability of the pathogen in response to osmotic shock. These contributions to the field of mechanobiology and channel biophysics suggest that environmental feedback during osmoregulation is recognized by the cell, provide a potential method to monitor the partitioning of antibiotics into a cell membrane, and lastly detail the mechano-electrical response of a relevant, disease-causing bacteria.

The gating of the bacterial mechanosensitive channel MscS reflects its function as a sensor of both crowding and lateral pressure as well as its role in osmoregulation

By

Ian Donald Rowe

Dissertation submitted to the Faculty of the Graduate School of the
University of Maryland, College Park in partial fulfilment
of the requirements for the degree of
Doctor of Philosophy
2014

Committee:
Professor Sergei Sukharev, Chair
Associate Professor Kwaku Dayie
Professor Marco Colombini
Associate Professor Jason Kahn
Associate Professor Wade Winkler

Dedication

I'd like to dedicate this work to my parents, Duane and Shirley Rowe, as well as my siblings Devin and Darby Rowe. Thank you for your unwavering love and support over the years.

Acknowledgements

I'd first like to express my gratitude to my research advisor Dr. Sergei Sukharev. His role as a guide and mentor during my time here at the University made me the scientist I am today and for that I'll be forever thankful. His good will, patience and persistence made this research possible.

To my committee members, Dr. Dayie, Dr. Colombini, Dr. Kahn and Dr. Winkler, I thank you for the guidance and other help you've provided along the way.

Thank you to those who contributed heavily to the work I've presented here: Andriy Anishkin for his modeling capabilities, Anthony Yasmann for his monolayer measurements and Dr. Sintim and Min Guo for analog preparation. Thanks to Dr. Huq for providing *V. cholerae* cells.

A special thank you to Vlad Belyy and Kishore Kamaraju for patiently teaching me how to patch clamp and Naili Liu for sharpening my micro and molecular biology skills.

Thank you to the following past and present members of the lab, all of whom helped to shape my work and made my time in the lab a great experience: Greg, Kenjiro, Abby, Claire, Ekta, Christina, Ugur, Anthony S., Miriam, Simona, and Deanna.

Lastly, thank you to all of the family and friends who have supported, housed-with and endured me during the entire process.

Table of Contents

Tables and Figures

Chapter 1

Chapter 2

Chapter 3

Chapter 4

Chapter 5

Supplement

Abbreviations

MS – mechanosensitive

MscS – mechanosensitve channel of small conductance

MscL – mechanosensitive channel of large conductance

TM – transmembrane helicies

WT – wild type

IPTG - Isopropyl thiogalactopyranoside

HEPES - 4-(2-hydroxyethyl)-1-piperazineethanesulfonic acid

HSPC – high speed pressure clamp

LB - Luria Bertani medium

EDTA – Ethylenediaminetetraacetic acid

BSA – bovine serum albumin

MD – molecular dynamics

MTSET – [2-(Trimethylammonium)ethyl]methanethiosulfonate Bromide

Preface

Declaration of intent to use author's own previously published text

The main text and figures in their entirety for:

> Chapter 2: The cytoplasmic cage domain of the mechanosensitive channel MscS is a sensor of macromolecular crowding

And

> Chapter 4: The mechano-electrical response of the cytoplasmic membrane of *Vibrio cholerae*

Were used and only slightly modified for accessibility and formatting purposes. Full citations are as follows:

> **Ian Rowe**, Andriy Anishkin, Kishore Kamaraju, Kenjiro Yoshimura and Sergei Sukharev. "The cytoplasmic cage domain of the mechanosensitive channel MscS is a sensor of macromolecular crowding." *Journal of General Physiology* 2014 (*in press*)
>
> **Ian Rowe**, Merina Elahi, Anwar Huq and Sergei Sukharev. "The mechanoelectrical response of the cytoplasmic membrane of *Vibrio cholerae*." *Journal of General Physiology* 2013 142(1):75-85

Chapter 1: An introduction to mechanosensitive ion channels and their role in osmotic regulation.

Introduction to mechanosensation

One of the defining characteristics of life is the ability to sense and respond to environmental stimuli. Perhaps the most basic of these inputs is mechanical stimulation, which affects all life forms, from bacteria to humans. Because organisms perceive various external forces and at the same time generate their own, mechanosensation arises in many obvious forms, such as hearing, touch sensation in skin, proprioception in joints, cardiovascular responses mediated by aortic baroreceptors, gauging fluid flow rates by the endothelium and managing large osmotic gradients by the kidney. The latter case is especially interesting because common osmotic forces are strong and ubiquitous throughout nature. A mere 100 mM gradient of glucose across a water-permeable membrane creates a hydrostatic pressure of 2.42 atm. Therefore, when the first membrane bound primeval cells began to accumulate metabolites, their cytoplasm became hypertonic in comparison to their environment and the problem of containing the hydrostatic pressure arose. Perception of osmotic forces is likely the most ancient from of mechanosensation.

To prevent uncontrolled swelling and possible lysis resulting from metabolite accumulation, various techniques were developed in nature. One is the rigid wall surrounding the cell membrane (in bacteria, fungi and plants) that could withstand high hydrostatic pressure [1]. But the rigid wall obviously restrained motility. In motile animal cells, the firm cell wall is replaced by a strong internal dynamic cytoskeleton that could resist swelling [2] and assist in regulatory volume decrease after hypoosmotic exposure

[3]. As a separate measure of reducing excessive osmotic gradients, channels arose which would open as membrane tension approached the lytic limit, letting out solutes. It is possible that these early channels functioning as simple osmotic 'release valves' became the evolutionary predecessors of more specialized channels that are currently associated with the meachanoelectrical transduction in sensory organs as well as in many non-sensory cells. Examples of such channels in higher organisms include the DEG/ENaC (degenerin-epithelial Na channel) family found in many animal mechanosensory and somatosensory neurons [4], TRP channels involved in both osmo- and mechano-sensory functions in yeast [5] and humans [6],the K2P family of neuronal K+-selective channels [7] and the recently identified channels from the Piezo family, which appear to be the main touch sensitive channel in eukaryotes. [8]. Higher plants (*A. thaliana*) are completely devoid of TRP and Deg/ENaC type channels but do have a Piezo homolog and their mechanosensation relies in part on MscS-type mechanosensitive channels that are present in the plasma membrane [9] and mitochondria [10], where they regulate volume and plastid division, respectively.

Mechanosensitive (MS) channels are not the only type of molecular mechanotransducers found in cells. Other types include proteins of the cytoskeleton, extracellular matrix (ECM) and adhesion molecules [11, 12]. Enzymes such as kinases, phosphatases, GTPases and cyclases, as well as G-protein coupled receptors [13] also respond to mechanical stimuli. Many of these proteins change conformation with force, and that change may send messages in many ways, such as exposing previously hidden binding sites for recruitment of new components and reversible modification of stress-bearing elements. However, MS channels are the fastest and most efficient transducers

because they activate directly by mechanical force without chemical intermediates and can utilize pre-existing electrochemical gradients of ions to convey information by altering the membrane potential of excitable cells[14].

The first experimental data suggesting the ion-conductive nature of primary mechanotransducers was obtained on frog muscle spindles, which depolarized under mechanical stress [15]. Similarly, depolarization with deflection was reported for insect mechanosensory hairs [16]. The ionic nature of the deflection-induced auditory hair cell receptor potential was reported by Hudspeth and Corey in 1979 [17], suggesting that the primary auditory mechanotransducer is an ion channel. At about the same time Neher, Sakmann and coauthors published the first recordings of single-channel currents using membrane patches isolated at the ~1 um tip of a glass pipette, allowing for the first examination of membranes via the technique that became known as 'patch-clamp'[18]. Because the tight gigaohm seal formation on the glass pipette involves application of negative pressure (suction), the technique inherently delivers a mechanical stimulus to the membrane as well. The first observation of activation of cationic channels in embryonic chicken myoblasts by stretching the membrane patch in this manner was published by Guharay and Sachs [19]. While in some preparations mechano-activated currents were readily recorded from on-cell or excised patches as a result of mechanical perturbation, mechanosensation was elusive in whole-cell mode and it was suggested to simply be an artifact of patch-clamping[20]. It took several years to convince the community that MS channels are real objects with a physiological function. The decisive piece of information came with the isolation and cloning of the first mechanosensitive channel, which was bacterial MscL [21]. The channel was purified and reconstituted in artificial liposomes

and shown to be fully functional, confirming the existence of channels which gate via tension conveyed through the lipid bilayer.

Os*moregulation*

A cellular membrane is tasked with separating the interior of the cell from the outside environment. Water from the aqueous environment most bacterial cells live in has two pathways for entering the cell. One is simple diffusion (osmosis) down its concentration gradient. Though the lipid bilayer has a very low partition coefficient for water, the concentration (or activity) of surrounding water is large enough that it can partition into and permeate the membrane[22]. The other mechanism of water movement is through specific water channels (aquaporins). If these aquaporins are inhibited, leaving bilayer permeation as the only route for water diffusion[23], there is only an approximate 60% drop in the water permeability rate across the membrane, meaning that a significant portion of water movement occurs without specialized channels. Unlike many biological responses which depend on specific ligands or receptors, osmoregulation relies on an overall physical property, which in this case is the osmolarity of the environment. In situations where the concentration of water is higher on the extracellular side of the membrane (hypoosmotic shock), there is a net flow of water into the cell, causing an initial increased cellular volume and a dilution of intracellular ions and metabolites. Metabolites and ions have their own specific concentration requirements so osmoregulation during hypoosmotic shock is interwoven with metabolic and ionic regulation in addition to its primary function in protection against osmotically induced lysis. Conversely, in hyperosmotic shock, water diffuses out of the cell and the same

precious ions and metabolites are limited in their ability to increase in concentration and serve as osmoregulatory solutes. Therefore, there is an accumulation of specific, compatible osmolytes which do not effect enzymatic activity [24] and keep the internal volume constant. These two conditions demonstrate that osmoregulation through the accumulation and release of osmolytes and the parallel water fluxes is tightly linked to many cellular processes.

Upon the onset of hyperosmotic shock, bacteria initially respond by increasing the internal concentration of K^+ [25]. The bulk of this work is done by the PMF-dependent potassium transport systems TrK(18) and an ATP-driven high-affinity Kdp transporter [26]. The promotor controlling Kdp has been shown to be insensitive to K^+ concentration[27] yet changes in external osmolarity (and thus turgor pressure [28]) induce the operon, increasing K+ influx. This effect is mirrored by a K^+ efflux during adaptation to lower osmolarity (low salt), which is primarily carried out through three different systems, MscK (formerly KefA), KefB, and KefC [29]. Concurrent with the K^+ accumulation during a rise in osmolarity, glutamate synthesis is induced, providing a counterion [30]. Since high concentrations of potassium glutamate can lead to disruptions of cellular metabolism[31], other osmolytes are needed to do the majority of osmotic regulation. Thus, to further increase internal osmolarity, the acquisition and synthesis of inert osmoprotectants (trehalose, proline and glycine betaine) is induced by increased levels of potassium glutamate [32, 33].

In an event of hypoosmotic shock, the problem is now reversed and the interior of the cell has a higher concentration of proteins and ions than the external environment. When two solutions are divided by a semipermeable membrane, the chemical potential of

the solvent on the solute-rich side (inside of the cell) decreases. In this situation, the flow of water down its chemical potential gradient generates hydrostatic pressure which counters the influx of solvent across the membrane until the chemical potential of the solvent on each side becomes equal. This is the pressure which presses against the cell membrane and develops turgor. Upon a 50% drop in external osmolarity, *E. coli* cells which were pre-adapted to high osmolarity media were shown to release most of their internal trehalose, potassium and glutamate stores within 20 seconds [34], however concentrations of other intracellular compounds (such as ATP, arginine, lysine and sucrose) did not become membrane-permeable. This indicates that the reduction of compatible osmolytes from the cells was the result of some type of controlled selective release and not simply an overall increase in permeability resulting from some type of fracturing of the membrane. As was described above, the resulting hydrostatic pressure inside the cell translates to lateral tension in the membrane, providing the mechanical input which opens MS channels. The main proposed avenue of osmolyte release from bacterial cells is through a set of several tension-activated channels characterized by different activation thresholds and unitary conductances.

Electrophysiological studies in bacteria

Bacterial cells are small and their cytoplasmic membranes are covered with a cell wall and often outer membrane. Initially, this prevented the application of patch-clamp technique to intact bacterium. The needed breakthrough came in a 1985 bacterial fusion experiment where Ruthe and Adler grew *E. coli* cells in the presence of cephalexin, (which inhibited cytokinesis) and caused cell wall digestion (via lysozyme), creating

giant spheroplasts in the range of 2-10 μm in diameter [35]. This cell preparation technique allowed for the first direct recording of channel activities in *E. coli* by applying the patch-clamp technique to giant spheroplasts; in 1987 Martinac et al. documented the presence of 1 nS pressure-activated channels in the *E. coli* cell envelope[36]. This was followed by solubilization and reconstitution of extracted *E. coli* membrane proteins into liposomes by Sukharev (1993) which identified a 1 nS MS channel similar to that described by Martinac, designated MscS, and another of larger conductance (3 nS), termed MscL [37].

In the following year, the MscL protein was identified, isolated and the *mscL* gene was cloned. A *mscL*$^{-}$ (null) strain was prepared which lacked MscL activity. When *mscL* was reinserted via an expression plasmid in the knockout strain, it restored MscL activity [21]. Purified MscL reconstituted with synthetic lipids was active in mechanically stimulated patches, which led to the conclusion that MscL is gated solely by tension in the surrounding bilayer. Levina et. al later isolated the *yggB* gene which encodes for MscS [38], the protein responsible for the bulk of the 1 nS conductance seen in wild-type *E. coli*. Another channel with a large amount of C-terminal homology to MscS, termed MscK, was identified along with its gene *kefA*; this channel opens with a conductance similar to MscS but is less abundant, has a degree of potassium dependence and has a stable open state [39]. Either MscS or MscL can single-handedly save MS-null cells from osmotic shock, while MscK is insufficient.

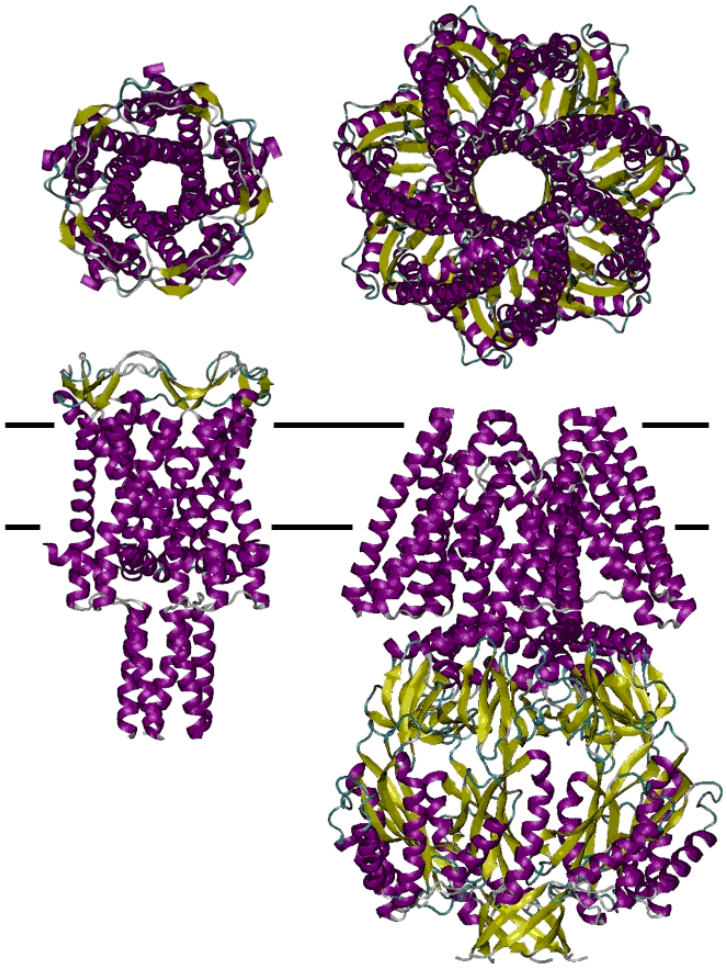

Figure 1.1. Crystal structures of MscL and MscS. (**Left**) The 136 amino acid homopentameric mechanosensitive channel MscL from *Mycobacterium tuberculosis* at a resolution of 3.5 Å (PDB 2AOR) [40]. The N-terminal transmembrane portion of the protein consists of two helices, followed by the molecular pre-filter C-terminal. (**Right**) The 286 amino acid homoheptamer mechanosensitive channel MscS from *Escherichia coli* at a resolution of 3.5 Å (PDB 2OAU)[41]. Three helics form the transmembrane domain while the C-terminus comes together to form a large hollow vestibule named 'cage.' Black lines represent the boundaries of the cytoplasmic membrane and the half of the figure shows the pore as view from the extracellular side of the membrane.

MscL and MscS are structurally unrelated yet both protect from osmotic shock by opening at the appropriate time and tension to release small osmolytes, partially dissipating the osmotic gradient and thus rescuing the cell from imminent osmotic lysis. MscS transiently opens its 1 nS pore at moderate sub-lytic tensions (midpoint tension~5.5-8 mN/m) and likely provides adjustments to mild osmotic downshifts. MscL, the 3 nS high-threshold channel opens at near-lytic tensions (10-13 mN/m) serving as a

'last resort' for survival. The major functional difference between these two is the ability of MscS to adapt to tension and enter an inactivated state, while MscL opens and closes but does not inactivate. This ability to release osmolytes and then disengage the gate to avoid repetitive openings and loss of metabolites allows MscS to act as the main volume regulator in non-emergency situations.

Relating MscS channel structure with its functional cycle.

MscS is a homoheptamer of 286 amino acid subunits with a crystal structure first resolved to 3.5 Å by Bass et. al, 2002[42] and then refined in 2007[41]. Each subunit contains three transmembrane helices (TM1-TM3) and the C-termini from all subunits jointly form a hollow cytoplasmic domain termed 'cage' (PDB ID 2OAU). The initial crystal structure shows the TM1-TM2 pairs surrounding an inner core of tightly packed TM3 helices which form the pore. The TM1-TM2 helices have a 30° splay from the pore axis. The central pore formed by a nearly cylindrical assembly of TM3 segments bears two rings of leucines (L105, L109) that form a hydrophobic gate inside the channel. However, the constriction is not completely occluded by the side chains and has a ~6 Å hole. Just below the gate, at residue G113, this crystal structure displays a kink and the rest of the TM3 (TM3b segment) forms the top portion of the cytoplasmic domain.

The first crystal structure of MscS was interpreted as the open state of the channel due to the incompletely-occluded pore [42]. Molecular dynamics (MD) simulations later suggested that the pore is too small and too hydrophobic to be permanently hydrated and thus it must be nonconductive[43]. Also, the splayed peripheral helices in the 2OAU crystal structure show a substantial crevice separating TM2 and TM3, indicating there is

no way to transmit tension on the membrane-facing helices (TM1-TM2) to the pore-lining helices (TM3). Further studies [44-46] then suggested the packing of the transmembrane domain *in situ* should be different from that in the 2OAU crystal structure and the splay of peripheral helices is likely due to the absence of the lipid bilayer. It was proposed that TM1 and TM2 are more tightly packed against the TM3 helices when they are in the membrane. To support this, a computationally restored TM2-TM3 hydrophobic contact was shown to play an important role in transmitting membrane tension from the outer helices facing the membrane (TM1-TM2) to the central pore-lining TM3 helices[44]. A more recent crystal structure (2VV5) [46] of the A106V MscS mutant shows a wider pore which, according to simulations, is hydrated and passes ions. It also shows a 45° twist of the TM1-TM2 helices relative to their positions in the 2OAU structure of wild-type MscS. This structure is likely a better representation of the open state of the channel.

Since crystallization requires the replacement of lipids with detergent around the protein, it is possible that a delipidated crystal structure misrepresents a native state of the protein. Also, the tension of at least 8 mN/m required to capture the open state of the protein is extremely difficult to recreate in crystallization[47]. To solve this issue, several computational protocols were used to explore the structure of MscS and determine a possible path of opening, starting with the 2OAU structure [48]. Anishkin et al., utilized an ‘extrapolated motion protocol’ (EMP) [49], which is based on repeated cycles of small displacements of the protein domains, short relaxing simulations, energy minimizations, and atom displacement based on previous coordinates, in the path most preferred by the protein itself. Candidate models generated by using EMP, which also satisfied

experimental parameters of conductance and in-plane pore-expansion, were reintroduced into the all-atom simulated environment and equilibrated with the fully hydrated lipid bilayer. The results confirmed that the TM2-TM3 interactions are stable in both the resting and open states [48, 49]. Also, this modeled resting state differed from the starting crystal structure in the placement of the kink in the TM3 helix, moving it from G113 in the crystal structure to G121 in the model [49].

Extrapolated motion simulations suggested that the opening of the channel occurs through a straightening and tilting of the TM3 helices [48]; a tilting and axial rotation of this helix produced a pore diameter of 16 Å, which is 9-10 Å wider than in the original 2OAU structure, and approximately 6 Å wider than that of the 2VV5 partially open structure [46]. This helical rotation exposed buried glycines to the channel while reorienting the L105 and L109 gate residues into contact with other hydrophobic residues on the neighboring TM3 helices, creating a much more hydrophilic environment inside the pore [48].

The resulting open state model depicts kink-free TM3s acting as collapsible ‘struts’, stabilizing the frame of the open pore [50]. Since the C-termini of the TM3 helices form the ‘top’ of the cytoplasmic cage domain and are far separated in the model, the only way for the proper hydrophobic residues to reform the constriction of the pore is to kink the helices. Repeated simulations showed a preferential bending of the TM3 helix at the highly-conserved G121 [50], not at G113 as suggested in the crystal structure, permitting better packing of TM2s along TM3s. Thus, TM3 kinking of the helices at the alternative hinge point of G121 was proposed as the nonconductive closed state of MscS.

Experiments have shown that there are two nonconductive forms of the channel which likely correspond to these different kink positions: one which can reopen and one which remains tension-insensitive [50, 51]. In a typical patch-clamp experiment, upon exposure to prolonged membrane tension just above the gating threshold, wild-type MscS channels gradually enter a tension-insensitive, nonconductive state. These channels are defined by their lack of response to super-saturating tension and termed as inactivated [38, 50, 51]. It is thought that this inactivation may play a role in preserving membrane barrier function by preventing the channels from reopening under sustained tension near the MscS gating threshold yet far below the lytic threshold. The kink present at G113 in the original crystal structure was attributed to the inactivated state. Experiments which increased helical propensity of G113 through a G113A mutation inhibit channel inactivation [50]. Conversely, a Q112G mutation creating a double-glycine motif made that kink region of the helix more flexible and this increased inactivation[51]. A double mutation at both proposed hinges (G113A/G121A) produces channels which remained in the open state for minutes at a time under zero tension, suggesting that TM3 exists in a kink-free form in the open state of the channel. This would suggest that the original crystal structure with a kink at G113 resembles an inactivated state of MscS, whereas the closed (ready-to-fire) state might have an alternative kink at G121 [50].

The crystal structure and the proposed closed state (Fig. 1.2) differ in the interpretation of the crevice between TM2 and TM3: could this helical separation and hydration of the crevice in the 2AOU structure represent disengagement of the gate in the inactivated state? Belyy et al. answered this by showing that serine mutations of the hydrophobic contact between TM2 and TM3 (F68S and L111S) result in channels which

became difficult to open, had a much higher rate of inactivation, and recovered much more slowly [44]. Serine mutations situated deeper in the crevice had no effect on inactivation or recovery. Also, the cysteine at the L111 site was only accessible to MTSET reagents when the channel entered the inactivated state, indicating that this site is not exposed to the solvent environment until the channel enters the inactivated state. Similar experiments showed that the sites located deeper in the hydrophobic crevice remained inaccessible throughout the gating cycle of MscS, meaning that a large separation of TM2 from TM3 does not happen in the course of inactivation[44].

Though the above experiments support the 'crevice' model of helix uncoupling, it is very possible that this placement of the helices is energetically unfavorable in the lipid environment [52]. The native inactivated state may have a different arrangement of transmembrane helices than those in the crystal structure, which was determined in the absence of a lipid bilayer. Since only the L111 site near the entrance to the crevice was accessible upon inactivation, it's possible that TM1-TM2 pairs do not swing outward to form a wide crevice, but rather bend and twist around TM3s and thus expose L111 to the solvent.

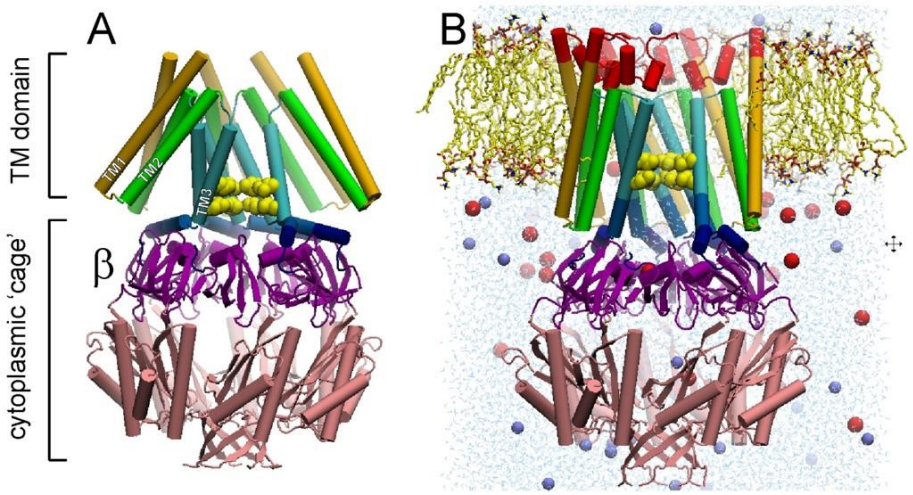

Figure 1.2. **The crystal structure and proposed closed state of MscS.** (**A**) The original crystal structure of MscS (PDB 2OAU) is believed to closely represent the inactivated state, with the TM1/TM2 contact with TM3 removed. The characteristic kink of TM3 at G113 is also present, putting the C-terminal end of TM3 in contact with the top of the cage. (**B**) The lipid-equilibrated model of the closed state of MscS, with the break of the helix now positioned at G121. This model also returns the contact between the lipid facing TM1/TM2 pair and the pore lining TM3. (Figure from Rowe et al. 2014, in press)

Macromolecular crowding and its effect on MscS

In solution, no two solute molecules can simultaneously occupy the same space. A single *E. coli* bacterium has an internal volume between 0.4 and 0.7 μm^3[53]. Within this space, macromolecules are present at concentrations of approximately 0.3 to 0.4 g/ml [54], creating an environment where free space is at a premium. Around all of these macromolecules inside the cell (or in any solution), there is a volume from which the center-of-mass of an approaching molecule is excluded [22]. The total space in which other molecules cannot occupy is the actual volume the molecule occupies plus a certain 'shell' around the molecule; the thickness of this shell is equal to the radius of the macromolecule which approaches it (Fig. 1.3). The larger the hydrodynamic radius of the approaching macromolecule, the larger the excluded volume, meaning that a long, rod-shaped particle will exert a greater crowding effect than a smaller protein. This

phenomenon of crowding and excluded volume has been linked to many processes such as an increased rate of protein folding [55], enzymatic activity [56], and protein aggregation.

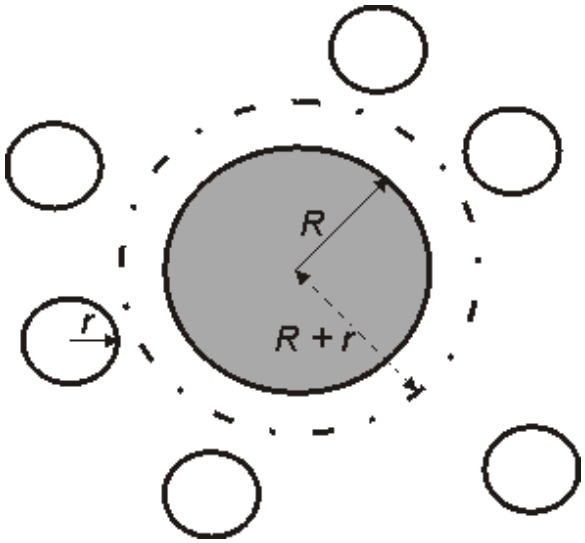

Figure 1.3. Excluded volume interactions. The total volume of which the small sphere of radius *r* cannot occupy when approaching the larger sphere of radius *R* is the entire volume within the dashed sphere. This excluded volume is defined as the sphere of radius *R* + *r*. (Figure credit: Rowe)

Previous studies [57] have found that large molecular crowding agents exert pressure on the channel complex, perhaps causing a more compact state of the cytoplasmic cage of MscS to be preferred. While there is debate as to whether this compaction is the result of osmotic stress in the form of water removal from the surface of the protein due to a change in water activity [58], some direct association of the channel protein with crowders [59], an increase in internal osmotic pressure, or an excluded volume effect, it is generally accepted that the state of smaller protein volume is preferred in the presence of inert crowding molecules[60].

The cage domain of MscS was originally viewed merely as a pre-filter at the cytoplasmic entrance to the pore [61]. Koprowski and coworkers [62] found that MscS adapts faster in the presence of polymers (PEGs, dextrans, Ficoll) on the cytoplasmic side

of the patch and speculated that this effect may be caused by the dehydrating action of polymers on the cage. Through random mutagenesis studies [63] they also discovered that the crystallographic interface between the beta domain of the cage and the C-terminal end of TM3 plays an obvious role in gating and adaptation. However, the pressure protocol for patch stimulation used by that group was not designed to separate the effect of stimulus adaptation from complete channel inactivation, and the question of which functional state of the channel and what transition the polymers act on remained unanswered. Multi-step pressure protocols probing the kinetics of both reversible adaptation and also complete inactivation have been devised in our laboratory and, as will be described below, they suggest that the polymers increase the rates of both closing and inactivation.

MscS as a sensor of lateral pressure asymmetry

Transmembrane proteins are embedded in a lipid bilayer matrix of the cell membrane, which creates a highly anisotropic environment due to the presence of local interfacial forces. The two leaflets of the cell membrane are made of various phospholipids which are joined together by polar interactions between the adjacent phosphate head groups of each monolayer and interfacial tension at the boundary with aliphatic chains. At rest, the repulsive force of the tight packing of the phosphate heads and acyl chain tails is countered by the attractive force of surface tension at the water/lipid interface, creating a lateral pressure profile which spans the membrane (Fig. 1.4). Aside from delineating the intracellular environment from the outside, the membrane can serve a reservoir for lipid-derived messengers or a place for preferential

distribution of lipophilic drugs. As lipophilic compounds penetrate between head groups of a monolayer or bilayer, they exert a lateral pressure on adjacent lipids and alter the lateral pressure profile by increasing the repulsion in the acyl chain region of the bilayer. The functions of channels [64, 65] and other integral proteins are likely dependent on lateral pressure changes in the membrane [66, 67]. Hence, the amphipathic properties of many general anesthetics cause them to preferentially partition into the membrane, altering the lateral pressure profile and generating the desired effects on transmembrane proteins.

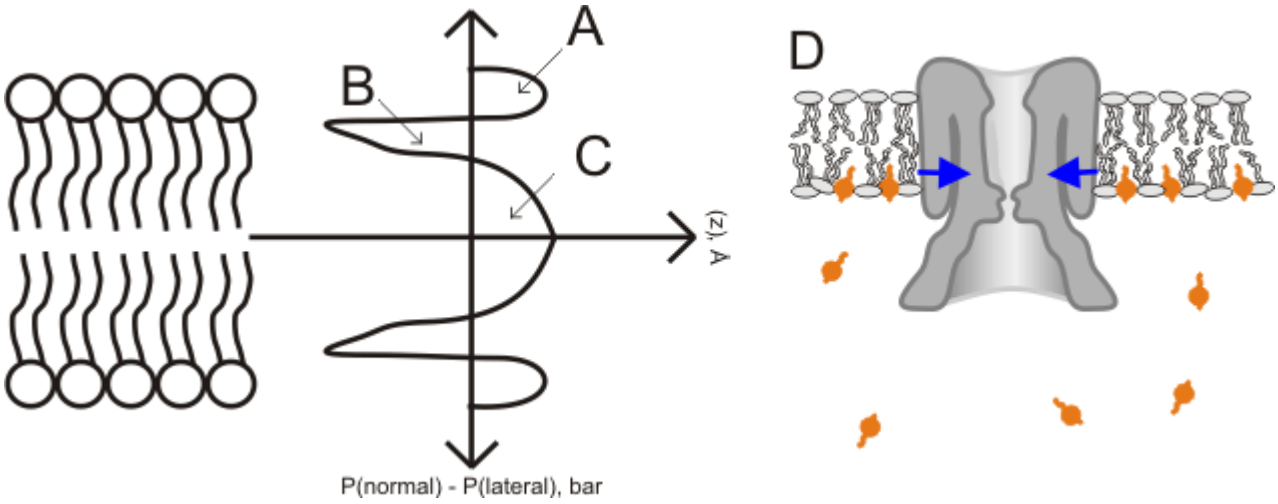

Figure 1.4. An example of a lateral pressure profile. On the far left is a lipid bilayer and in the center is a theoretical lateral pressure profile associated with it. Due to the aliphatic nature of lipids, the head groups pack tightly together to reduce the exposure of the hydrophobic tails to solvent while the tail groups are also forced into close proximity. On top of this, surface tension at the boundary between the hydrophobic and hydrophilic groups creates a large attractive force. The area under the curve in the profile describes an attraction or repulsion at that particular position in the membrane and since the bilayer is at equilibrium the sum of these forces (the area under the entire curve) must equal zero. (A) indicates head group repulsion, (B) describes the attractive force of surface tension and (C) represents the repulsion due to the hydrophobic tail packing. (D) depicts the hypothesized mode of action of intercalating agents.

The first effects of amphipathic substances (trinitrophenol, chlorpromazine) on bacterial MS channels were reported by Martinac and coworkers [68]. Subsequently,

even smaller substances such as fluorinated alcohols were found to be potent modifiers of MS channel gating. It has been shown that 2,2,2-trifluoroethanol (TFE) disrupts interhelical contacts and strongly prefers the organic bulk phase in solution [69]. TFE has an octanol/water partitioning coefficient of 0.41, implying that it would have a strong tendency to occupy the membrane if given the chance. As stated earlier, MscS gates via tension in the membrane and thus would be susceptible to TFE in the membrane. In patch-clamp studies, TFE (<5%) reversibly right-shifts the activation curve of MscS, implying that higher tension is then required to open the channel. The increase of lateral pressure in the inner leaflet of the lipid bilayer upon TFE addition acts asymmetrically on the gate of the channel, which is closer to the cytoplasmic side of the membrane. Similarly, it was found that esters of parabenzoic acid (parabens) of different length (ethyl, propyl, and butyl) shift the activation midpoint of MscS according to the length of their sidechain; this data was found to correlate with the ability of the parabens to alter both the surface tension of an air/water interface and the surface pressure of a monolayer [70]. More recently, partitioning of amphipathic autoinducer molecules (AI-1, AI-2, indole) into the inner E. coli membrane was assessed using WT MscS as a lateral pressure sensor in a study that combined patch-clamp experiments with tensiometry and Langmuir monolayer experiments [71]. The observed correlations between MscS activation curve shifts and changes of lateral pressure in Langmuir experiments asserted that MscS can be used as a lateral pressure sensor for monitoring of partitioning of exogenous lipophilic substances into the native bacterial membrane.

Problem statements and questions

Probing of the cytoplasmic domain of MscS

When I joined the Sukharev Lab in the fall semester of 2008, ongoing experiments and simulations suggested that the cytoplasmic cage of MscS was not a rigid structure and could occupy different conformations of varying volume. The role of the cytoplasmic domain was still unclear but it clearly had a more important function than simply acting as a size-exclusion filter. Some initial experiments suggested that macromolecular crowding exerted by large polymers changed channel closure and increased inactivation[62]. Initial studies of this phenomenon in the Sukharev Lab supported this notion yet a detailed portrait of how crowding changed the channel structure has not been obtained. Thus, I sought to describe:

- What is the actual mechanistic effect of large macromolecular crowding agents on channel opening, closing and inactivation?
- How does the packing of the beta-domain of the cytoplasmic cage affect channel opening, closure and inactivation and does the modeled closed state accurately predict the packing of residues in this region?
- What is the physiological role of MscS inactivation and is it related to osmotic regulation of the interior of the cell?

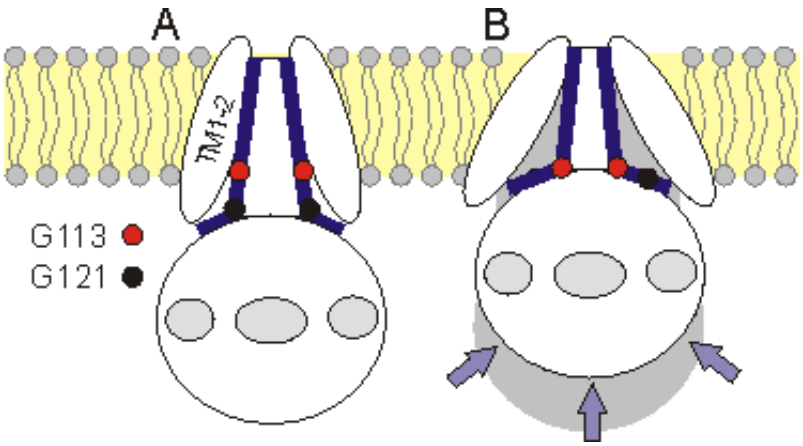

Figure 1.5. Proposed effect of cytoplasmic crowding. (A) Cartoon representation of the resting state with a relaxed round cage.TM3 (blue) is coupled with peripheral TM1-2 helices and the kink in the pore-lining TM3 helix is at G121. (B) The inactivated state in which macromolecular crowding causes compression of the cage and breaks TM3 at G113 instead of G121. TM1-2 helices become uncoupled from TM3 and the grey area shows the change of excluded volume.

Utilizing MscS as a sensor of drug partitioning

Permeability through membranes is a key determinant of drug efficacy; if it cannot enter a cell it cannot perform its task. The common ways to estimate membrane permeability use surface activity, oil-water partition coefficients, partitioning into artificial lipid-impregnated filters or liposomes. Langmuir lipid monolayers is a system that permits direct measurements of lateral pressure changes exerted by an amphipathic compound as it intercalates between lipid molecules on a surface. Currently, no simple probe-based technique exists to predict the partitioning of a lipophilic or amphipathic substance into the native bacterial membrane. Since MscS activation has been shown to be sensitive to membrane-intercalating substances, is it possible that it can act as a sensor of drug partitioning? The main issues which need to be addressed are:

- Can MscS be optimized as a probe for asymmetric partitioning?

- Do amphipathic drug analogs, which alter the surface tension of water and exert lateral pressure in lipid monolayers, similarly affect the activation of MscS channels in patch-clamp experiments?
- Can the changes in MscS activation be interpreted as a membrane partitioning coefficient (K_{mem}) and are these values comparable to other partitioning coefficients obtained in more classic manners?
- Can the redistribution of amphipathic analogs to the opposite leaflet of the membrane be monitored?

The mechanosensitive channels in facultative pathogens Vibrio cholerae

E. coli has been the main organism used to study bacterial mechanosensitive channels since their discovery in 1987. Since then they have been well characterized but the field is lacking in understanding of how such channels operate in other pathogenic bacteria. The ability to investigate the electro-mechanical properties of the membrane in more harmful bacteria has obvious potential for drug development and targeting. The first hurdle to this is the generation of spheroplasts; the procedure for making such cells is well documented for *E. coli* but has not yet been developed for other species. Thus, expanding the patch-clamp technique to other organisms would be a worthwhile endeavor.

V. cholerae is an enteric bacteria which causes severe diarrhea and is responsible for infecting about three million people annually [72]; in 2010, Haiti alone suffered a cholera epidemic that killed approximately 8,000 to 10,000 people. During its transmission cycle, *V. cholerae* must regularly be subjected to environments of varying

salinity, meaning that it likely utilizes mechanosensitive channels to cope with osmotic shock. The medical relevance each of these bacteria present make them optimal choices for spheroplast development.

The promise of membrane susceptibility to partitioning agents and the medical relevance of both these species makes them perfect candidates for membrane exploration. Here, I set out to address the following:

- Is it possible to make spheroplasts of *V. cholerae* such that they can be easily studied for mechanosensitivity similarly to the way *E. coli* is examined?
- What is the mechanosensitive channel population of *V. cholerae* and how does it compare (in both number and activity) to that in *E. coli*?
- How do compatible osmolytes effect the mechanosensitive activity of the *V. cholerae* membrane?

Chapter 2: The cytoplasmic cage domain of the mechanosensitive channel MscS is a sensor of macromolecular crowding

Ian Rowe[1,2], Andriy Anishkin[4], Kishore Kamaraju[1], Kenjiro Yoshimura[1], and Sergei Sukharev[1,3]

[1]Department of Biology, [2]Department of Chemistry and Biochemistry, [3]Maryland Biophysics Program, University of Maryland, College Park, MD 20742
[4]Center for Computational Proteomics, Huck Institutes of the Life Sciences, Pennsylvania State University, University Park, PA 16802;

Abstract

Macromolecular excluded volume of the cytoplasm is a critical parameter maintained by cells, but mechanisms of its sensing remain unknown. MscS, the major turgor regulator in bacteria, mediates efflux of small osmolytes in response to increased membrane tension. Under moderate sustained tensions, MscS exhibits slow adaptive inactivation, but it inactivates sharply in the presence of cytoplasmic crowding agents. To understand this mechanism, we explored possible transitions of MscS and generated models suggesting that the coupling of the gate formed by TM3 helices to the peripheral TM1-TM2 pairs depends on the axial position of the core TM3 barrel relative to the TM1-TM2 shaft and the state of the associated hollow cytoplasmic domain (cage). Tension-driven inactivation separates the gate from the peripheral helices and promotes kinks in TM3s at G113; this conformation is stabilized by association of the TM3b segment with the beta domain of the cage. Mutations destabilizing the TM3b-beta interactions preclude inactivation and make the channel insensitive to crowding agents and voltage. Mutations that strengthen

this association result in a stable closed state and immediate inactivation. Simulations show that pressure exerted on the bottom of the cage in the inactivated state reduces the volume of the cage in the cytoplasm and at the same time increases the footprint of the TM domain in the membrane, implying a coupled sensitivity to both membrane tension and crowding pressure. The cage, therefore, provides feedback on the increasing crowding that disengages the gate and prevents excessive draining and condensation of the cytoplasm. We discuss the structural mechanics of cells surrounded by an elastic cell wall where this feedback mechanism specific for MscS may be necessary.

INTRODUCTION

Life, as we know it, is inseparable from water. Solvation sets chemical potentials for all soluble components inside and outside the cell, affects intermolecular interactions, drives hydrophobic assembly, and provides free space for diffusion and macromolecular dynamics. Crowding effects are strong since many equilibria and reaction rates inside the cell have generally steeper dependencies on the macromolecular excluded volume than on ionic strength or osmolarity per se [73-77]. Although mutual compensatory mechanisms between increased ionic strength and macromolecular excluded volume exist, the primary purpose of osmoregulation is the maintenance of sufficient amount of free water in the cytoplasm [78]. Cells actively regulate their water content by accumulating or releasing ions and small compatible osmolytes [79], but the mechanisms that sense and define the setpoints for water activity and volume fraction are still unclear. While several candidates for primary osmosensors in different organisms and cell types

have been proposed [80-82], no mechanistic hypothesis that would connect their function with the fractional volume of water exists.

Free-living microorganisms are frequently subjected to hydration stresses and possess robust osmoregulatory systems. In hyperosmotic conditions, bacteria accumulate ions and compatible organic osmolytes to retain water [83-85]. Under steady growth conditions, the internal turgor (hydrostatic pressure) inside bacterial cells decreases with an increase in external osmolarity[86]. However, in the event of a sudden drop of external osmolarity, bacteria release accumulated osmolytes through several types of mechanosensitive channels acting as tension-activated release valves. Gradual increase of tension in the cytoplasmic membrane of *E. coli* opens the low-threshold YbdG channel [87] exhibiting a MscM-like activity, followed by more conductive MscK [88], MscS [38], and several other species such as YbiO, YjeP, and YnaI [89]. When tension in the membrane approaches the lytic limit (11-14 mN/m), large-conductance mechanosensitive channels (MscL) released larger osmolytes [21] and rescues the cell from lysis [38]. One should remember that in the event of moderate osmotic adjustments, even brief opening of the non-emergency MscS valve results in dissipation of vital ionic gradients, and clearly comes at a metabolic cost. Apparently, to suppress spurious openings at sustained moderate tensions, MscS shows adaptive behavior which leads to closure and subsequent inactivation [50, 51, 90, 91].

In the inactivated state, MscS does not conduct or respond to tension [51]. Examination of the WT MscS crystal structure (PDB ID 2OAU, [41]) obtained in foscholine (in the absence of lipids) suggests that its conformation resembles a non-conductive inactivated state [92]. This state is characterized with the gate uncoupled from

the external stimulus due to the splay of peripheral TM1-TM2 helical pairs being separated from the gate formed by sharply kinked TM3 helices. For the same reason the structure does not possess functionally important D62-R131 bridges. A more recent crystal structure of WT MscS obtained in a partially open state in dodecylmaltoside (PDB ID 4HWA [93]) shows a different splay of unsupported TM1-TM2 pairs, indicating that the conformations of these domains are very sensitive to the type of detergent replacing the membrane and that their positions in the lipid bilayer are likely to be different. Several attempts were made to create a model of the resting state, which would have a direct connection to transmit force from the lipid-facing helices to the gate [44, 49, 50, 94]. This conformation is likely characterized by a more parallel packing of TM1-TM2 helices, forming a buried hydrophobic interface with TM3s (Fig. 2.1) providing a mechanism by which the channel would be able to open by membrane tension transmitted through the peripheral helices to its gate [44]. The previous searches for the gating-competent resting state and models for opening and inactivation considered primarily conformational changes in the transmembrane (TM) domain, although there were indications that the movements of the TM domain generates coupled movements in the cage [95-97].

The possibility of a salt bridge formation between the tips of the TM1-TM2 loops (D62) with the equatorial region of the cage (R128/R131) was first noted in MD simulations [52], and then the functional role of these bridges was experimentally demonstrated by Nomura and coworkers [96] who found that disruption of these bridges with mutations strongly speeds up channel adaptation. Another important observation was made by the Kubalski group who first reported that adaptive closure of MscS occurs

more rapidly in the presence of indifferent polymers such as PEGs, dextrans or Ficoll on the cytoplasmic side, implying involvement of the hollow cage domain [57]. Subsequent genetic screens for gain- and loss-of-function mutants performed by the same group [63] revealed multiple new loci affecting gating, including one potent mutation at the interface between TM3b and the beta domain of the cage (G168D) that strongly affected the process of adaptation.

In the present paper we go beyond previous studies and show that MscS inactivation is exquisitely sensitive to excluded volume effects and the cage domain directly participates in sensing the cytoplasmic crowding of large-molecular weight compounds and voltage. We develop a new molecular model of the resting state that includes several previously unexplained features and propose a consistent explanation for the role of the cage and specifically the TM3b-beta interface in the functional cycle of MscS. We show opposite effects of interface-stabilizing and destabilizing mutations on MscS inactivation and provide data suggesting that in active states the mutual arrangement of TM3b and beta domains are likely to be different from that in the crystal structure. Molecular simulations of the resting and inactivated state models illustrate how geometrical parameters of the molecule (lateral expansion of the transmembrane domain and compaction of the cytoplasmic cage) lead to the coupling between membrane tension and crowding pressure both acting synergistically in driving the inactivation transition. We propose the first structural mechanism of crowding sensing by a mechanosensitive channel and describe a physiological context in which cells surrounded by elastic peptidoglycan would benefit from this ability.

MATERIALS and METHODS

Modeling and simulations

We used the extrapolated motion protocol (EMP) [48, 50] to generate a set of non-random models from the crystal structure of WT MscS (PDB ID 2OAU) [41] with the missing N-terminal domain modeled with Rosetta [49]. Arranged as cycles of small (0.1-0.5 Å) displacements extrapolated from the previous step, energy minimizations and short relaxing MD simulations (see details in Supplement), this protocol generates strings of interconnected conformations covering 5-15 Å domain displacements within 50-100 steps. The protocol was implemented with the Tcl/Tk language in NAMD2-VMD [98]. The library of about 86000 models generated from different starting points was sorted using automated searching scripts identifying spatial proximities of specific groups or domains. The specific search criteria included (a) sufficiently tight rings of L105 and L109 forming a non-conductive gate; (b) salt bridge between the tip of the TM1-TM2 loop (D62) and the equatorial region of the cytoplasmic 'cage' domain (R128 or R131) [96]; (c) an extensive buried contact between TM2 (A63-F80) and TM3 (V99-L115) in the resting state, and separation of these helices in the inactivated state [44] and (d) TM3 helix straightened near G113 in the resting state or kinked in the inactivated [50]. An additional criterion for the choice of the pair of resting and inactivated states was the difference of the effective in-plane areas of the TM barrel that was estimated from the inactivation and recovery kinetics as about 8 nm^2 [90].

The candidate models without perturbations of the secondary structure were embedded in the fully hydrated and pre-equilibrated lipid bilayer assembled from 220 POPC molecules, energy-minimized and then equilibrated in all-atom MD simulations for 20 ns followed by refinement using a 5 ns symmetry-driven simulated annealing [99].

To explore the structural changes in MscS under increased crowding in the cytoplasm we visualized the effect of cytoplasmic cage compression using steered molecular dynamics. We have approximated the pressure of the large macromolecules by a force acting on the C-terminal half of the cytoplasmic cage (residues 183-280 in each subunit, 2751 atoms per complex). The force acting towards the midplane of the bilayer was set for slow exponential growth from 0.001 to 0.1 kcal/mol/Å/atom over the course of 20 ns simulations. To prevent the net displacement of the protein and membrane under the force, we have restrained the center of mass of non-hydrogen backbone atoms of TM1-TM2 helices in its position inside the lipid bilayer only in the direction normal to the membrane midplane (see more details in the Supplement).

Mutagenesis and electrophysiology

The *mscS* gene was inserted and induced via IPTG in a pB10b vector and expressed in the MJF465 triple-knockout *E. coli* strain (*mscS-, mscL-, mscK-*) [38] or PB113 (*mscS-*, *mscK-*) [88], which retained a native copy of *mscL*. Mutants of MscS were created using a QuikChange mutagenesis kit (Strategene/Agilent).

Spheroplasts were generated as described in previous works [36, 51, 100] and all electrophysiological recordings were made in excised inside-out patches exposing the cytoplasmic side to the bath. The experimental bath solution contained 400 mM sucrose,

200 mM KCl, 50 mM $MgCl_2$, 5 mM $CaCl_2$ and 5 mM HEPES and was titrated to pH 7.4 with KOH. For crowding experiments, Ficoll 400 was perfused into the bath manually at the desired wt/vol concentration. Osmolarities of solutions were measured with a Wescor 5520 vapor pressure osmometer. Membrane patches were obtained with borosilicate glass pipettes (Drummond, cat# 2-000-100) and recorded at the desired voltage set by a microelectrode amplifier (Axopatch 200B); unless otherwise noted, all recordings were performed at 30 mV pipette potential. Negative pressure (suction) was applied using a high-speed pressure clamp apparatus (HSPC-1, ALA Scientific). Pressure and voltage protocol programming and data acquisition/analysis were performed with the PClamp 10 suite (Axon Instruments). Linear triangular ramps involve a steady 1 s increase in pressure followed by a symmetric reduction of pressure back to zero and were used to determine activation midpoints and hysteresis. Pulse-step-pulse protocols are defined by an initial pulse of saturating pressure to visualize the entire population, followed by a step (5 to 10 s) of sub-saturating pressure and ending with another saturating pulse to show the number of channels still available for opening; these elucidated the extent of tension-driven inactivation. Pulse-step protocols were performed with a saturating pressure pulse opening the entire channel population followed by a step down to some sub-saturating tension, which allowed the channels to adapt/close and gave insight into the closing rate dependencies on tension.

Conversion of the pressure amplitudes into the tension scale was achieved by using the previously-established midpoint tension values for WT MscS (7.8 mN/m) and MscL (13 mN/m). Assuming that the radius of curvature of the patch (r) does not change in this pressure range, the ratio of tension and pressure midpoints should be the same.

The pressure midpoint of each patch was determined via a 1s ramp of pressure and set equal to the tension midpoint of MscS (7.8 mN/m) after it was determined that the specific mutant had the same p0.5MscS/ p0.5MscL (~0.6) as WT MscS through expression in a cell like containing native MscL. [101-103]

RESULTS

Modeling

The existing crystal structures of *E. coli* MscS [42, 46, 93] and its homologs [104] solved in detergents obviously do not represent the complex functional cycle of the channel entirely. The non-conductive structures likely resemble the inactivated state with an uncoupled gate [41], whereas conductive conformations [46, 93] appear to be partially open. Modeling and simulations may help envision the channel structure in the native membrane environment and reconstruct the missing parts of the functional cycle [48-50]. Here we combined a computational algorithm allowing us to explore the conformational space of MscS with multiple constraints derived from functional experiments to generate models for the resting and inactivated states. All modeling was done by Dr. Anishkin.

A database of non-random models was generated from the revised crystal structure of WT MscS. This library of 86000 non-random models generated from

different starting points was sorted using automated searching scripts identifying spatial proximities of specific groups or domains. The criteria included non-conductive gate; salt bridge formed between D62 and one of the arginines (R128 or R131) on the cytoplasmic 'cage' domain, buried contact between TM2 and TM3 engaging the gate in the resting state, or separation of these helices in the inactivated state.

It soon became obvious that imposition of the D62-R131 bridges results in a more upright orientation of the peripheral helices and vertical displacement of the TM3 barrel inside the TM1-TM2 shaft. In EMP trials, this transformation generally (not always) correlates with straightening of the crystallographic G113 kink and reformation of a less prominent kink near G121. In the crystal-like inactivated state, D62 formed a salt bridge with R128. We did not stipulate the in-plane area change in the transmembrane domain between the modeled resting and inactivated states, but we found it very close to the experimentally estimated 8 nm^2 area change [90].

The candidate models were embedded in the fully hydrated and pre-equilibrated POPC lipid bilayer, energy-minimized and equilibrated in all-atom MD simulations for 20 ns followed by symmetry-driven simulated annealing [99]. The models are shown in Fig. 2.1 (A, B) with the detailed structure of the gate region and surrounding domains below.

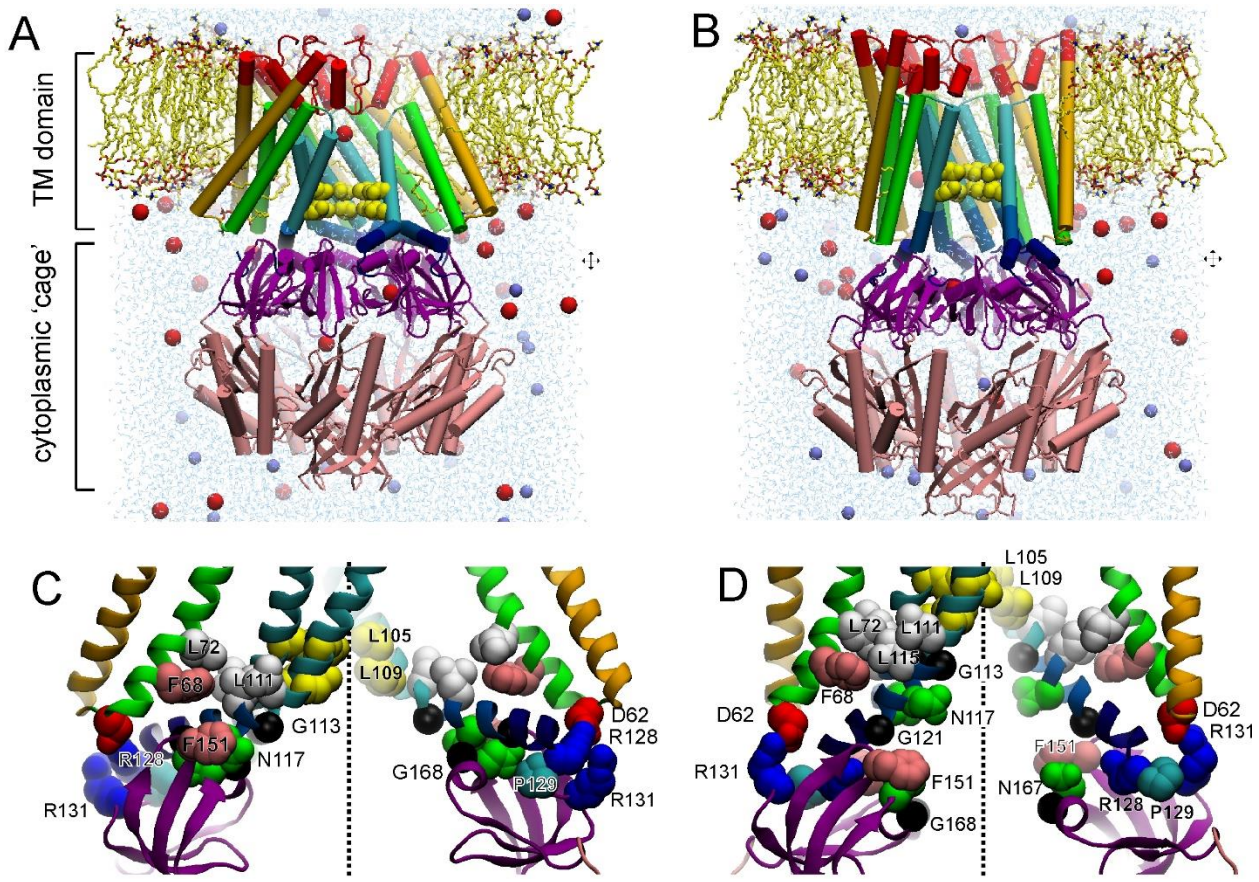

Figure 2.1. MD-equilibrated models of the inactivated (A) and resting (B) states in the explicit lipid bilayer. The details of TM-cage domain interactions with critical sidechains shown for the inactivated (C) and resting (D) state where the gate (L105, L109) is coupled to the peripheral helices through the hydrophobic (F68, L72 – L111, L115) contact. The model of inactivated state resembles the crystal conformation (2OAU), however the splay of the peripheral TM1 and TM2 helices (ocher and green) is less. In both conformations, D62 residing on the TM1-TM2 loop forms a salt bridge with either R128 in the inactivated or R131 in the resting state. The resting state model predicts straightening of the crystallographic G113 kink, a substantial separation of TM3b (dark blue) from the beta cytoplasmic domain (purple) and a translation of the gate region upward.

The conformation assigned as 'inactivated' (Fig. 2.1A) is similar to the initial crystal state, with prominent kinks at G113 and tight packing of the TM3b-beta interface. In this putative inactivated conformation, the peripheral TM1/TM2 helices are splayed but they form a smaller angle than in the crystal structure, allowing the D62-R128 salt bridges to form. The TM1-TM2 pairs are partially detached from the gate region such that the hydrophobic sidechains in the buried zone are packed more loosely than in the

resting state. The TM1-TM2 splay increases the effective in-plane area of the lipid-embedded TM domain compared to the resting state (Fig. 2.1B). In most of the candidate models for the resting conformation, the TM3 helices were reproducibly kink-free until G121, the entire TM3 barrel was moved up inside the sheath of peripheral TM1-TM2 helices and the TM3b helical segments were dissociated from the beta domains within the cytoplasmic cage.

The transition from left to right would represent recovery from inactivation to the gating-competent resting state. Experimental measurements of recovery kinetics show that it is a relatively slow process on the molecular scale, taking 1.3-2 s for WT MscS [51]. It involves several changes: compact packing of helices and formation of a more extended and tight contact between TM2 and TM3 (see panels C and D), which are accompanied by movement of the TM3 barrel inside the TM1-TM2 sheath by approximately 2 helical turns (from the cytoplasmic interface towards midplane of the membrane), straightening of TM3s and detachment of the TM3b helical segment from beta domains and re-formation of D62-R131 bridges which stabilize the resting state. The inactivating transition is likely to involve the same changes in reverse, which results in a decrease of the cage profile in the cytoplasm. While its own internal volume does not change much, due to the vertical displacement the cage occupies a smaller volume when the sharp kinks at G113 are in place and the TM1-TM2 pairs are separated from the inner TM3 barrel.

MscS inactivation is increased in the presence of crowding agents

Like activation, MscS inactivation is driven by tension; both transitions originate from the closed state [90]. The ability of MscS current to adapt with time under sustained tension [51, 102] produces decaying current traces which represent the sum of sequential processes of adaptive closure and complete inactivation. The two kinetically intertwined processes are distinguished by the 'comb' pressure protocol that includes a prolonged conditioning step of tension with interspersed short saturating pulses testing for the availability of non-inactivated channels. In control experiments, the amplitude of current responses to test pulses gradually decays with time, representing the number of channels in the closed state as well as kinetics of tension-dependent inactivation (Fig. 2.2).

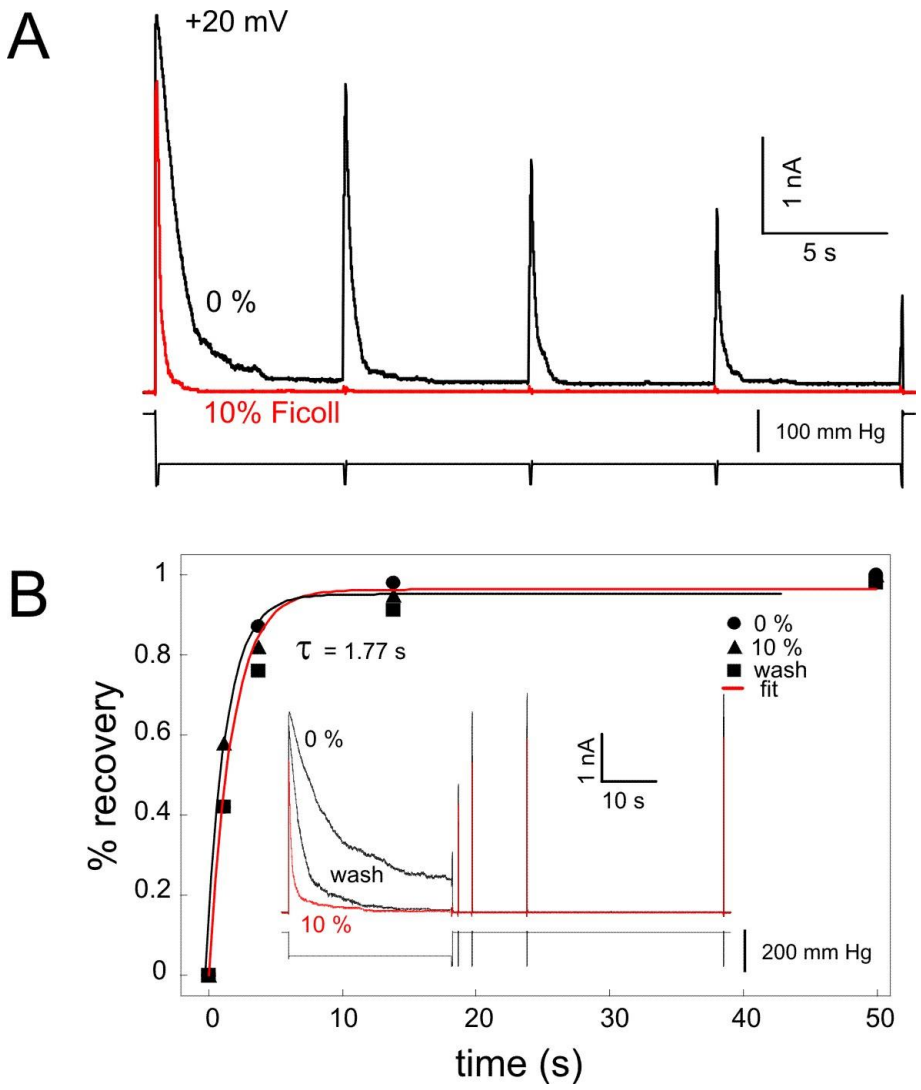

Figure 2.2. Responses of WT MscS to crowding agent Ficoll 400. The top trace (A) was recorded at +20 mV pipette voltage with stimulation by a 30 s step of constant pressure with five evenly interspersed saturating test pulses of 0.1 s in length ('comb' protocol). The peaks of current responses to test pulses in the control (0% Ficoll 400) reflect the kinetics of inactivation. In the presence of 5% Ficoll, the MscS population opens in response to the first pulse and then completely inactivates. The bottom figure (B) shows the kinetics of recovery after inactivation. The inset shows the pressure protocol consisting of a prolonged step of pressure followed by a series of test pulses. The kinetics of recovery is not influenced by 10% Ficoll.

The presence of crowding agents such as Ficoll 400 on the cytoplasmic side shifts the activation curve in response to ramp stimuli toward higher pipette pressures (Fig. 2.4A), signifying that the crowding pressure acting primarily on the cytoplasmic domain interacts with the gate and counteracts the tension. The presence of crowders also

changes the character of response to the ‘comb’ protocol (Fig. 2.2), leading to immediate inactivation after the first test pulse. In the presence of 10% Ficoll the rate of inactivation increases by more than one order of magnitude as measured at the same amplitude of conditioning pulse equal to the midpoint pressure (p0.5) of MscS activation determined in ramp experiments. Surprisingly, the presence of 10% Ficoll did not visibly change the kinetics of recovery. Polyethylene glycol (PEG 3300) in concentration of 25 mM (~7.5 vol %) exerted the same strong effect on inactivation, but also slowed down the recovery.

The TM3b-beta domain interface

In order to proceed with analysis of mutations, we first investigated (Fig. 2.3) and analyzed the residue interactions at the TM3-beta domain interface which underwent a substantial rearrangement upon modeled transition from the inactivated to resting state. In the TM3b-beta bound conformation representing crystal-like inactivated state (panel A) we observe several critical interactions. The sidechain of N117 interacts with the backbone nitrogen of N167 and packs with F151. The backbone of N117 forms alpha helical hydrogen bonds with the backbone of both critical hinge residues, G113 and G121 [50]. Besides the terminal oxygen of N117, the backbone of N167 also interacts with the backbone amide oxygen of F151. G168 packs in close proximity of G113 and N117. The crystallographic TM3-beta contact is predicted to be essentially desolvated. Upon straightening of TM3 in the resting state (panel B), the hydrophobic neighborhood is largely dispersed, liberating the sidechains of N117 and N167. The separation of many hydrophobic sidechains is energetically feasible because N167 and N117 become favorably solvated. The general prediction is that crystallographic packing will be

stabilized by isovolumic replacement of N117 or N167 by apolar valines. The G168D mutation identified by Koprowski and coworkers in the random mutagenesis screen [63] is located at the interface between the cytoplasmic beta domain and the c-terminal end of TM3b. Introduction of a charged and bulkier substitution is expected to stabilize the open conformation which has the most unfolded TM3b-beta contact. We have analyzed 10 single and 3 double substitutions in this region. The most drastic and interpretable effects of several mutations are described below.

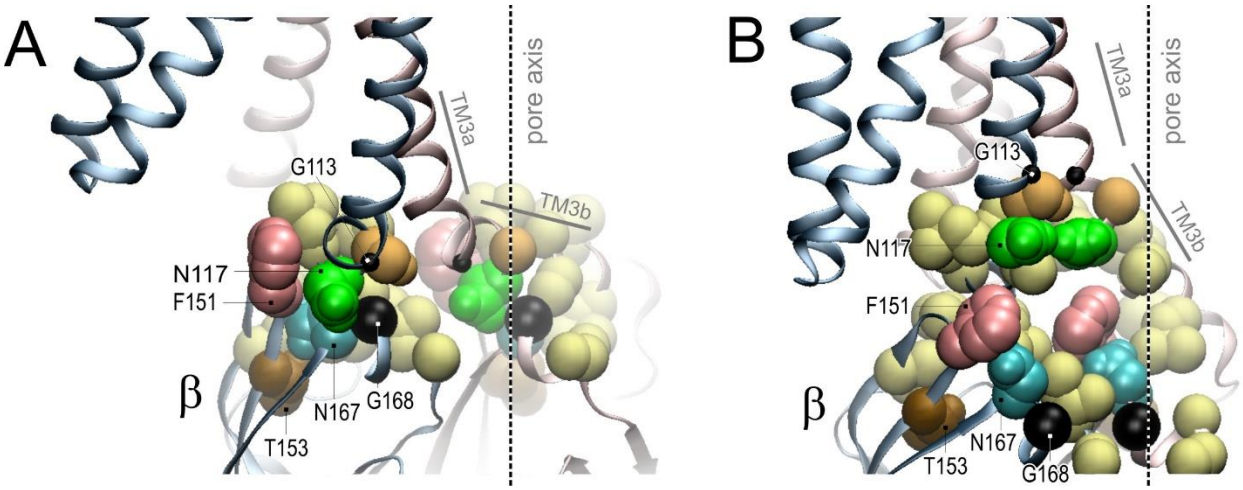

Figure 2.3. Detailed view of sidechain packing at the TM3b – beta domain interface in the crystal conformation (PDB ID 2OAU) (A) and in the modeled resting state with TM3b and beta domains separated (B).

The G168D mutation affects the gating transitions and sensitivity to crowding agents

Current responses to triangular ramps of pressure for WT and G168D MscS are presented in Fig. 2.4A. WT exhibits moderate asymmetry of response (hysteresis), showing a lower midpoint of the current-pressure curve on the descending limb of the ramp in comparison to the ascending limb, while G168D exhibits much stronger hysteresis and closes only at tensions near zero. The hysteresis is the manifestation of a

slow closing rate (k_{off}), which appears to be especially slow in the mutant. This closing transition was confirmed with a specific (pulse-step) protocol; the population was subjected to a full activation by a short saturating pulse followed by a prolonged step of lower pressure, during which the closing kinetics were recorded. The resultant decaying current traces (Fig. 4B) were fitted with monoexponential functions, producing a linear dependency of the natural log of k_{off} on tension (γ, mN/m) (Fig. 2.4D). The same range of decay times was achieved for the G168D mutant at much lower pressures (red arrows), which shifts the position of the ln(k_{off}) curve to much lower tensions (by 2 mN/m). Extrapolation of the fitting line to zero tension (the y-intercept) gives estimations of 'intrinsic' closing rates of $2430 \pm 270\ s^{-1}$ (n = 6) for WT and only $107 \pm 24\ s^{-1}$ (n = 6) for G168D MscS. The slopes of these curves represent the tension dependency of their closing rates and can be interpreted as the difference of in-plane areas between the open state and rate-limiting barrier for closing, based on a putative single-barrier energy profile (Fig. 2.4D, inset) for the tension-gated transitions [105]. The slope of the WT curve was found to be $-1.54 \pm 0.16\ s^{-1}/(mN/m)$, n = 6, which is smaller than that found for the G168D mutant ($-2.0 \pm 0.17\ s^{-1}/(mN/m)$, n = 6). This suggests that the open state of G168D is more stable and might have a deeper and/or wider energy well than WT. Alternatively, the mutant may have a different position of the rate-limiting barrier, which is farther from the open-state well compared to WT.

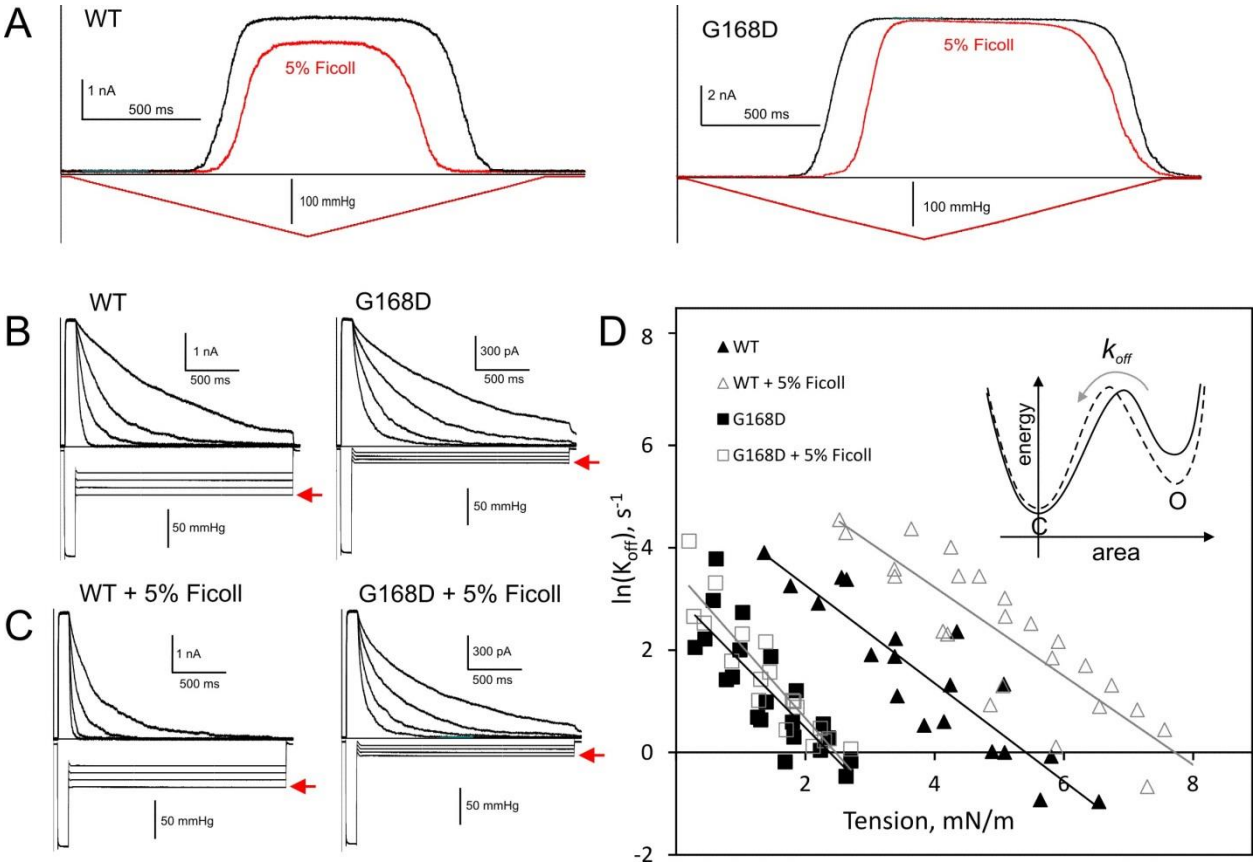

Figure 2.4. The crowding effects of 5% Ficoll 400 on Wild Type and G168D MscS opening and closing. Under symmetric ramps of saturating pressure (A), both WT and G168D MscS open at similar tensions yet G168D closes much more slowly, resulting in greater hysteresis of the closing portion of the activation curve. Upon the addition of 5% Ficoll, activation curves for both WT and G168D shift ~10% to the right (shown in red). Pulse-step protocols for both WT and G168D are shown both before (B) and after (C) the addition of 5% Ficoll. Arrows indicate the pressure that was applied for the two second step during which the closing kinetics were monitored. The closing rates from each of these curves (before and after 5% Ficoll) were plotted against the applied tension (n = 3 for each) (D). The alteration of closing kinetics after 5% Ficoll is more pronounced for WT than G168D MscS. The inset shows a theoretical single barrier energy profile. The solid line represents the transition from closed to open in WT MscS while the dotted line corresponds to G168D; the deeper and wider energy well for the open state of the mutant indicates a stabilization of the open state and a slower closing rate.

Ramp responses measured in the presence of 5% wt/vol Ficoll 400 showed a 10% ± 6% (n = 10) shifts of the activation curve midpoint toward higher pressures for WT MscS, as measured on the ascending limb of the ramp (Fig 2.4A, red traces). The midpoint on the descending limb also shifted toward higher pressures (22% ± 10%, n = 10), signifying stabilization of the resting state comparing to the open. The maximal

current amplitude at saturating tensions also tended to decrease by 10-20% due to partial inactivation of the channel population. For the G168D mutant, the response to the ascending limb shifted comparably to WT, however the rate of channel closure did not appear to increase as dramatically as in WT and a decrease of maximal current was less pronounced. The alteration of closing rates by Ficoll was further investigated by repeating the pulse-step protocol for WT and the mutant (Fig. 2.4C). The closing rate versus tension plot, based on three separate patches of both WT and G168D in the presence of 5% Ficoll, shows that the WT MscS curve shifts by about 40% toward higher tension, while the G168D curve only has a 4% shift (Fig. 2.4D, grey lines). This indicates that the G168D mutant is less susceptible to crowder-induced alterations of the closing rate of the channel.

Fig. 2.5 shows the typical responses of WT and G168D MscS to pulse-step-pulse protocols revealing the degree of tension-dependent inactivation. After a 10-s conditioning step of approximately half the tension required to open all the channels (p0.5), an average of about 70% of the WT population remains active while the remaining channels recover from inactivation with a time constant τ of 1.4s $\pm$ 0.4 s, n = 10. However, in the presence of 10% Ficoll WT MscS inactivates completely, as demonstrated in Fig. 2.5A. The G168D population generally resists inactivation under similar conditions (10-s conditioning step of sub-saturating tension), even in the presence of Ficoll (Fig. 2.5B). To compare the inactivation resistance of G168D with another non-inactivating mutant, G113A, we applied the same protocol. The G113A mutation favors a straight pore-lining helix and has been shown to impede inactivation in the absence of crowders [50, 90] (Fig. 2.5C). Upon the addition of 10% Ficoll, G113A shows moderate

inactivation. Fig. 2.5D shows data from three WT MscS patches and describes the inactivation of the channels in response to 10s conditioning steps of varying tension. WT MscS shows its maximal inactivation of roughly 40-50% of channels upon exposure to a 10s step of tension of approximately 8 mN/m, seen as a dip in the data. Upon addition of 5% Ficoll, this inactivation drastically increases, with 80-90% of the population becoming inactivated. G168D is much less susceptible to tension-driven inactivation in identical procedures, with less than 15% inactivation (Fig. 2.5E). After exposure to 5% Ficoll, inactivation remains below 20% for G168D (n = 3). G113A shows intermediate inactivation (approximately 40%, n = 3) in the presence of Ficoll, as seen in Fig. 2.5F, indicating that the mutant is more sensitive to crowding than G168D. The fact that G168D inactivates much less than G113A in the presence of crowders indicates that the intact TM3b-beta interface has a stronger contribution in the stability of the inactivated state than helical flexibility at G113 and the cage is intimately involved in conveying the crowding pressure perturbation to the gate. Notably, the active channel population is entirely present in the first saturating test pulses in the 10s protocol for both WT, G168D and G113A (Fig. 2.5A-C); this shows that crowding agents at these concentrations do not drive the channel directly into the inactivated state and tension is absolutely required to inactivate MscS.

We have also tested the disaccharide trehalose, a compatible osmolyte for similar effects in a concentration range up to 1 M, which constitutes 24 vol%. While at this concentration trehalose also shifted activation curves to the right, it did not change the extent of inactivation of WT or G168D MscS (see Fig. 5.4).

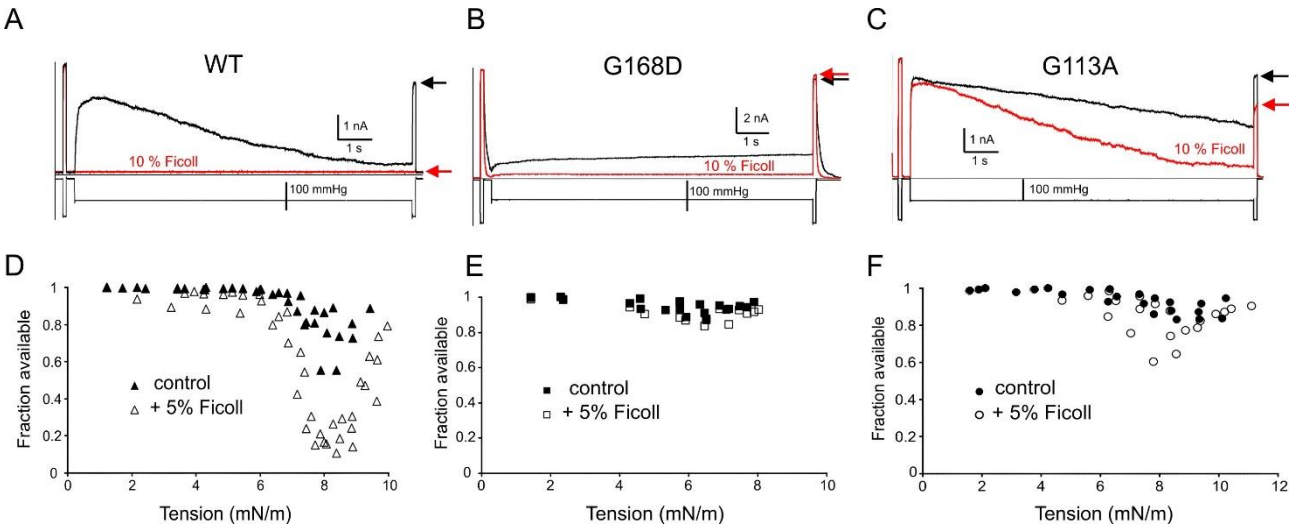

Figure 2.5. The crowding effect of Ficoll 400 on Wild Type and G168D MscS inactivation. Pulse-step-pulse protocols were used to investigate the tension-driven inactivation of WT (A), G168D (B) and G113A MscS (C), with the difference between the initial and final pulse (black arrows) representing the relative amount of inactivation. After exposure to 10% Ficoll on the cytoplasmic side of the patch, WT MscS completely inactivates, G168D resists inactivation and G113A displays an intermediate amount of inactivation (red arrows). The same pulse-step-pulse protocol was applied at varying step pressures to several different patches of WT, G168D and G113A (n = 3 for each) in the absence and presence of 5% Ficoll 400. The resulting fraction of available channels was plotted against tension to illustrate inactivation. The inactivation of WT MscS channels was greatly increased in the presence of Ficoll (D) while G168D remained largely unchanged (E) and G133A inactivated moderately (F).

G168D MscS is insensitive to voltage

Fig. 2.6 shows traces of MscS currents evoked by the same step-pulse pressure protocol recorded at different voltages. The near-saturating step kept the entire population open for 5 s whereas the super-saturating step at the end was applied to indicate any adaptive closure or inactivation that could occur during the step. As seen from the traces, WT population reduces its conductance at -60 mV pipette voltage (depolarizing) and quickly closes and completely inactivates at -80 and -100 mV, consistent with the previous results [51]. An alanine substitution at residue 168 does not change this behavior. The G168E mutant displays slight inactivation at -100 mV and the G168D mutant shows no inactivation at all. This data suggests that the conformational changes in the cage are also critical for voltage-dependent inactivation, which likely proceeds

through the common pathway with tension-dependent inactivation involving kink-stabilizing TM3b-beta interactions. Based on a recent study [106], it is also possible that the cage acts as a voltage sensor, in contrast to previous conjectures that charges on TM1 may be responsible for voltage-dependent gating [42]. It is likely that the driving force for closure is electroosmotic water flux [48] which may lead to partial desolvation and shrinkage of the cage and would be analogous to the desolvating effect of crowders.

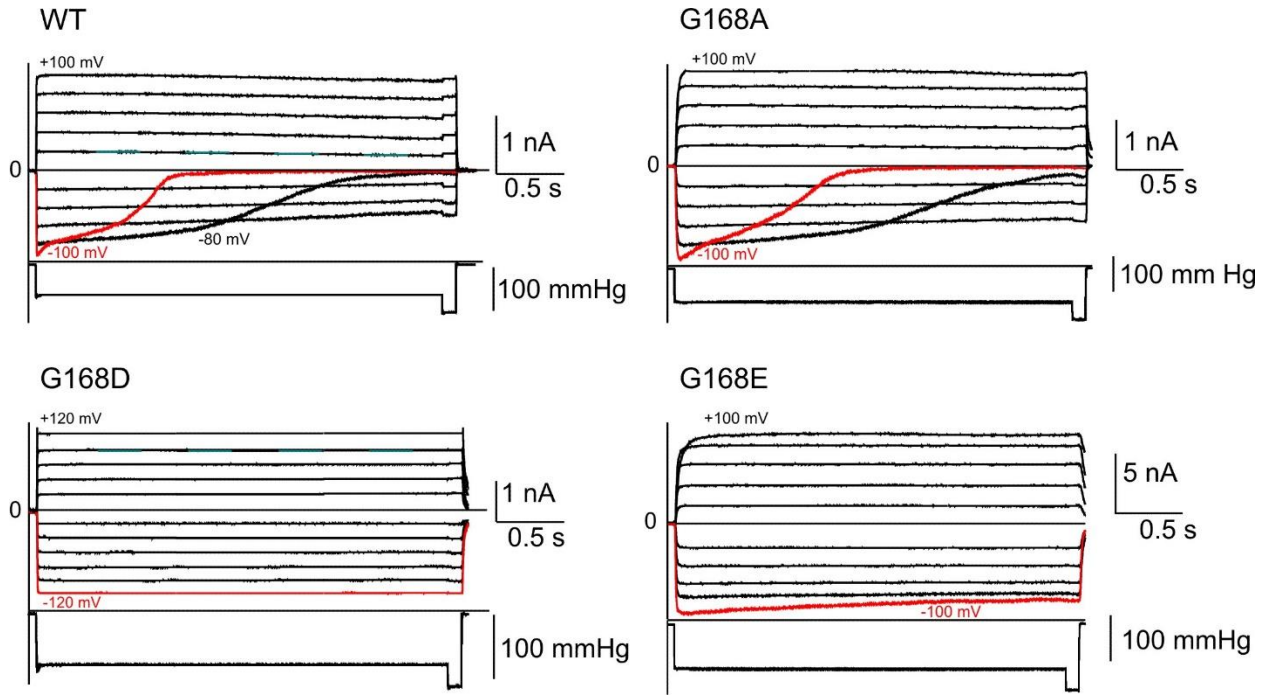

Figure 2.6. Inactivation of MscS under strong depolarizing voltages is obliterated by negatively charged substitutions for G168. Responses of a 3 s step-pulse pressure protocol activate the entire population of channels in an excised membrane patch. This protocol was repeated at varying voltages between ±20 mV and ±120 mV to demonstrate the voltage-dependent adaptation and inactivation of WT MscS at -80 mV and -100 mV. A substitution of alanine at residue 168 did not cause a phenotypic divergence from WT MscS in terms of voltage-dependent adaptation. However, this voltage sensitivity is completely lost in G168D while G168E shows little adaptation.

Hydrophobic substitutions near the TM3b-beta interface stabilize non-conductive states

As suggested by the comparison of the inactivated and resting conformations (Fig. 2.1 and 2.3), disruption of the hydrophobic neighborhood of residues forming the TM3b-beta domain interface is facilitated by the presence of two polar residues, N117 and

N167. Isovolumic replacement of these asparagines with more hydrophobic valines is predicted to stabilize the tightly assembled crystallographic state.

Fig. 2.7 compares the traces of N117V and N167V MscS populations versus WT obtained with ramp, pulse-step and pulse-step-pulse protocols. WT shows full activation with 1 s ramps, its closure within a 10 s period takes place at tensions near the midpoint and it moderately inactivates during a 5 s step and recovers with a characteristic τ of 1.4s $\pm$ 0.4s (n = 10) (see also Table S1). In the presence of high concentration of crowders (10-15%), ramp responses show only partial activation of MscS, whereas the rest of the population inactivates silently without opening (red trace). As indicated by measurements in the PB113 *mscL*-positive strain, both valine mutants activate at much higher tension than WT (~13 mN/m). N117V shows reduced activation with a 1 s ramp and closes with a τ of about 0.1s at tensions close to 90% of saturating tension. This indicates substantial silent inactivation and a destabilized open state in this mutant. Under a 5s conditioning step of sub-saturating tension, N117V closes very quickly and inactivates almost completely. However, this mutant recovers three times faster than WT, with a τ of 0.5 $\pm$ 0.02s (n = 3). N167V could not be readily activated by a 1 s ramp, also indicating massive silent inactivation preceding opening. It was impossible to keep this mutant population in the open state for longer than 500 ms even under saturating pressure, indicating a strongly destabilized open state. Under pulse-step-pulse protocols, N167V inactivated silently and completely yet also recovered much more quickly than WT MscS, with a τ of 0.6 $\pm$ 0.2s (n = 3). When these two valine mutations were combined to create N117V/N167V MscS, the channel was again nearly impossible to activate with a 1s ramp and showed complete inactivation under moderate tension (not shown).

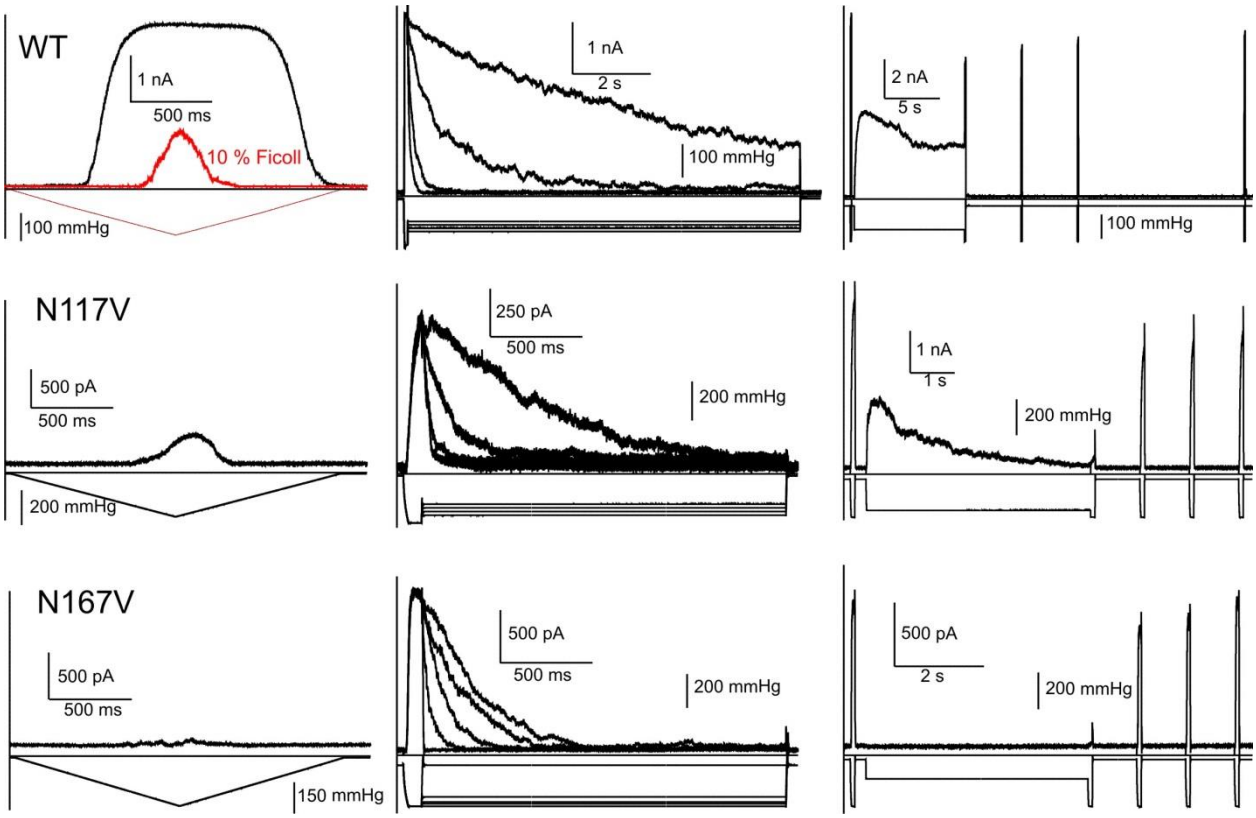

Figure 2.7. Effects of hydrophobic substitutions for N117 and N167 on the resting, open and inactivated states. Above displays three similar protocols for WT MscS and the mutants N117V and N167V. (Column 1) Upon being subjected to a 1 s pressure ramp, WT MscS displays its characteristic opening and closure, while both N117V and N167V refuse to open. (Column 2) The patches were then subjected to a closure protocol similar to those from Fig. 2.4 B, C. N117V and N167V required near-saturating pressure to hold the channels open long enough to monitor closure and both closed much faster than WT MscS. (Column 3) Lastly, the patches were subjected to an inactivation protocol beginning with a saturating pulse followed by a conditioning step and ending with several pulses of saturating pressure to monitor the process of channel recovery from the inactivated state. The N117V and N167V MscS mutants showed more inactivation than WT MscS following the conditioning step yet both mutants recovered faster, with a characteristic time of recovery (τ) of 0.5 s + 0.02 s (n = 3) for N117V and 0.6s $\pm$ 0.2 s (n = 3) for N167V. Both of these recovery rate values were lower than that found for WT MscS (1.4 s $\pm$ 0.4 s, n = 10).

Silent inactivation from the resting state and quick recovery suggests that in these mutants the resting state is conformationally closer to the inactivated state. It appears that these transitions occur without substantial separation of TM3b from the beta domain and may only involve the separation of TM1-TM2 pairs from TM3. It is also possible that the

unstable open state in valine mutants has a different conformation compared to WT, which is predicted to have kink-free TM3 helices in the open state [50].

The predicted inactivated state is susceptible to axial compaction coupled to lateral expansion of the transmembrane domain.

The data above show that crowding acts synergistically with tension in driving inactivation. However, the question of how tension and crowding perturbations communicate within the channel remains. We designed steered simulations to mimic crowding pressure acting on the channel from the cytoplasmic side and observe a susceptibility of the resting and inactivated states to this type of perturbation. Although crowding pressure of smaller macromolecular components might be acting normally to the cage surface, larger crowders which are unable to approach the membrane too closely would primarily exert pressure along the main axis of the channel toward the membrane. In the following simulations we have approximated the pressure acting on the cage domain in the direction normal to the membrane. The membrane-equilibrated models of the resting and inactivated state were subjected to gradually increasing steering force applied to all main chain atoms of the lower hemisphere of the cage directed toward the membrane midplane. The force increased exponentially from 0.001 to 0.1 kcal/mol/A. These forces were purposely much larger than the actual osmotic forces acting on the cage in experiments in order to observe the character of domain interactions in the 20 ns time frame accessible in all-atom simulations. Fig. 2.8 shows the initial and 16 ns frames of a 20 ns simulation of the resting (A) and inactivated models (B) (after the 16^{th} ns the exponentially increasing force was causing non-physiological distortion of the

structures). Analysis of these two states indicates that the upward cage displacement resulted in sharpened TM3 kinks (at G113) and increased splay of TM1-TM2 pairs, stabilizing and somewhat exaggerating the inactivated state and causing a significant in-plane expansion. Steered motion of the cage in the resting model does not lead to such distortions and caused an increase in the in-plane channel area only half as large. Panel C shows the changes in the molecule's geometry with time, tracing the distances between the cage and TM domain's centers of masses in the course of compression. Panel D depicts simultaneous changes of the volume that the cage takes in the cytoplasm and the average in-plane area of the TM domain. It is clear that the vertical displacement of the cage, especially in the inactivated state, is coupled to a large lateral expansion of the TM domain. A volume change of ~20 nm^3 experienced by the cage is substantial. Since the thermal energy of 1 k_BT = 4.1 atm ×1 nm^3 , the pressure that would generate this energy over a 20 nm^3 compression path is ~0.2 atm, which in corresponds to osmotic imbalance of only ~9 mOsM (Note that 10% w/v Ficoll 400 used in our experiments has osmotic pressure of 70 mOsm, meaning that it creates an energy bias toward more compact state by ~8 kT). A coupled expansion of the transmembrane domain by ~8 nm^2 under tension of 7 mN/m would by itself generate a bias of ~14 kT toward the inactivated state. The observed coupling between the two geometrical parameters (Fig. 2.8E, F) appears to be the structural underpinning of the enhancement of tension-driven inactivation by crowders.

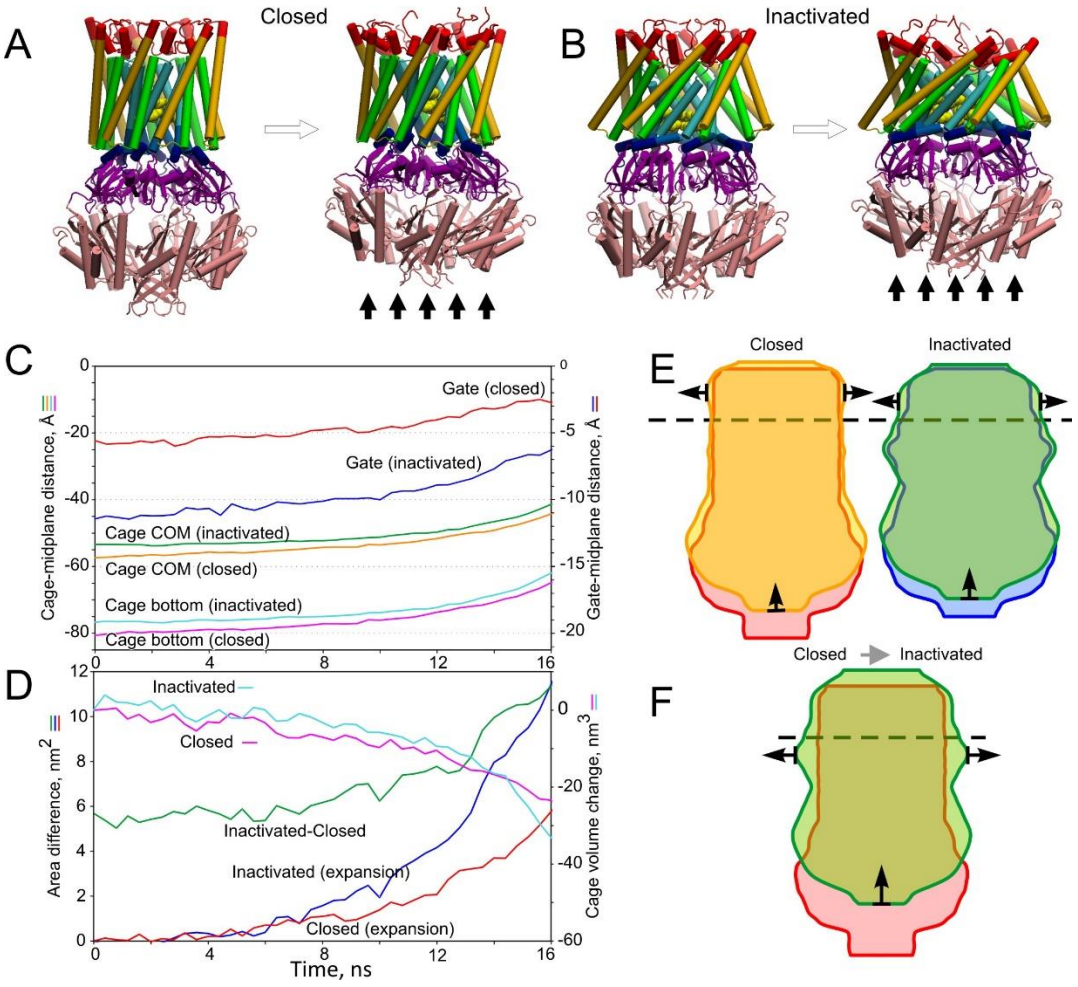

Figure 2.8. Results of MD simulations in which the cage domain in the resting and inactivated states was subjected to a compressive force applied to the lower half of the cage normally toward the plane of the membrane. Panels A and B show closed and inactivate conformations at start and at eight nanoseconds (marked with black arrows). The applied force causes similar displacement of the bottom and center of mass (COM) of the cage in both closed and inactivated states (C), however the gate region displaces more towards the center of the membrane in the inactivated state (blue line), apparently due to the detached state of TM1-TM2 pairs from the TM3 barrel. Cage volume decreases similarly under compression in both conformations, however cage pressing on the transmembrane barrel cause twice as larger increase of the in-plane area of the inactivated conformation as it has lipid-facing helices detached from the pore-lining TM3 barrel (D), thus favoring the transition from the closed to inactivated state under tension. Cage compression and the barrel expansion are illustrated by the contours of cross-section radii (E), while overlay of the closed state with no compression and inactivated state under force (F) explain the geometry change with inactivation and the reason for the synergy between tension and crowding pressure in driving inactivation.

Experiments presented on Fig. 2.4 show that crowding agents also shift activation curves to the right, making opening harder. Based on simulations, crowding pressure could stabilize the resting conformation relative to the open by making it slightly wider in

the membrane and thus decreasing energy gain from tension on opening. Another stabilizing contribution might be increasing the number and stability of TM1-TM2 linker contacts with the beta-domains (in particular, D62-R131 salt bridge). Such closed conformation would still be capable of opening because of the stable TM2-TM3 contact (membrane stress transmission route to the gate), but may open at a slightly higher tension, as observed in experiments .The inactivated state is predicted to be more strongly stabilized because of increased TM2-TM3 separation which facilitates expansion of TM1-TM2 barrel.

Consistent with the slow kinetics of inactivation (5-10 s at near-midpoint tensions), in our 20 ns steered simulation of the resting state we did not observe any tendency to switch to the inactivated conformation even at highest axial pressures exerted on the cage. Neither had we observed recombination of the beta domain with the TM3b helix. Apart from the timescale, it could be also because we did not apply high enough tension which is required for triggering the transition as observed in experiments. To visualize the transition, it would take a set of specially designed long simulations with simultaneously applied tension to the TM domain and pressure on the cage, and possibly with enhanced sampling techniques to overcome the energy barriers underlying the slow rate of inactivation.

DISCUSSION

The experimental measurements of MscS activity in excised patches using advanced pressure protocols (Fig. 2.2) show that the channel is exquisitely sensitive to crowding agents on the cytoplasmic side, which shift activation curves to higher tensions and drive immediate inactivation after the first activating pulse. Since resting MscS can undergo two parallel tension-driven transitions, to either the open or inactivated state, crowding appears to bias the process toward inactivation. The volume percent of the crowders present in our experiments (5-10%) was lower than the typically estimated macromolecular excluded volume for *E. coli* cells grown under standard conditions (~30%) [54, 78]. This means that the observed effect is not caused by exaggerated experimental conditions and pertains to the physiology of osmoregulation. How can this crowding-dependent MscS disengagement be beneficial for bacteria?

Solute-accessible volume of the cytoplasm (reciprocal to macromolecular excluded volume) is a parameter tightly regulated by cells through accumulation or release of small osmolytes. Bacterial MS channels perceive excessive internal pressure in the form of membrane tension which is generated in the cytoplasmic membrane in a curvature-dependent manner according to the law of Laplace ($\Delta p = 2\gamma/r$). The cytoplasmic membrane of *E. coli* is not free but is instead covered by both an elastic peptydoglycan layer (cell wall) [107, 108] and the outer membrane which are stressed under normal turgor pressure of ~ 1-3.5 atm [86] and undergo additional distension under osmotic downshock. We propose that the presence of an elastic cell wall acting as a

‘corset’ stipulates a feedback system that would sense and modify the efflux of small osmolytes depending on the degree of cytoplasmic crowding.

Let us first consider a cell devoid of a cell wall that is initially in osmotic equilibrium with the external medium. On moderate medium dilution, hypoosmotic swelling will dilute internal osmolytes and reduce the osmotic gradient, but stronger swelling and building membrane tension will activate MS channels, which would release part of the internal osmolytes and thus relieve the pressure inside. Once this tension drops to the sub-threshold level, the channels close. As a result, this cell would gain some extra volume after the osmotic down-shock and this sequence cannot result in a return to previous levels of small solute accessible volume (illustrated in Fig. 2.9) unless the conditions suddenly reverse toward higher external osmolarity. Even if mechanosensitive channels remain open after establishing the new equilibrium in a more hypoosmotic medium, this would not result in a cell volume decrease.

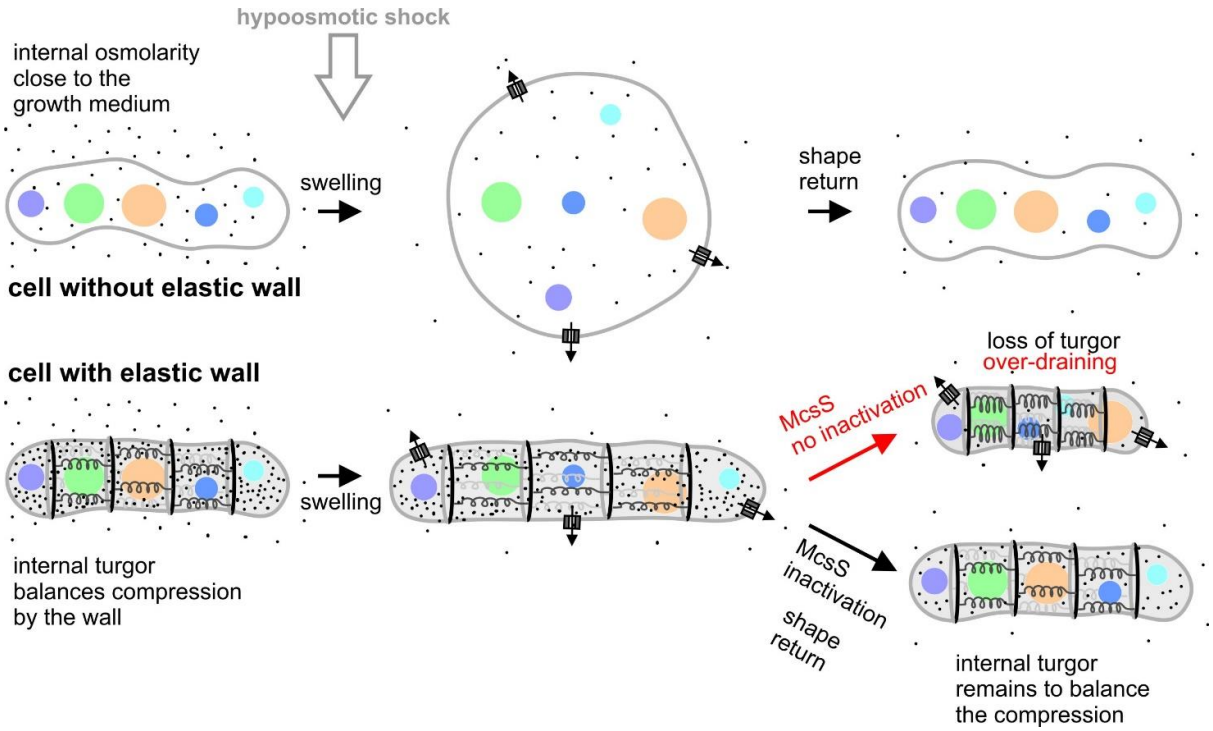

Figure 2.9. A cartoon representation of wall-less and walled cell responses to osmotic downshifts. The wall-less cell (above) behaves like an osmometer with release valves, it swells first and opens osmolyte release channels and partially returns to its initial state which is close to equilibrium with the new more dilute medium. Shrinkage is not expected. The walled cell maintains its volume by generating turgor pressure that counters the restoring force of the elastic cell wall. Swelling and opening of MS channels will release osmolytes and water, but if the channels remain open for too long, the compression may extrude water and shrink the cell beyond its normal volume. Channels that sense the increasing cytoplasmic crowding will inactivate and prevent 'ovedraining' of the cytoplasm.

MscS, which is located almost exclusively to walled cells [109, 110], functions in a different context. Due to metabolite accumulation, bacterial cells typically have relatively high internal hydrostatic (turgor) pressure [86]. This pressure acting on the cytoplasmic membrane from the inside is counteracted by the compressing force from the cell wall and this balance maintains cell volume and shape [111]. Therefore, not only the internal volume but also the fraction occupied by macromolecules is the result of fine balance between the external compression and turgor created primarily by small metabolites. When in special experiments intracellular components were chemically washed away, the sacculus shrunk substantially [108]. A qualitatively similar effect is

expected in the event of osmotic membrane permeabilization. When MS channels are open under osmotic downshock, the release of osmolytes and simultaneous water efflux are greatly assisted by the elastic recoil of the peptidoglycan. A prolonged action of channels in this case can potentially let out more osmolytes than needed resulting in excessive condensation of the cytoplasm. A feedback system that would detect excessive crowding and in a timely fashion disengage the channels will prevent cell shrinkage and cytoplasm 'overdraining'. The behavior of MscS in the presence of crowders described above clearly indicates the presence of such feedback.

Our data show that the crowding-sensing mechanism increases the rate of tension-driven inactivation which involves the hollow cytoplasmic domain (cage). Searches for conformations that satisfy the presence of functionally important D62-R128/R131 salt bridges [96] resulted in a new arrangement of helices in the transmembrane domain, which straightened the G113 crystallographic kink and led to the separation of TM3b segment from the beta-domains in the cage. This conformation characterized by tight interactions between the peripheral (TM1-TM2) helices and the gate region (TM3) was assigned as the resting state, whereas the splayed crystal-like model was considered inactivated. The detachment of the beta domain from TM3b resulted in a slightly more prolate conformation of the cage as compared to the inactivated state with beta domains attached to TM3b (Fig 2.1A and B). Subjected to steered compression in MD simulations (Fig. 2.8), the two conformations exhibited similar compliances in the axial direction, but very different lateral expansions of the transmembrane domain. These suggested that when the closed channel experiences tension and starts switching from the resting to the inactivated state [90], not only does it expands in the plane of the membrane, but also

becomes more receptive to crowding forces acting on the cage. The simulations strongly suggest an allosteric interplay between the geometries of the transmembrane and cytoplasmic domains which makes the bulk parameter of macromolecular pressure inside the cell act synergistically with the interfacial parameter of membrane tension.

How does this coupling occur? Our data suggest that crowding pressure by itself (in the studied range) does not produce inactivation, but moderate tension applied to the peripheral TM helices is required to trigger the transition. Under super-threshold tension and low/no crowding pressure the channel willingly activates. When crowding increases, the resting state is stabilized and the activation threshold increases. However, when this threshold is reached, tension diverts the population into the inactivation path (Fig. 2.2 and S1). We have pinpointed several loci in the channel that change in the course of inactivating transition. The major event is kink formation at G113 [50] which accompanies detachment of the TM1-TM2 pairs from the gate and produces lateral splay, which in turn increases the 'footprint' of the channel inside the membrane [90]. The G113-kinked conformation of TM3s is then critically stabilized by association with the beta domains in the cage. This last step is supported by the effect of the contact-destabilizing mutation G168D (Fig. 2.5), the mutant which barely inactivates and is practically insensitive crowder-induced inactivation. Importantly, G168D MscS does not inactivate with strong depolarizing voltage either (Fig. 2.6), indicating that voltage-driven inactivation [112] [51] proceeds through the same pathway as the crowder-assisted inactivation. According to the inflected traces in Fig. 2.6, it may not be not voltage per se, but more likely ionic current and associated electroosmotic efflux of water [48] that tends to reduce the internal volume of the cage and collapse TM3s, which might be analogous

to the effect of crowders. Previous studies [50, 102] have shown that this buckling of TM3 at G113 (and thus inactivation) can be inhibited via a G113A substitution, which increases the helical propensity at that point. The fact that G113A is more susceptible than G168D to crowder-induced inactivation indicates that the association of TM3 and the beta domain not just a major requirement of inactivation but can impose a kink in TM3 even in the presence of G113A.

In steered simulations under normal force mimicking the effect of crowding pressure we observed a clear difference in the behavior of the modeled resting and inactivated states. In the latter case, the detachment of the TM1-TM2 pairs from TM3s and lateral barrel expansion is reinforced by the normal pressure. Thus, under conditions where both a normal force (crowding) and membrane tension are applied, the inactivated state of the channel is favored.

The effects of mutations stabilizing the TM3b-beta association were more complex. These mutations strongly destabilized the open state even at saturating tensions leading to speedy inactivation in the absence of crowders. The recovery of these mutants from the inactivated state was unexpectedly fast (Fig. 2.7), suggesting that the closed and inactivated states in these mutants are more similar than in the WT and the conformational path is shorter. The modeling predicted that even with the stable G113 kink imposed by stable association with the beta domain the TM1-TM2 loops can salt-bridge to the equatorial arginines (R128 or R131) and the helices themselves can form a buried contact with the gate such that the channel can open, although at tensions higher than normal. The effectively ‘shorter’ pathway between the closed and inactivated states

in these mutants is likely due to absence of the vertical TM3 barrel displacement impeded by the stabilized G113 kinks.

In conclusion, the fraction of cell volume allocated for macromolecules is a parameter tightly regulated by cells through accumulation or release of small osmolytes. We have only begun to understand mechanisms that regulate the crowding-dependent transport of osmolytes across the membrane. In the present work we show that the mechanosensitive channel of small conductance, MscS, the primary turgor-regulating valve in *E. coli* is also one of the sensors of internal crowding. Following the earlier observations by the Kubalski group [57, 63, 95] we have characterized MscS as the first sensor of cytoplasmic crowding and explained its adaptive inactivation mechanism in the context of a small cell encased in an elastic peptidoglycan sacculus. Although not all MscS homologs found in other species inactivate [113, 114], this mechanism has implications for the entire family of MscS-like channels carrying similar cytoplasmic 'cages' which are structurally connected to the gate through the pore-lining helices. This domain, previously considered as a pre-filter [115], was recently shown to impart some ion selectivity to MscS and its homologs. Our data now provides the first conjecture as to why MscS-like channels are ubiquitously distributed in all domains of life characterized by cell walls and a reliance on turgor for the maintenance of their volume, shape and mechanical strength.

Acknowledgement. The work was supported by NIH GM075225 and GM107652 grants to SS. The authors thank Dr. Miriam Boer and Mrs. Abigail Cember for assistance with cloning, mutagenesis and primary characterization of some mutants.

Chapter 3: Partitioning of platensimycin and dialkylamine analogs into the bacterial membrane gauged by the lateral pressure-sensing channel MscS

Ian Rowe[1,2], Min Guo[2], Anthony Yasmann[1], Abigail Cember[1], Herman Sintim[2] and Sergei Sukharev[1,3]

[1]Department of Biology, University of Maryland, College Park, MD 20742 [2]Department of Chemistry and Biochemistry, University of Maryland, College Park, MD 20742 [3]Maryland Biophysics Program

Abstract

Membrane permeability is a desired property of most newly synthesized drugs, but there have been difficulties quantifying direct drug partitioning into native membranes. To assess forces that drive the molecule into and across the membrane, here we compare surface activity, affinity to phospholipid monolayers and partitioning into the inner *E. coli* membrane for three synthetic analogs of platensimycin. Biosynthetic production of this new antibiotic targeting prokaryotic and eukaryotic beta-ketoacyl synthases is costly, driving the development of synthetic analogs, among which dialkylamine compounds were found promising. For three analogs of platensimycin synthesized with identical dihydroxyl benzoate pharmacophores but different sidechains, biological activity varied by more than two orders of magnitude. To test whether the activity of some of them is limited by low membrane permeability, we calculated their polarity, measured surface activity and ability to insert into phospholipid monolayers. We found that affinity to phospholipids for all three compounds directly correlated with the ability to intercalate into the native bacterial membrane gauged by activation curve shifts

of a re-engineered mechanosensitive channel MscS used as a lateral pressure sensor. The highest propensity toward membranes was observed for QD-11, the analog with two myrtenal sidechains, which exhibited the strongest antibacterial effect. Discrepancies between surface activity, monolayer and patch-clamp measurements emphasize different contributions to the total thermodynamic force driving membrane partitioning and permeation for different substances. We discuss the capacity of endogenous tension-activated channels to detect asymmetric partitioning and permeation of exogenous substances into the native bacterial membrane.

Introduction

Permeation through the membrane is the first step in the mechanism of any drug that targets intracellular components or processes. When developing high-affinity pharmacophores, drug designers also try to balance the overall hydrophobicity of the drug that would confer direct permeability through the lipid bilayer without any special transport mechanisms. Generally, hydrophobicity measured as an oil-water or octanol-water partitioning coefficient reasonably correlates with membrane solubility and permeability [116]. While these equilibrium measurements of two-phase partitioning take a long time, reverse phase HPLC on hydrophobic media [117] gives a faster answer but is still only an approximation. An uneven distribution of polar and apolar groups defines amphipathicity of the substance which is manifested as propensity toward interfaces and quantified as surface activity at the air-water interface [118]. This parameter was also found to be a good corollary of the general membrane and blood-brain barrier permeability [119]. Neither an oil-water system nor an air-water interface accurately represent the membrane or properly account for drug-phospholipid interactions. The more recently developed system based on phospholipid -impregnated filters (PAMPA) [120] does mimic membrane composition but the presence of bulk solvent inside the filter does not precisely recreate the bilayer structure. Lipid monolayers previously used to assess affinities of anesthetics [121, 122] represent only half of the membrane with an artificially controlled lateral pressure and area per lipid, both of which are important parameters for partitioning. Direct partitioning into native cellular membranes can be done in a straightforward fashion with either radioactive, spin-labeled or fluorescent compounds, but not with any substance of interest.

Early patch-clamp recordings in giant bacterial spheroplasts indicated that amphipathic substances known to deform erythrocytes (such as chlorpromazine or trinitrophenol) due to unilateral intercalation into the lipid bilayer [123, 124] also change the open probability of bacterial mechanosensitive channels. This observation was initially interpreted as a curvature-inducing effect of amphipaths. Later analysis suggested that, independent of the spontaneous curvature the substances induce, insertion of a new material into one leaflet will lead to a redistribution of tension between the leaflets which may explain the observed changes of channel activity [125]. When MscS, the mechanosensitive channel of small conductance from *E. coli*, was first crystallized [42] the cytoplasmic position of the gate relative to the mid-plane of the membrane suggested a greater sensitivity to tension/lateral pressure in the inner leaflet as opposed to the outer. This notion was fist supported by experiments involving an asymmetric addition of trifluoroethanol [69], which shifted activation curves to the right when presented to the cytoplasmic side and, conversely, to the left when incorporated into the extracellular leaflet. A comparative study of three esters of parabenzoic acid (parabens) indicated that the magnitude of right shift of the MscS activation curve reflected the extra tension needed for opening and closely correlated with the lateral pressure exerted by intercalation of these substances into the Langmuir monolayer formed of bacterial lipids [70]. The transient character of activation curve shifts leading to a return to the original position was interpreted as a time-dependent redistribution of intercalating substances to the opposite leaflet (i.e. permeation) and thus a restoration of lateral pressure symmetry. A subsequent study of autoinducers (AI-1, AI-2, indole) in these two systems confirmed

the ability of MscS to detect lateral pressure changes caused by the permeation of strongly amphipathic quorum signaling molecules across the bacterial membrane [71].

In the present study we further develop this approach. We optimize MscS as a sensor of lateral pressure asymmetry by introducing a mild gain-of-function mutation that increases its sensitivity and then focus on the membrane partitioning of platensimycin and three synthetic analogs. This broad-spectrum antibiotic targets beta-ketoacyl synthases (FabF/B) in many prokaryotes and is active against eukaryotic fatty-acid synthesizing enzymes as well [126-128]. The high cost of its biosynthetic production drives the development of synthetic analogs, among which dialkylamine compounds were found most promising. For three analogs of platensimycin synthesized with identical dihydroxyl benzoate pharmacophores but different sidechains, biological activity varied by more than two orders of magnitude [129]. We hypothesize that the inactivity of some of them might be caused by low membrane permeability. To address this property, we calculated polarity, measured surface activity and determined the ability to insert into phospholipid monolayers and native bacterial membranes for each compound. One specific analog with two myrtenal sidechains stands out in terms of its ability to intercalate into membranes and shows the highest antibacterial activity. However, this correlation does not hold for other compounds, suggesting that not only membrane permeability but other factors define the biological activity of these analogs.

Materials and Methods

Synthesis of Platensimycin analogs

Platensimycin analogs were synthesized following published procedures [129, 130]. Briefly, compound **1** was reacted with excess aldehyde and sodium cyanoborohydride to form ester **2**. The ester group in compound **2** was hydrolyzed into the carboxylic acid **3**, using sodium hydroxide, followed by hydrochloride acid.

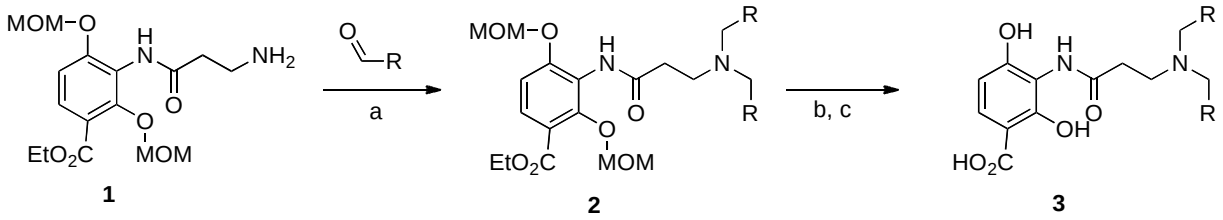

Scheme 3.1. Synthesis of platensimycin analogs. a) Aldehyde (3 equiv), $NaCNBH_3$ (1.5 equiv.), HOAc (3 equiv.), EtOH, rt, 1.5 h; b) NaOH (4 equiv.), EtOH/H_2O (v/v) = 3/1, 40 ^oC, 7 h; c) 6M HCl aq. (20 equiv.), 40 ^oC, 6h.

Computations of polarity and partial charges

Optimized structures, electrostatic potential maps and partial charges were obtained using Gaussian 09 [131] at B3LYP/6-31G(d) level. Solvent effect (water) was taken into account using a polarizable continuum model (PCM). EPIWEB 4.1, ALOGPS 2.1 and molinspiration software were used to calculate the octanol-water partition coefficient (K_{ow}) and polar surface area.

Tensiometry and Langmuir monolayer experiments

Surface tensions of subphase solutions of varying concentrations of platensimycin analogs were quantified using the Wilhelmy method with a piece of filter paper (Whatman, No. 1, 10.5 mm wide and 0.25 mm thick) used as a probe. The subphase

buffer consisted of 150 mM NaCl and 25 mM Tris titrated to a pH of 7.0 with NaOH. The pressure sensor (model 601, NIMA, Coventry, UK) was calibrated using a 100 mg weight. Water surface tension was measured to be −72 mN/m, after calibration. The sensor was hence zeroed, with further surface tension readings giving positive values for surface pressures. The surface activity and values for molecular area at the surface of the air-water interface (As), the partition coefficient at the air-water interface of the surface active molecule (K_{AW}), and the membrane partitioning coefficient (K_{mem}), were determined as described previously [71, 132].

All monolayer experiments were performed in a dust free enclosed bench. All Langmuir measurements were done with a two-barrier rectangular 22 × 6 cm trough (Kibron MicroTrough XS) utilizing a Dyneprobe metal alloy needle as the Wilhelmy plate. Lipids used were *Escherichia coli* total polar lipid extract from Avanti Polar Lipids (Alabaster, AL) dissolved in chloroform or hexane to a final concentration of 0.2 mg/ml. Distribution of lipids onto the subphase was accomplished using a gastight 50 µl Hamilton® syringe. The subphase buffer was identical to the tensiometry buffer. Pressure – area isotherms (monolayers) were performed at room temperature (~ 20 °C) from 100 cm^2 to 20 cm^2 at a barrier rate of 18 cm^2/ min. All concentrations of the analogs were measured at least three times.

Strains, spheroplast preparation and electrophysiology

A pB10b vector was used to house and express the mscS gene in the triple-knockout *E. coli* strain MJF465 (*mscS*$^-$, *mscL*$^-$, *mscK*$^-$). The A98S MscS mutant generated and characterized previously [71] was chosen for its higher sensitivity to inner leaflet drug partitioning.

Spheroplasts were generated as described previously [36, 51, 100]. The experimental bath solution contained 400 mM sucrose, 200 mM KCl, 50 mM $MgCl_2$, 5 mM $CaCl_2$, and 5 mM HEPES and was titrated to pH 7.4 with KOH. Membrane patches were obtained on borosilicate glass pipettes and recorded at 30 mV pipette voltage set by a microelectrode amplifier. The midpoint of activation for channels in each patch was determined at two-minute intervals for the duration of the experiment via a 1 s ramp of saturating pressure. Analogs of platensimycin were pre-diluted in either ethanol or bath solution and perfused into the bath to achieve the desired concentration. Negative pressure (suction) was applied with the HSPC-1 high speed pressure clamp device from ALA Scientific. Programming of the pressure protocols and data analysis were performed with the PClamp10 suite (Axon Instr.). The principle of lateral pressure measurements using two experimental systems, lipid monolayers and patch-clamp, is illustrated in Fig. 3.1.

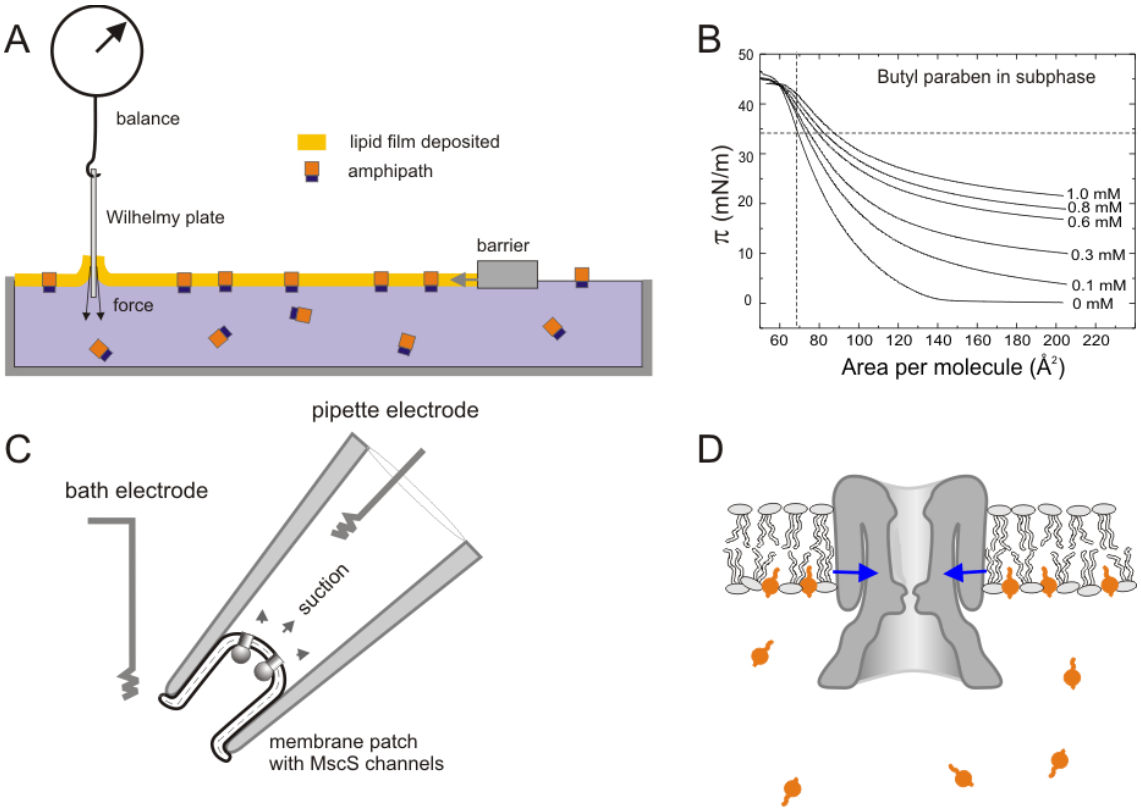

Figure 1. Experimental systems used for studies of lateral pressure perturbations. (A) Langmuir monolayer with amphipathic substance in the subphase. (B) A set of compression isotherms obtained with *E. coli* polar lipids in control and in the presence of varying concentrations of butyl paraben. The upward shift of isotherm signifies additional pressure in the film due to intercalation of paraben. (C) Excised patch configuration for electrical recording of MscS population currents evoked by pressure ramps. Applied negative pressure to the pipette (suction) produces tension in the patch membrane according to the law of Laplace. The intercalating paraben exerts additional lateral pressure in the inner leaflet of the patch membrane and shifts the activation curve to the right (D). Cartoon depicting the intercalation of parabens into the inner leaflet of the bilayer and exerting a lateral pressure on MscS.

Interfacial partitioning data analysis

The analysis of all interfacial adsorption data was performed in the general framework of Gibbs equation

$$d\pi = \sum \Gamma_i d\mu_i$$

where $d\pi$ represents a small change in surface pressure, Γ_i is surface excess of component i and $d\mu_i$ is the small change of chemical potential of that component. For one adsorbing component, the Gibbs isotherm takes the form

$$d\pi = RT\Gamma \ln C$$

where surface excess is defined as the surface density of molecules $\Gamma = 1/(N_A A_S)$, N_A is Avogadro's number and A_S is the area requirement for the molecule at the surface. Generally, Γ is not constant, however, beyond a certain concentration in the bulk, Γ assumes a constant value of Γ_∞ and in that range of concentrations a linear relationship holds:

$$\Gamma_\infty = (1/RT)d\pi / d\ln C$$

To evaluate the partition coefficient for an air-water interface (K_{AW}), the integral form of this equation which was introduced by Szyszkowski and applied in Gerebtzoff et al. [133] was used:

$$\pi = RT\Gamma_\infty \ln(K_{AW}C + 1)$$

As was shown in Suomolainen 2004 [119], the x-intercept of the fitting line of experimental π(lnC) curve would approximate the inverse partitioning coefficient $1/K_{AW}$. The value of the bulk-monolayer (K_{lip}) partitioning coefficient was determined in a similar way, using the deviations of surface pressure of monolayers measured at constant area. Initially, we attempted determining $\Delta\pi$(C) starting from the monolayer-bilayer equivalence pressure of 40 mN/m achieved at 68.5 Å^2/molecule [70]. However, at this compression, strongly intercalating substances produced pressure shifts beyond the collapse pressure of 45 mN/m, which forced us to score $\Delta\pi$ from lower pressures achieved at 72 Å^2/molecule. The bulk-membrane partitioning coefficient (K_{mem}) was estimated from the values of relative increase in MscS activation pressure midpoint ($p_{0.5}$) measured in patch-clamp experiments at different concentrations of intercalating agents.

Results

Optimizing MscS as a lateral pressure sensing device

Previous studies of paraben partitioning into the inner *E. coli* membrane using wild-type MscS as a lateral pressure sensor [70] revealed direct correlations between the shifts of pressure midpoints ($p_{0.5}$) for MscS activation curves measured in patch-clamp experiments and the additional surface pressure created by the same concentrations of substances due to intercalation into lipid monolayers. This suggested that the pressure sensor of the Langmuir apparatus and MscS detect the same parameter of lateral pressure change. In contrast to the Langmuir system, MscS senses not the absolute value of lateral pressure, but rather the difference in pressures between the membrane monolayers (Fig. 3.1). The drawback of the original patch-clamp system employing WT MscS expressed in the MJF465 (*mscS*$^-$, *mscL*$^-$, *mscK*$^-$) *E. coli* strain was that positive shifts of activation curves required application of higher tensions, which destabilized the patches. Another problem was the massive amount of MscS inactivation upon exposure to the concentrations of intercalating agents required to produce large shifts [71].

We explored the A98S gain-of-function mutant of MscS and found it a more suitable sensor. In pressure ramp experiments this mutant activates earlier, but apparently has the same tension dependency of inactivation as WT [102]. Because the two competing processes of opening and inactivation both begin in the resting state (and open channels do not inactivate), at lower tension thresholds opening becomes a preferred path and these mutants generally do not inactivate [134]. The serine-for-alanine substitution hydrophilizes the outer portion of the hydrophobic pore (Fig. 3.2A,B). As a result, this mutant activates at 5.8 mN/m ($p_{1/2}$) versus 7.8 mN/m for WT MscS [134], and shows

reduced inactivation. We tested this mutant against WT with a cytoplasmic addition of 0.6 mM paraben, which has been characterized previously [70]. The typical activation curves (normalized current versus pipette pressure) measured with pipettes of equal size for the two channels are shown in Fig. 3.2C. Not only is the absolute shift of activating pressure ($p_{0.5}$) greater for A98S, but the normalized shift averaged for six independent patches was 41 $\pm$ 6% for the mutant versus 14 $\pm$ 4% for WT. This illustrates the higher sensitivity of the mutant to a given lateral pressure perturbation.

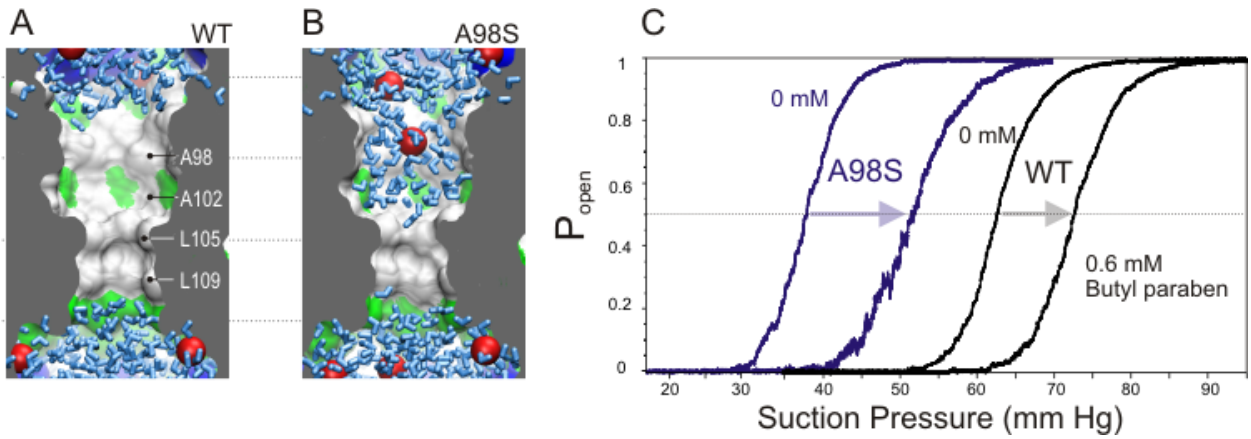

Figure 3.2. The A98S mutation of MscS increases the hydrophilicity of the pore region. The gating of MscS is defined by a dewetting transition from a hydrophobic pore in the closed state (A) to a hydrated, conducting channel. A serine substitution at position 98 pre-hydrates the closed pore of MscS, effectively shrinking and shifting the gate toward the cytoplasmic side of the membrane (B). A patch-clamp experiment showing the activation curve in response to a 1 s ramp of pressure (C) for both WT (black traces) and A98S (purple). Upon exposure to 0.6 mM butyl paraben, the activation curve of both patches shifts to the right, with the greatest change seen for A98S.

The set of three synthetic analogs of platensimycin

All of the platensimycin analogs described herein share the same benzoic acid pharmacophore and ethylene linker, but varied at the side chains. Figure 3.3 presents the structures of platensimycin and three analogs. The amino group in compound **1** (Scheme 3.1) facilitated the easy installation of alkyl and aryl groups of different hydrophobicity via reductive amination. The easy installation of alkyl groups on compound **1** contrasts

with the difficult synthesis of the tetracyclic core in platensimycin, which involved more than 10 synthetic steps and multiple chromatographic separations. QD-06, QL-03 and QD-11 (myrtemycin) were the first generation of platensimycin analogs previously reported [129]. QD-11 contains two bulky myrtenyl rings, QD-06 has two simple linear butyl chains and QL-03 contains only one myrtenyl ring. Partial charge distribution calculations revealed that in platensimycin, polar area constituted 36% of the molecule and that partial charges were largely distributed around the benzoic acid and partially on the oxygen atom of the tetracyclic ring. In QD-06, QD-11 and QL-03, partial charges are mainly on the benzoic acid. QD-06 and QD-11 are both more hydrophobic than platensimycin, with the percentage polar areas of 30% and 25% respectively (compared to 36% for platensimycin). The calculated hydrophobicity of QL-03 (percentage polar area of 34%) is similar to platensimycin. In water, the two side chain groups of QD-06 and QD-11 are predicted to form an open conformer and the aliphatic chains of QD-6 are predicted to be relatively easily solvated. All analogs were prepared, verified by NMR and visualized by Min Guo.

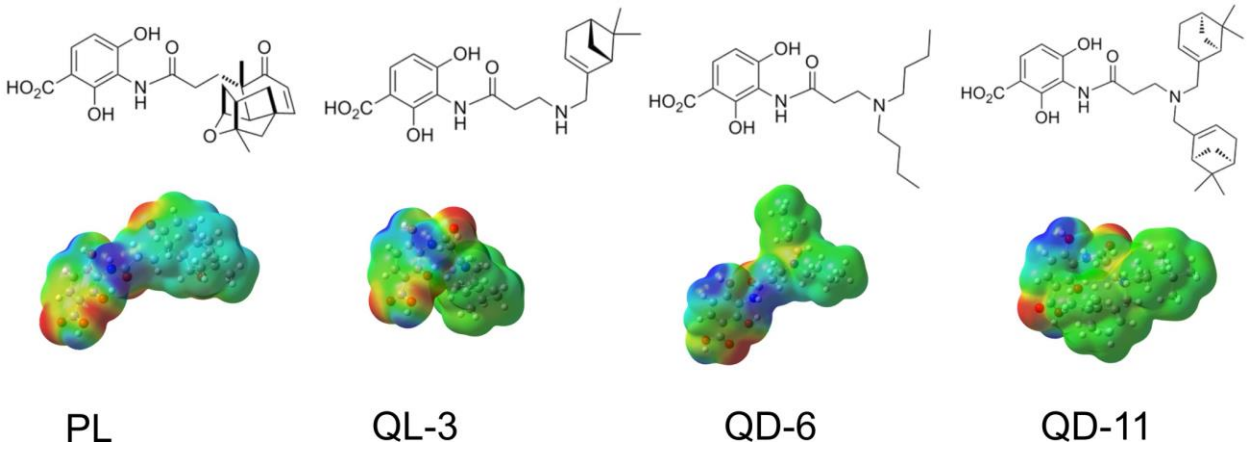

Figure 3.3. The chemical structures and calculated partial charges and the preferred conformations in water for platensimycin and three analogs (Gaussian computations by Min Guo).

1	2	3	4	5	6	7	8	9
Compound	Percent Polar area	ALOGPS $\log K_{OW}$	Molins-piration $\log K_{OW}$	Average $\log K_{OW}$	$\log K_{AW}$ (tensiometry)	$\log K_{lip}$ (monolayer)	$\log K_{mem}$ (patch-clamp)	MIC[a], μg/ml
QD-11	25%	7.44	6.067	6.75	6.09	7.59	6.09	4
QD-06	30%	3.52	3.702	3.61	4.07	5.60	5.54	128
QL-03	34%	3.79	2.852	3.32	4.04	5.95	4.52	>250
PL	36%	3.32	2.844	3.08	4.63	6.49	4.82	2-4

Table 3.1. Calculated and experimentally estimated partitioning parameters for platensimycin and its three analogs, compared with the anti-microbial activity. The first three columns are computational predictions by two programs and their average of the oil-water partitioning coefficient (K_{OW}) based on the exposed polar area of the molecule. The air-water (K_{AW}) partitioning coefficient was obtained from tensiometry. The lipid and membrane partitioning coefficients (K_{lip} and K_{mem}) were obtained from the x-intercepts of lateral pressure versus concentration and midpoint shift ($\Delta p_{1/2}$) versus concentration curves (Fig. 3.4). MIC represents the minimal inhibitory concentration for these substances determined with *Staphylococcus aureus, Streptococcus agalactiae and Bacillus subtillis*.

Tensiometry

The comparison of all data collected using tensiometry at the air-water interface, Langmuir technique and patch-clamp measurements with A98S MscS is summarized Figure 3.4. The resulting estimations of air-water (K_{AW}), lipid monolayer (K_{lip}) and membrane (K_{mem}) partitioning coefficients for platensimycin (PL) and three synthetic analogs are presented in Table 3.1 along with the predicted K_{OW} determined by the *ALOGPS 2.1* and *molinspiration* software. Below we provide some details and illustrations on how these data were obtained.

Tensiometry experiments were straightforward for QD-6, for which a decrease of surface tension was observed only in the sub-millimolar range, producing a linear $\Delta\gamma(\log C)$ dependence and a $\log K_{AW}$ of about 4.0 (Fig. 3.4, top). QL-3 and especially QD-11, containing one and two myrtenal rings, were considerably more surface-active with a $\log K_{AW}$ of 4.04 and 6.09, respectively. At higher concentrations, their Gibbs isotherms visibly rolled off, signifying micelleation/aggregation in water. Platensimycin, the most

hydrophilic substance, produced no visible effect on surface tension up to 30 μM. The tensiometry data generally agree with computed hydrophobicities with the exception of QL-3, which appeared more hydrophobic than predicted.

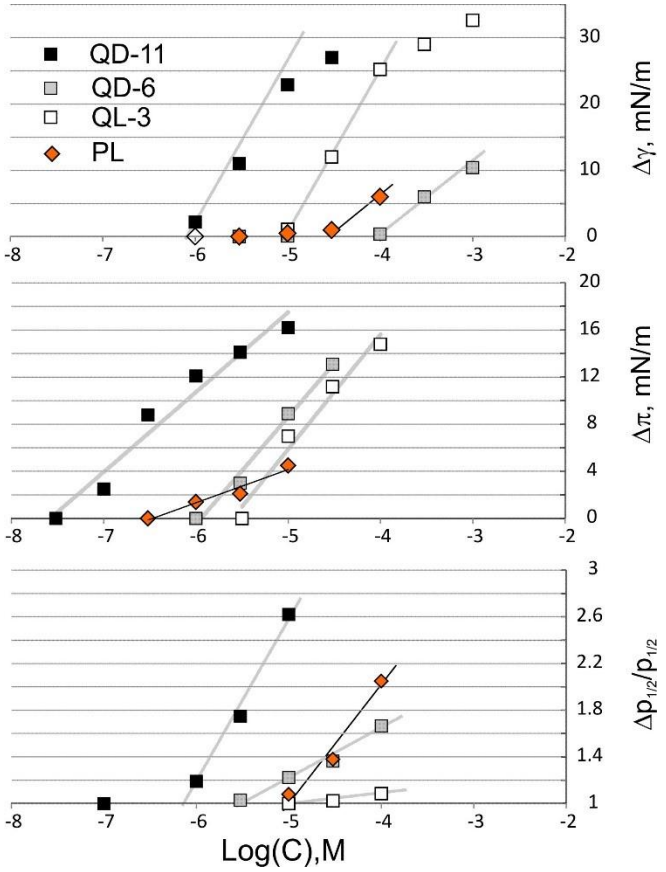

Figure 3.4. Shifts of the MscS activation curve correlate to changes in surface tension and lateral pressure in Langmuir monolayers. The changes in surface tension ($\Delta\gamma$), lateral pressure ($\Delta\pi$), and activation midpoint of MscS ($\Delta p_{1/2}$) are plotted against the logarithm of concentration. The plots on the left represent those obtained from platensimycin (PL), QD-6, QL-3 and QD-11. The straight lines represent fits of linear parts of the curves where x-intercept corresponds to the inverse partitioning coefficient in each system (see Methods).

Langmuir monolayer experiments

The families of isotherms for four compounds (platensimycin, QD-11, QD-6 and QL-3) are shown in Fig. 3.5. The upward-right shifts signify swelling of the film with intercalating substances. Note that the concentrations of substances which produce detectable shifts vary within 2 orders of magnitude. QD-11 characterized with the highest affinity is 'visible' at 10^{-7} M, whereas QD-6 produces appreciable shift only at 10^{-5} M. The fact that the right ends of the curves are elevated relative to control curves indicates that the antibiotics willingly partition into the rarified (expanded) lipid film. However,

with compression, as surface pressure approaches the monolayer-bilayer equivalence region (35-40 mN/m), substantial part of the intercalated substance partitions back to the subphase. At the highest studied concentrations, all substances except for platensimycin remain in the film all the way to the collapse (denoted by arrows), which is 3-7 mN/m above the monolayer-bilayer equivalence pressure. This suggests that these substances have substantially high propensity toward lipids and will be able to make their way (wedge) between the lipids in the native membrane that exists at the same density. This pressure-dependent shift in the monolayer-bulk equilibrium has been reported for other substances [135-137]. All monolayer experiments were performed by Anthony Yasmann.

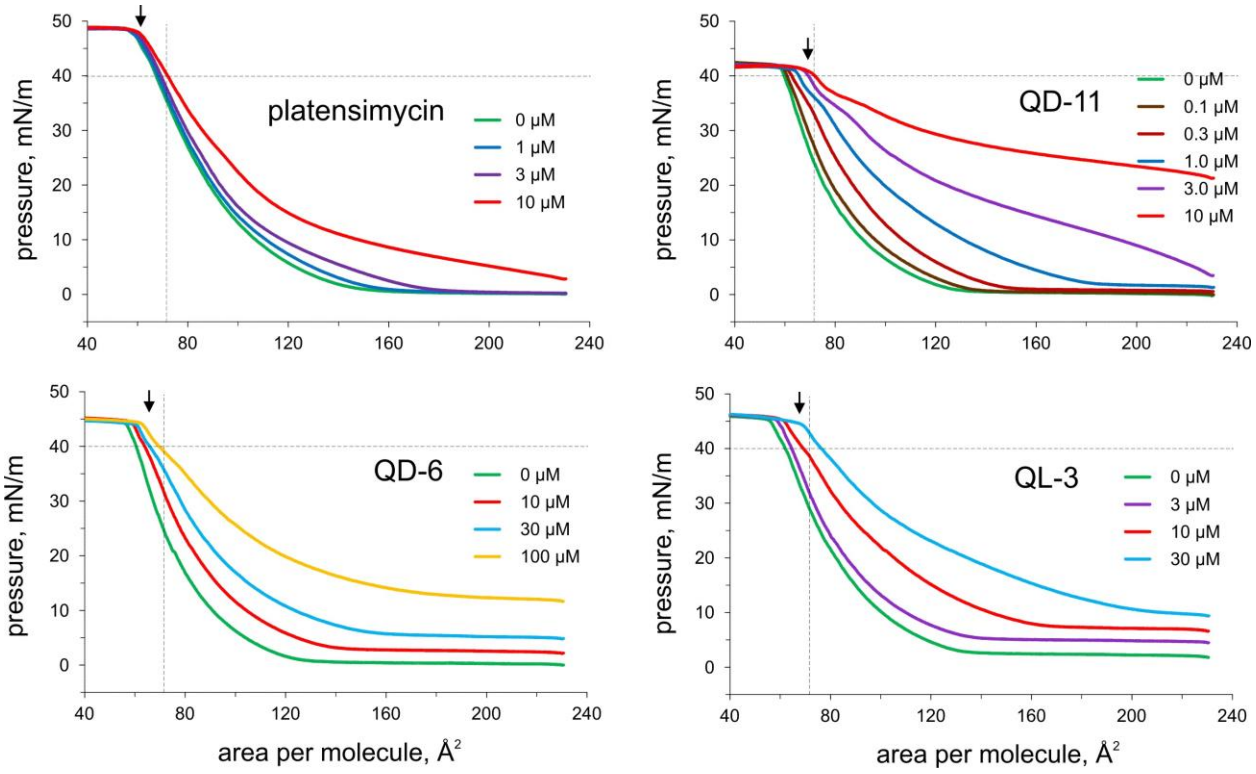

Figure 3.5. Langmuir pressure-area (p-A) isotherms for platensimycin and three analogs. Green curves in all cases are control isotherms taken without intercalating agents. The upward-right shifts of p-A curves with concentration indicate intercalation of the amphipathic substance from the subphase and 'swelling' of the monolayer. The dashed lines denote monolayer-bilayer equivalence pressure (40 mN/m) and the molecular area of 72 Å^2 at which the pressure elevation was scored.

The sections of these families of isotherms taken at 72 $Å^2$ per molecule produced pressure shift-concentration dependences (Fig. 3.4B) which were analyzed using Szyszkowski formalism [133]. The fits produced apparent $\log K_{lip}$ of 5.6 and 6 for QD-6 and QL-3 (Table 3.1). QD-11 was an exception, generating comparable shifts at 10^{-6} M with an estimated $\log K_{lip}$ of 7.59. These values demonstrate that K_{lip} is at least one order of magnitude above K_{AW} values, indicating favorable interactions of platensimycin analogs with lipids in the monolayer as compared with the bare air-water interface. Remarkably, the natural antibiotic was characterized with relatively low propensity toward the monolayer, showing essentially no surface activity in this concentration range.

Patch-clamp investigation of platensimycin insertion and its analogs

The responses of isolated patches containing multiple A98S MscS channels to linear pressure ramps produced sigmoidal activation curves with saturation. The saturating current estimates the population of channels ranging from 100 to 250 in a typical patch. All tested substances shift the position of activation curves to the right. The examples of curve shifts for platensimycin and three analogs are shown in (Fig. 3.6). Platensimycin produces the highest relative shift of the curve at 0.1 mM concentration and, as seen from the level of saturation, causes inactivation of a substantial part of the channel population.

The pressure ramps were applied every 2-5 min and the $p_{1/2}$ shifts were plotted as a function of time. The slightly smoothed time courses of $p_{1/2}$ for four tested substances are shown in Fig. 3.6. With QD-11, each sequential addition (arrows) leads to a rapid right shift with a gradual return toward the initial position with the time course of ~30 min. This relaxation of the initial shift signifies equilibration of the lateral pressure

profile suggesting permeation of the intercalated substance to the other side of the membrane. For QD-11, the process of initial unilateral insertion into the membrane appears to be 5-6 times faster than the process of flipping across the membrane. QD-6 and QL-3 show similar time courses of insertion, but less pronounced relaxation at each addition. Platensimycin and its analog QD-11 show not only faster insertion at the highest bulk concentration (0.1 mM), but also much faster relaxation. This suggests that massive intercalation in one leaflet generates tension in the opposite leaflet, which likely generates a strong large lateral pressure gradient across the membrane thus driving permeation.

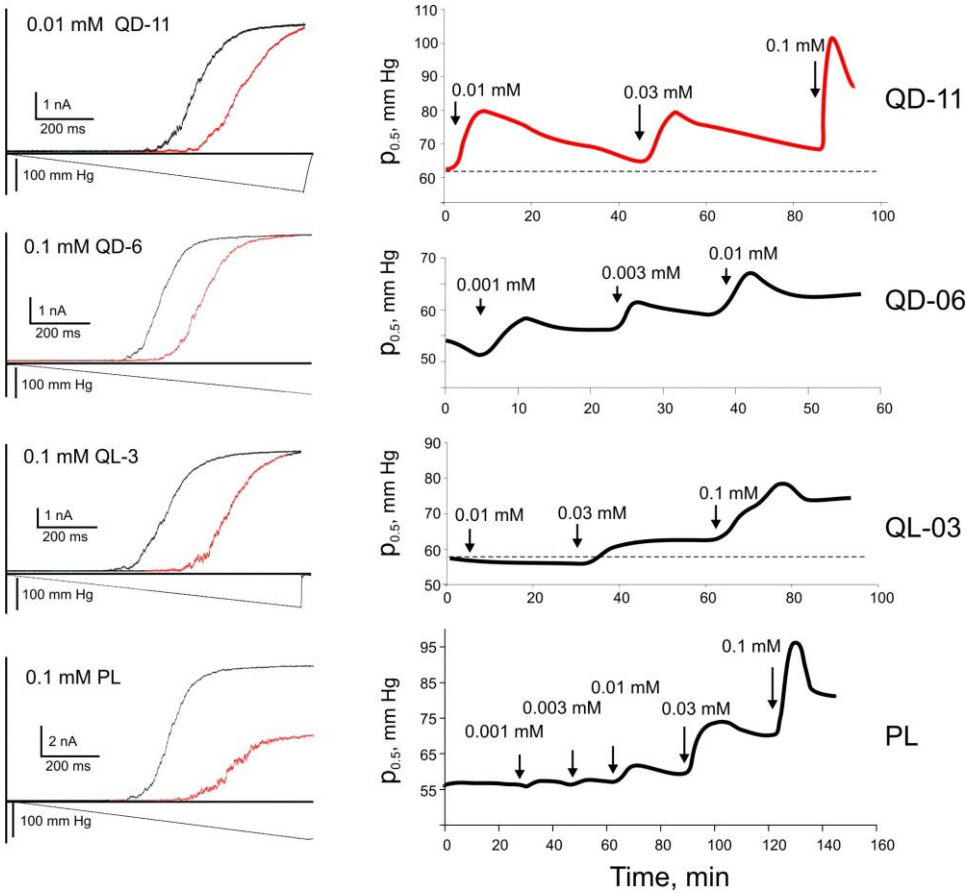

Figure 3.6. Ramp responses of A98S MscS following the addition of platensimycin and its analogs and the time dependencies of the resulting midpoint shift. The shift of the activation curve of A98S MscS toward higher tension after exposure to the denoted compounds is shown (left column). The activation midpoint of the curves ($p_{0.5}$) were then plotted against time (right column). Arrows indicate the point in time at which the given concentration of the compound was added to the bath.

The dose-response curves constructed from cumulative up-shifts of $p_{1/2}$ are shown in Figure 3.4C for all four substances. The intercepts of fitting lines produce $\log K_{mem}$ between 4.5 and 6, with the highest affinity for QD-11. The patch-clamp data ($\log K_{mem}$) is consistent with the monolayer data ($\log K_{lip}$) for the analogs, with the exception of QD-11, for which the indicated $\log K_{lip}$ was considerably higher. One possible explanation is that the bulky myrtenyl groups probably anchor the molecules during monolayer compression and thus preventing easy exchange and equilibration.

The last column in Table 3.1 presents minimal inhibitory concentrations (MIC) for all of these substances assayed with several gram-positive and gram-negative bacteria [129]. Remarkably, platensimycin which is the most biologically active compound, resides in the middle of the hydrophobicity range and shows one of the lowest K_{mem} among its analogs. The second most active compound is QD-11, which is shows the highest surface activity, propensity to phospholipids and affinity for the native bacterial membrane. As illustrated by the data in Table 3.1, the absence of a direct correlation between the ability to partition into the membrane and biological activity for this set of platensimycin-like compounds with identical pharmacophores indicates that our initial hypothesis of the defining role of membrane permeability was too simplistic and other factors need to be taken into account.

Discussion

A successfully engineered drug or synthetic analog of a natural, biologically active compound must satisfy many other criteria besides its required affinity to the target molecule. If the target is inside the cell, then the drug must be sufficiently permeable

through the cell envelope. Small hydrophilic molecules may be taken up via poorly specific nutrient transport systems. However, a more reliable strategy is to make substances moderately lipophilic or amphipathic such that they would still be sufficiently water-soluble and at the same time directly permeable through the lipid bilayer. Permeability should be high enough to overwhelm endogenous efflux pumps (MDR proteins) which many malignant cells or pathogenic microorganisms possess or acquire. If the drug is too hydrophilic, it may not go through the membrane and be simply excluded from the cell. Conversely, if the drug is too lipophilic, it will be insoluble and hard to deliver. And even if the delivery scheme works well, the substance may start accumulating in the membranes or be sequestered in other lipid reservoirs. Therefore, inactivity of some engineered drugs with perfectly computed pharmacophores may be due to one of these problems posed by 'non-specific' interactions with membranes. For this reason, development of methods that could trace substances of interest directly in the membranes of their target organisms is a timely task. These methods may help tuning the balance between hydrophobic and hydrophilic properties of a new drug, and find proper distribution of polar and apolar groups for optimal solubility and membrane partitioning.

Mechanosensitive channel MscS, naturally embedded in the cytoplasmic membrane of *E. coli* (with homologs in most known bacteria), readily detects partitioning of amphipathic drugs in the cytoplasmic leaflet of the membrane. The mild gain-of-function mutant A98S used in this work is a more sensitive sensor of lateral pressure asymmetry than WT MscS, activates at lower tension and exhibits a larger fractional shift of $p_{0.5}$ upon asymmetric intercalation of a well characterized test substance butyl paraben (Fig. 3.2). This technique provides a comparable, but somewhat lower estimation of drug

affinity to the native bacterial membrane compared to the Langmuir monolayer technique. By no means can this application of the patch-clamp technique be considered a 'high-throughput' approach since the patches are less stable in the presence of amphipaths, and a skilled patch-clamper may collect one or two complete datasets (Fig. 3.6) on a good day. Yet, the technique can play its role in the 'diagnostics' of why a promising drug that displays a high affinity to its target in the test tube becomes inactive in *in vivo* experiments.

As illustrated in a cartoon style in Fig. 3.1, the channel detects the difference in pressures/tensions between the leaflets, but not the absolute value of lateral pressure. The channel gate is approximately at the level of phosphates of the inner phospholipid leaflet of the membrane and the additional lateral pressure created by the substance intercalating in that leaflet (relative to the pressure in the extracellular leaflet) requires extra tension to activate the channel. As the concentration of intercalating substance is increased, $p_{0.5}$ progressively increases. We presume that the intercept of the $\Delta p_{0.5}$ curves with the concentration axis reasonably approximates $1/K_{mem}$, but we cannot interpret the slope of the curve the same way we interpret the slope of Gibbs isotherms as molecular area [132] (Methods). On one hand, this can be considered a drawback which precludes quantitative thermodynamic analysis; however it is this 'differentiating' property that permits the detection of the redistribution of the intercalating substance between the two leaflets, i.e. the process of permeation. The 'flipping' across the bilayer results in an equilibration of pressure profiles on both sides of the membrane and this is read by the system as midpoint relaxation back to its initial value. The kinetics of permeation appear to be

slower than the process of initial unilateral incorporation, and the exact time course of permeation is characteristic of each individual substance.

In the present work we have characterized platensimycin and its three synthetic analogs in terms of partitioning to the air-water interface, a phospholipid monolayer of *E. coli* lipids and the native *E. coli* membrane. The simple ranking by the percent polar surface area emphasizes the higher hydrophobicity of QD-11 but does not make a large distinction between the three other substances (Table 3.1, column 2). The separation of polar and apolar areas as well as curvatures of solvated regions are taken into account in the algorithms used in *EPIWEB 4.0, ALOGPS 2.1* and *Molinspiration* software (columns 3 and 4). The data summarized in Figure 3.4 and Table 3.1 shows that all three experimental techniques give comparable but consistently different partitioning coefficients in the three systems. These differences emphasize the different components of the thermodynamic force driving the substances out of the aqueous phase and into the membrane: hydrophobicity, ampipathicity (dictating propensity toward the interface as opposed to continuous bulk phase) and favorable interactions with the phospholipids. Estimations of oil-water partitioning ($\log K_{ow}$), from algorithm-based hydrophobicity computations surprisingly give a reasonable estimation for QD-11, the most hydrophobic substance, but are not accurate predictors of surface activity and membrane partitioning for less hydrophobic substances.

Estimations of $\log K_{AW}$ based on tensiometry measurements also underestimate compound partitioning into the membrane because they primarily take into account the hydrophobic effect (expulsion from water). Monolayer partition coefficients (K_{lip}) are consistently higher by 1-1.5 orders of magnitude than air-water partition coefficients

(K_{AW}), indicating that favorable interactions with lipids contribute to the affinity, contrasting the monolayer environment from the bare air-water interface (see discussion of this subject in Seelig and Suomolainen [119, 136]).

If we consider experimental $\log K_{mem}$ measured in patch-clamp as a parameter reflecting all physical factors driving drugs into the membrane (hydrophobicity, favorable interactions with lipids and the necessity to overcome lateral pressure of lipids [136, 138]), we would say that lipid monolayers would be an adequate system to study drug partitioning since it gives almost identical data for most of the substances in a wide range of hydrophobicities. The discrepancy, however, is obvious for the two myrtenal compounds QL-03 and QD-11, for which the monolayer technique overestimates the partitioning. First of all, bulkier myrtenal groups are expected to be solvated by water less favorably than thin aliphatic chains [139]. The reason for stronger retention in the monolayer of these two substances is the presence of unusual bulky ball-like hydrophobic groups that can strongly anchor the molecules in the monolayer, thus preventing fast exchange. Indeed, we can use the assumption that a monolayer (representing half of the membrane at the equivalence pressure) has the same interface with the bulk water as a complete bilayer, however, when we consider partitioning, we should remember that in these two systems we approach the same equilibrium from two different sides. In the monolayer, which in its expanded state harbors many more amphipathic molecules, we observe expulsion of these molecules with compression. In the native membrane, we expect a wedging of the intercalating molecules between lipids which are naturally pre-compressed to their normal density. It is possible that reaching true equilibrium in a compressed monolayer experiment with these compounds may require longer times since

the bulky myrtenal groups which easily partition into the expanded lipid monolayer may resist expulsion upon compression. Also, due to the large cross-sectional area of the myrtenal groups, it is more difficult for these compounds to intercalate into the bilayer in patch-clamp experiments, making the effective $\log K_{mem}$ lower than $\log K_{lip}$. Another important factor might be coupling between the two leaflets in the complete bilayer, in which substance intercalation on one leaflet should also produce work of expansion of the opposite leaflet since the two are coupled through the common midplane. Effectively, lateral compressibility of the monolayer might be higher, which would harbor grafted amphipathic molecules more easily.

In conclusion, the development of a patch-clamp based technique of estimating the partitioning of extrinsic amphipathic substances into the cytoplasmic membrane of *Escherichia coli* using mechanosensitive channel MscS as a natural sensor of lateral pressure opened new possibilities for characterizing membranotropic properties of natural or newly synthesized compounds. The comparison of partitioning coefficients for a particular set of substances obtained in different systems emphasizes not only the differences of the systems but different components of thermodynamic forces driving the substances into and across the membranes.

Chapter 4: The mechano-electrical response of the cytoplasmic membrane of *Vibrio cholerae*

[1,2]Ian Rowe, [1,3]Merina Elahi, [3]Anwar Huq and [1,4]Sergei Sukharev

[1]Department of Biology, [2]Department of Chemistry and Biochemistry, [3]Maryland Pathogen Institute, Department of Cell Biology and Molecular Genetics, [4]Maryland Biophysics Program, University of Maryland, College Park, MD 20742

Abstract

Persistence of *Vibrio cholerae* in waters of fluctuating salinity relies on the capacity of this facultative enteric pathogen to adapt to varying osmotic conditions. In an event of osmotic downshift, osmolytes accumulated inside the bacterium can be quickly released through tension-activated channels. With the newly established procedure of giant spheroplast preparation from *V. cholerae*, we performed the first patch-clamp characterization of its cytoplasmic membrane and compared tension-activated currents with those in *Esherichia coli*. Saturating pressure ramps revealed two waves of activation belonging to the small-conductance (~1 nS) MscS-like channels and the large-conductance (~3 nS) MscL-like channels, with a pressure midpoint ratio $p_{0.5}$MscS/$p_{0.5}$MscL of 0.48. We found MscL-like channels in *V. cholerae* present at a density three times higher than in *E. coli*, and yet, these vibrios were less tolerant to large osmotic downshocks. The *Vibrio* MscS-like channels exhibit characteristic inward rectification and subconductive states at depolarizing voltages; they also adapt and inactivate at sub-saturating tensions and recover within 2 s upon tension release, just like

E. coli MscS. Trehalose, a compatible internal osmolyte accumulated under hypertonic conditions, significantly shifts activation curves of both MscL- and MscS-like channels toward higher tensions, yet does not freely partition into the channel pore. Direct electrophysiology of *V. cholerae* offers new avenues for the *in situ* analysis of membrane components critical for osmotic survival and electrogenic transport in this pathogen.

INTRODUCTION

Strong osmotic forces constantly affect all microorganisms, probably with only a few exceptions of obligatory symbionts or parasites. A cell 2 μm in diameter, surrounded by a single unarmored membrane, would burst with only a 20 mOsM inside vs. outside osmotic gradient. At the same time, most gram-negative bacteria survive 600-1000 mOsm downshocks with uncompromised viability [34, 83, 84, 140]. The early perception was that bacteria can tolerate high internal pressure because they are surrounded by a rigid cell wall, but the peptidoglycan network was shown to be stretchable [107], and the more common opinion now is that the bacterium survives mostly because of its ability to rapidly dissipate excess osmolytes through a special emergency release system [36, 38] . This system consists of several types of mechanosensitive channels activated at different tension thresholds [87, 115, 141], with MscS and MscL mediating the bulk of osmolyte release. The success of the rescuing operation depends on one simple condition: the release of excess osmolytes must outpace the rate at which the lytic level of hydrostatic pressure inside the cell is reached. It is not surprising that expression of mechanosensitive channels is under the control of transcription factors regulating stress responses [142], especially responses to cell wall damage. It is now obvious that bacterial

mechanosensitive channels are capable of quickly dissipating ionic gradients [91] but their permeabilities to organic compatible osmolytes have not been studied. Functional properties of such channels are under intense scrutiny through the application of direct electrical recording [36], reconstitution [37], structural [41, 143] and computational [48, 144] techniques, but limited primarily to *E. coli*.

Facultative pathogens which spend part of their life as free-living forms face the same problem of osmotic adaptation. *Vibrio cholerae* populates an extremely broad range of aquatic environments, from rain water to deep sea water of high salinity [145-147] and estuarial zones, where the salinity and osmotic pressure can broadly fluctuate. Pathogenic strains of *V. cholerae* are transmitted predominantly through fresh water, in which it is typically dropped from the intestines [148]. The fact that microorganisms survive these abrupt changes in osmolarity implies a very efficient osmoregulation system [149, 150] which enhances environmental stability and transmission from one host to another. Extension of the electrophysiological platform to *Vibrio cholerae* may uncover new aspects of its osmoregulation system that are critical for osmotic survival. Previously, biophysical properties of the outer membrane channels (porins) from *V. cholerae* were studied in reconstituted systems [151-153] with the emphasis on adaptation to the intestinal environment. The membrane aspects of *V. cholerae* osmotic survival in fresh water have not been studied in direct electrophysiological experiments before.

In this work we adapted the giant spheroplast preparation technique to *Vibrio cholerae,* previously developed for *E. coli,* and completed the first patch-clamp survey of its cytoplasmic membrane. We found two dominant channel activities similar to MscS and MscL in *E. coli*. Despite a higher overall density of mechanosensitive (MS) channels,

V. cholerae exhibits lower tolerance to large osmotic shocks. We present the first comparison of channel activities between the two enteric species, emphasizing differences which suggest parameters that may define environmental fitness of these bacteria.

MATERIALS and METHODS

Strains, spheroplast preparation and electrophysiology.

Wild-type (WT) *V. cholerae* (N16691) from Dr. Anwar Huq's laboratory (UMD) and WT *E. coli* strain AW405, a gift from J. Adler (University of Wisconsin), were used in the study. The original procedure of giant spheroplast preparation from *E. coli* [35, 36] includes a 1.5-2 hr incubation in the presence of 0.06 mg/ml cephalexin, during which bacteria produce long filamentous cells. The filaments are resuspended in 1 M sucrose buffer and subjected to lysozyme digestion (0.2 mg/ml) in the presence of 5 mM EDTA. Within 5-10 min of lysozyme treatment, filaments collapse into spheres 3-6 μm in diameter, at which point the reaction is stopped with excess Mg^{2+}. Spheroplasts are separated from the rest of the reaction and debris using quick sedimentation through a 1-step sucrose gradient. Spheroplasts were stored in a high-sucrose/BSA medium at -80ºC. This procedure was used to make AW405 *E. coli* spheroplasts and was applied to N16961 *V. cholerae* with adaptations as described in Results.

Borosilicate glass (Drummond, cat# 2-000-100) was empirically shown to be suitable for tight seal formation with bacterial membranes. Channel activities in giant spheroplasts were recorded from excised membrane patches at voltages between -80 mV and 80 mV. Negative pressures (suction) were applied to patches with a high-speed

pressure-clamp apparatus (HSPC-1, ALA Scientific Instruments). Pressure protocol programming, data acquisition and analysis were performed using PClamp 10 software. Ensemble and single-channel currents were analyzed after Rs-correction of the traces by the equation, $G_P = I/(V - IR_S)$, where G_P is the patch conductance and V and I are the transmembrane voltage and current, respectively. The series pipette resistance ($R_S \approx 2.5$-3 MΩ) was determined in each experiment after the patch broke.

To analyze the effect of trehalose on single-channel conductance, we used the macroscopic equation accounting for the pore (R_p) and access (R_s) resistances separately: $R_{ch} = R_p + R_s = (l + 0.5\pi a)\rho/\pi a^2$, where l and a are the length and radius of the pore [154, 155]. Specific resistances (ρ) of recording buffers with and without trehalose were measured using CDM230 conductivity meter (Radiometer, Copenhagen).

The midpoint of activation was determined with 1-s saturating pressure ramp protocols and the change in midpoint was monitored before and after the addition of trehalose to the bath. A combination of ramps of varying duration was used to visualize single-channel events in order to determine the current passing through a single channel. Inactivation of the MscS-like channel was examined with protocols which compared the number of channels available both before and after the patch was held under a subsaturating tension for 10-s. Specific protocols are explained in figure legends.

Osmotic survival experiment

After observing large tension-activated conductances and anticipating corresponding osmotic permeability responses, we compared osmotic shock survival for *V. cholerae* and *E. coli*, in parallel side-by-side experiments. Both species grow well in

LB+3% NaCl (HiLB, 1180 mOsM). Fresh overnight cultures were diluted 1:100 in this medium and pre-grown for 2 hrs to OD600 of ~0.4. The high-osmolarity adapted cultures (50 μl aliquots) were then abruptly shocked into 5 ml of diluted media (LB, LB/2, LB/4, LB/8, LB/16 and distilled water). After 15 min incubation and quick 1:200 dilution in the medium it was shocked, each culture was plated in duplicates and the colonies were counted the next morning. Osmolarities of media were measured using a Wescor 5520 vapor pressure osmometer (Logan, UT). All osmotic shock experiments were performed by Merina Elahi.

RESULTS

Vibrio spheroplast preparation.

The original procedure of giant spheroplast preparation from *E. coli* [35] was adapted by Martinac and coworkers [36] for patch-clamp; it includes a 1.5-2 hr incubation in the presence of 0.06 mg/ml of the septation blocker cephalexin, during which bacteria grow but do not divide, producing filamentous cells. Our results show that *V. cholerae* is susceptible to both cephalexin and lysozyme. Filamentous forms grew in LB broth in the presence of 0.1 mg/ml of cephalexin at the approximate rate of ~100 μm/hr. Filaments 80-150 μm long remained stable after sedimentation at 2000 g and gentle pipetting. The concentration of lysozyme (0.4 mg/mL) and EDTA (25 mM) required for spheroplast formation in *V. cholerae* was twice what was needed for analogous *E. coli* preparations and on average took 20-30 min, which is also double the requirement of *E. coli*. Spheroplasts were separated from the debris by centrifugation through 1 M sucrose. Fig. 4.1 illustrates relative sizes of intact bacteria, filamentous

forms and giant spheroplasts. Spheroplasts often had a slightly irregular non-spherical shape, signifying remnants of undigested peptidoglycan.

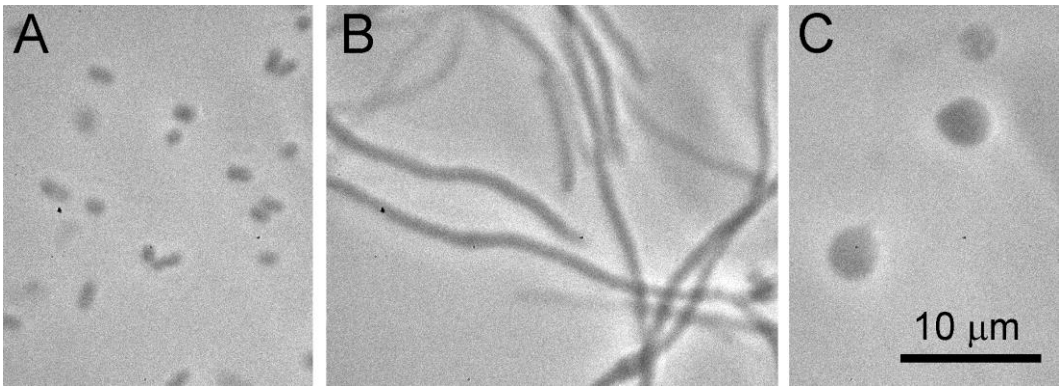

Figure 4.1. Phase contrast images of the intact *V. cholerae* cells (A), cephalexin-induced filaments (B) and giant spheroplasts after 20 min incubation with EDTA and lysozyme (C).

Mechanoelectrical responses of the inner membrane to pressure ramps.

Under sustained 20-40 mm Hg suction delivered from the pressure clamp apparatus, *V. cholerae* spheroplasts formed tight seals with borosilicate glass pipettes typically within 2-15 min. As with *E. coli*, patch excision was achieved by tapping on the base of the micromanipulator. Inside-out patches stimulated by triangular ramps of saturating pressure under a 30 mV hyperpolarizing voltage exhibited 2-7 nA currents in both types of preparations, which invariably displayed two-wave responses (Fig. 4.2A). In *E. coli*, the first wave was ascribed to the MscS population, possibly with a mixture of a few MscK channels [88] and the second, activating at higher tensions, represents a uniform MscL population. In *V. cholerae* we observed very similar two-wave responses, usually with a lesser relative amplitude of the first wave. Relative amplitudes of the two waves were essentially independent on the speed of the pressure ramp. To avoid voltage clamp errors due to pipette series resistance (Rs) under high (>2 nA) currents, Rs-

correction was introduced (see Methods). The corrected traces provided fractions of the total conductance ascribed to each type of channels and pressure mid-points for activation. The ramp responses clearly show that in both enteric bacteria, MscL is the dominant conductance responsible for the bulk of tension-activated permeability increase. MscS-like channels in *Vibrio* represent considerably smaller fraction of conductance compared to MscS of *E. coli*; also they show no activation hysteresis (difference in midpoints on the ascending and descending legs of the triangular ramp), while half of *E. coli* MscS de-activate at a considerably lower pressure compared to the activation midpoint, producing an asymmetrical ramp response (Fig. 4.2B).

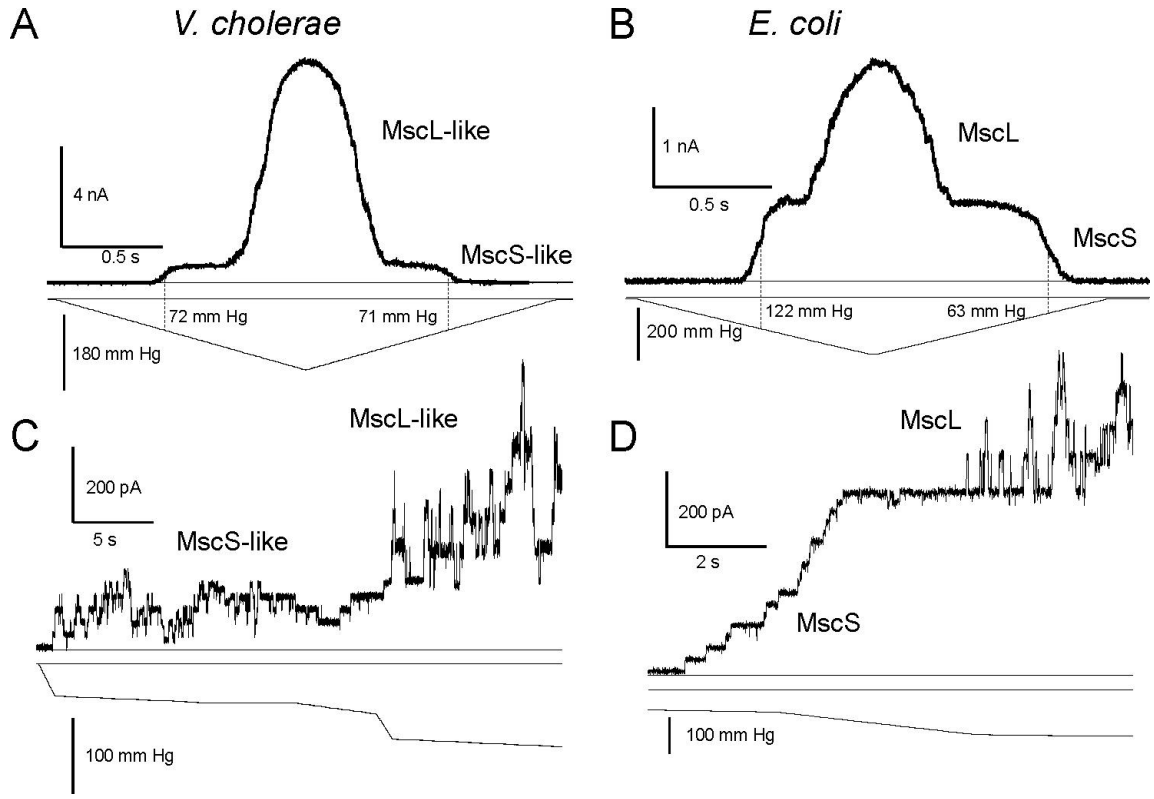

Figure 4.2. Mechano-electrical responses of *Vibrio cholerae* and *Escherichia coli* membrane to ramps of pressure. (Top) Typical response of an excised inside-out patch to a 1-s saturating triangular ramp in *V. cholerae* (A) and *E. coli* (B). Responses of the same patches to a slow non-saturating ramp protocol designed to reveal single-channel conductances for *V. cholerae* (C) and *E. coli* (D).

In order to determine unitary conductances, we applied sequences of slower ramps to visualize single-channel events (Fig. 4.2 C, D). From multiple traces taken at different voltages, we created I-V plots and determined slope conductances at hyperpolarizing voltages (pipette positive) for single MscS-like (1.0 ± 0.1 nS) and MscL-like channels (2.6 ± 0.1 nS, or 2.9 nS after Rs-correction) of *V. cholerae* (Fig. 4.3). This information permitted us to quantify the numbers and densities of channels in each preparation. Based on the previous results that the pressure midpoints for *E. coli* MscL correspond to ~12 mN/m tension [103, 105], we estimated the radius of curvature and area for each *E. coli* patch using the law of Laplace. Since we used the same 2.5-3 MOhm pipettes throughout this project, we first assumed that the average geometry of patches in both preparations was the same. The second assumption was that the tension midpoints for *E. coli* MscL and *V. cholerae* MscL-like channel are the same[156]. Using these two different assumptions we estimated patch areas and densities of channels in each preparation. The first assumption (Table 4.1, columns 4,5) gave a 20% lower estimation of channel density in *V. cholerae* relative to the second assumption (columns 8, 9) due to a slight difference in estimated mean patch radius (1.37 versus 1.50 μm).

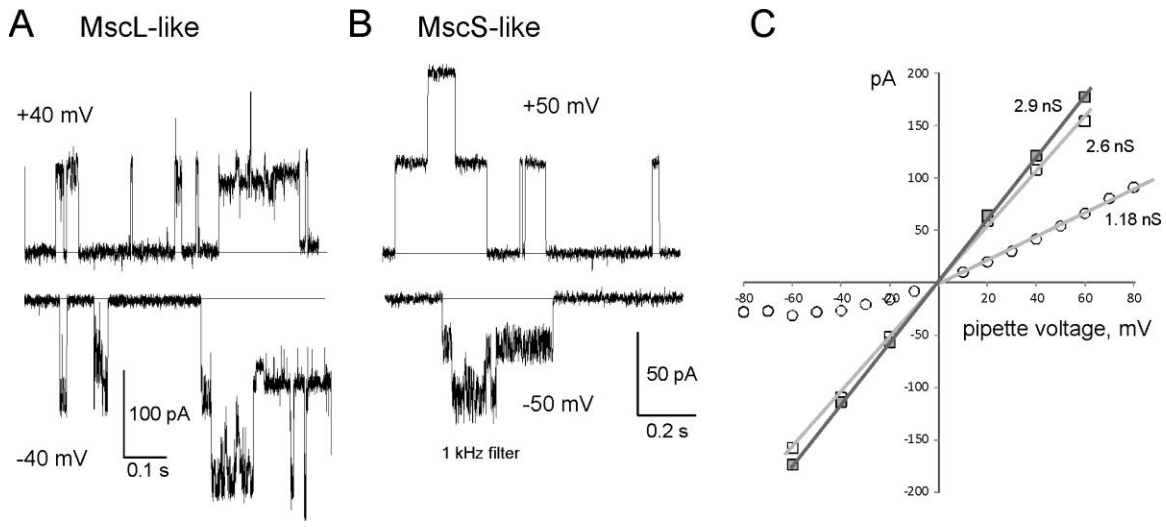

Figure 4.3. Current-to-voltage relationships for the two dominant channel conductances in *V. cholerae*. (A, B) Examples of single-channel currents at opposite voltages for both the MscL- and MscS-like channels. Note fast-flickering sub-conductance levels in MscS at negative pipette potentials. (C) Current-to-voltage plot of MscL-like (squares) and MscS-like channels (circles). Filled squares represent the Rs-corrected curve for MscL. MscS shows obvious inward rectification.

The comparison of the ensemble currents in multiple patches (Fig. 4.2) reveals modest but statistically significant differences in activation midpoint ratios and substantial differences between channel numbers and densities in the membranes of *E. coli* and *V. cholerae* (Table 4.1). In *E. coli* (AW405), MscS and MscL are present on average at 3.6 and 4.3 channels/μm2, with a ratio of midpoint pressures of 0.60 ($p_{0.5}$MscS/$p_{0.5}$MscL). The MscS-like and MscL-like channels occur in *V. cholerae* (N16961) at densities of 1.2 and 11 channels/μm^2, respectively, with a midpoint ratio of 0.48. Based on the data in Fig. 4.2 and Table 4.1, MscL-like channels are present at a 2.5x higher density and MscS-like channels are present at third the density in *V. cholerae* compared to *E. coli.* These differences in channels densities, confirmed in three independent batches of spheroplasts, prompted us to compare resistances of the two strains against acute osmotic down-shock. The inference was that the higher overall density of channels in *V. cholerae* should correlate with higher osmotic survival.

	1	2	3	4	5	6	7	8	9
	#MscS per patch	#MscL per patch	$p0.5_{MscS}$/ $p0.5_{MscL}$	MscS/μm² (r=1.5μm)	MscL/μm² (r=1.5μm)	Patch r, μm (γ0.5 = 12 mN/m)	Patch Area, μm²	MscS/μm²	MscL/μm²
E coli	46 ± 14	61 ± 40	0.60 ± 0.05	3.6 ± 1.8	4.3 ± 2.2	1.5 ± 0.3	14.7 ± 5	3.6 ± 1.8	4.3 ± 2.2
V cholerae	17 ± 9	164 ± 100	0.48 ±0.04	1.2 ± 0.7	11 ± 4	1.37 ± 0.3	12.4 ± 6.3	1.5 ± 0.8	14 ± 5

Table 4.1. Experimental occurrences of MscS-like and MscL-like channels in patches of wild-type *E. coli* and *V. cholerae.* Multiple traces, as shown in Fig. 4.2, were Rs-corrected and numbers of MscS-like and MscL-like channels as well as midpoint pressures for each population were determined. The pressure midpoint ($p_{0.5}$) for Eco MscL was equated to membrane tension $\gamma_{0.5}$ = 12 mN/m acting on channels, from where the radii of patch curvature and areas were calculated according to the law of Laplace ($\gamma=\Delta pr/2$). The densities (channels/μm²) were then deduced for MscS- and MscL-like channels individually, first on the assumption that the average patch radius for *V. cholerae* preparations is the same as for *E. coli* (columns 4 and 5), and independently with the assumption that MscLs in both preparations gate with the same midpoint $\gamma_{0.5}$ = 12 mN/m (columns 6 through 9). Data are presented as mean ± std (n=12 for *E. coli* and n=19 for *V. cholerae*). The midpoint ratios $p0.5_{MscS}/p0.5_{MscL}$ for the two species (column 3) are significantly different at a 0.006 level according to two-tailed unequal variance t-test.

Osmotic survival of Vibrio cholerae

Survival rates of estuarial/enteric *V. cholerae* were compared to that of primarily enteric *E. coli* in parallel osmotic dilution-and-plating experiments. Both cultures were pre-adapted in high-osmotic LB medium (LB base with 0.52 M NaCl, 1180 mOsM) where they grew for 2 hrs to OD_{600}~0.5. The cultures were then abruptly diluted 1:100 into media of different osmolarity (1180, 425, 212, 106, 70, 48 mOsM and distilled water). As seen from Fig. 4.4, both cultures easily survived a 970 mOsM downshift, after which the number of colonies for *V. cholerae* decreased. *E. coli* remained completely viable after ~1100 mOsM drop, but beyond that point its survival precipitously declined as well. Remarkably, between the final osmolarity of 48 mOsM (LB/16) and distilled water there was almost no difference in the survival rates, ~2-4% *E. coli* and ~0.3-0.1% *V. cholerae.* Although osmotic shock tolerance is comparable in the two enteric species, *V. cholerae* is clearly more sensitive despite the fact, that it had the overall higher density of MS channels. We hypothesize that this higher density of MS channels may be a

compensation for some other vulnerable traits of *Vibrio*, such as cell geometry, elasticity of the cell wall or limited permeability of channels to specific osmolytes. The possible reasons for *Vibrio* vulnerability are presented in Discussion. The repeated observation of surviving colonies in distilled water suggest that bacterial populations are non-uniform and always contain a small fraction of highly resistant cells.

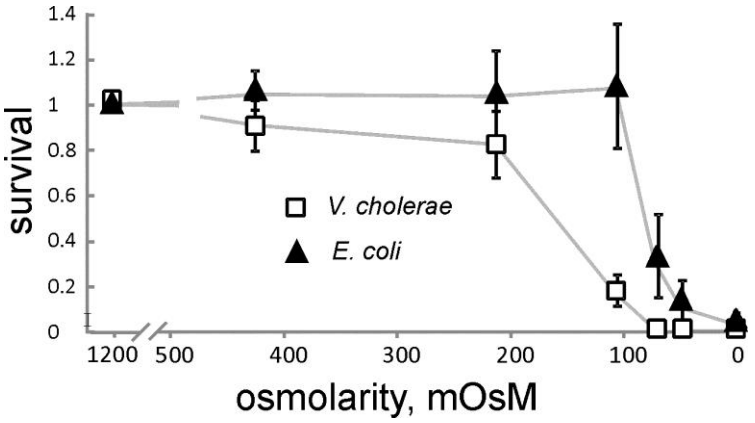

Figure 4.4. Viability of *V. cholerae* and *E. coli* upon osmotic downshifts of different magnitude. Both cultures were pre-grown at 1180 mOsM (LB containing 0.52 M NaCl) for 2 hrs and then abruptly diluted into media of different osmolarity as indicated on the horizontal axis. After 15 min of incubation the cultures were further diluted and plated in duplicates. The survival is expressed as the number of colonies relative to the unshocked control. The data points are averages of 6 independent experiments with error bars representing standard deviation.

Current-to-voltage relationships for the two dominant activities.

To investigate how closely mechanosensitive channel activities in *V. cholerae* resemble those in *E. coli* we measured current-to-voltage (I-V) curves in a broad range for the two dominant activities. It was easier to record single MscS-like channels, which activate at a relatively low threshold, when the patch was initially silent. Conversely, to characterize MscL-like activities we had to saturate the population of MscS-like channels first and record single MscL-like activities on top of a 1 nA current plateau. Due to reduced patch resistance in the presence of 8-10 open MscS-like channels, the MscL-like

channels conducted at apparent 2.6 nS. After Rs correction (Rs = 2.9 MΩ, the open pipette resistance), the conductance was close to the 3.0 nS activity reported for MscL channels recorded in MscS-null *E. coli* strains [38, 157]. In parallel experiments, *E. coli* MscL exhibited an apparent conductance of 2.4 nS when recorded at the background of ~20 saturated MscS channels, 22% lower than the previously established unitary conductance of *E. coli* MscL. We also observed that the large-conductance channel from *Vibrio* also had a stronger propensity toward the uppermost subconductive state than *E. coli* MscL (compare Fig 4.3 A and B).

The *Vibrio* MscS-like channel displayed a substantial inward rectification; the I-V curves were linear at hyperpolarizing voltages (pipette positive), but had a lower slope at depolarizing voltages. This MscS-like channel exhibited open-state noise at depolarizing (negative pipette) voltages, similar to what was observed in *E. coli* MscS [51]. These fast-flickering substates are likely to be the reason for rectification.

MscS-like channel inactivates and recovers.

The earlier saturation of MscS-like channel population (plateau in Fig. 4.2A) allowed us to choose a pressure range at which we could see activity only from this channel. Traces presented in Fig. 4.5 show patch responses to a pulse-step-pulse protocol, revealing the processes of adaptation and inactivation. In each protocol, the first short saturating pulse applied in the beginning revealed the entire active population while the following prolonged step of pressure conditions the process of inactivation. The short saturating pulse delivered at the end tests for the remaining active population. The trace presented in Fig. 4.5A shows a noticeable inactivation under a sub-threshold step which

did not invoke any activity. When the conditioning pressure step was at the midpoint for channel activation (determined with a 1 s ramp) inactivation was maximal (Fig. 4.5B). The recovery experiment (Fig. 4.5C) employed a similar protocol; after the conditioning-step pressure was dropped to zero, the patch was probed by a sequence of saturating pulses, tracing the process of recovery from inactivation. As illustrated in Fig. 4.5D, inactivation of the MscS-like channel is tension-driven. The *Vibrio* MscS-like channel thus behaved very much like *E. coli* MscS [51, 90], with one subtle difference: it shows a small amount of silent inactivation at tensions which invoke no activity (Fig. 4.5A).

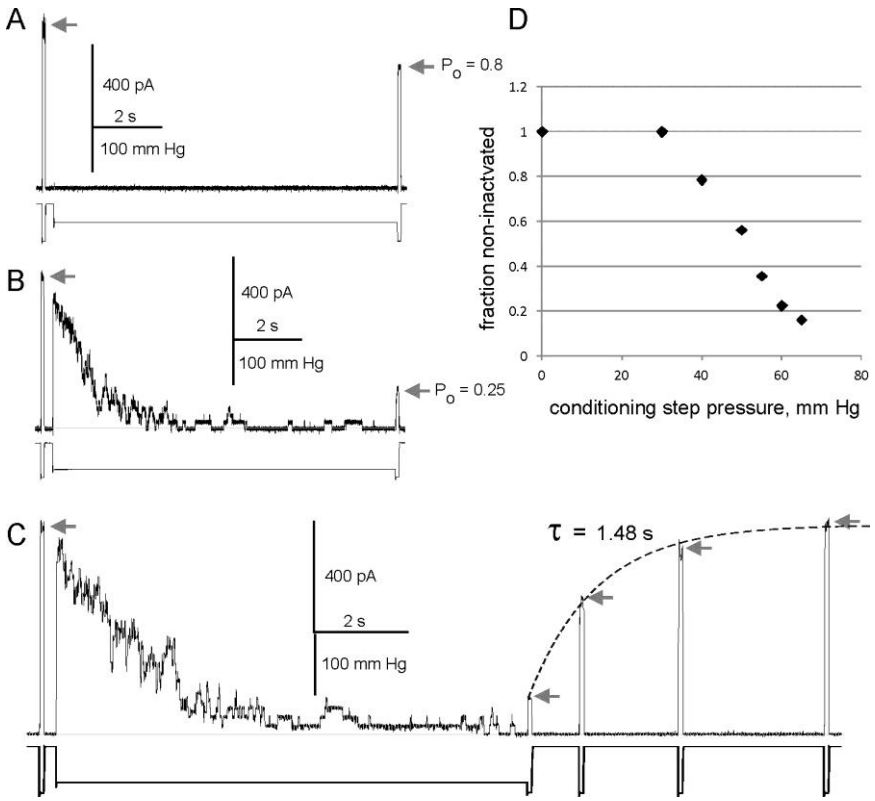

Figure 4.5. Inactivation and recovery of the Vibrio MscS-like channel. (A) Patch response to the pulse-step-pulse protocol with a sub-threshold step amplitude. Saturating pulses before and after the step reveal the initial and remaining active population (B) A similar experiment with activation of nearly the entire population during the step. (C) The recovery experiment. Fitting of the tips of the test pulse responses reveals tau recovery of 1.5 ± 0.2 (n = 3) s. (D) Dependence of the non-inactivated fraction of MscS-like channels on the amplitude of intermediate pressure step illustrates that inactivation is tension-driven.

Both MscS-like and MscL-like channels are modulated by compatible osmolytes.

Ramp responses of the entire channel population in control and in the presence of 0.5 or 1 M trehalose on the cytoplasmic side of the patch are demonstrated (Fig. 4.6). *V. cholerae* (A) and *E. coli* (B) are both shown to be sensitive to the presence of this compatible osmolyte, evident by a right shift of the activation curve and a decrease of the active population. The lower panels (C, D) show the magnified responses of MscS-like channels at the foot of the trace in both control and with 1 M trehalose traces. In four independent experiments, the average shift of MscS activation midpoint in the presence of 1 M trehalose was 24± 16% for *V. cholerae* and 12± 5% for *E. coli*. Shifts of MscL-

like channels were 24±4% and 11±2%, for *V. cholerae* and *E. coli*, respectively. It is clear that trehalose modulates channel activity, possibly through tension-driven intercalation into the bilayer [158-160] or perhaps through an osmotic or crowding effect, which has been shown to promote MscS inactivation [62]. We have also observed right-shifts of MscL-like channel activation in the presence of 1 M glycine-betaine, another compatible osmolyte. glycine-betaine exerted no visible effect on MscS-like channel of *Vibrio.*

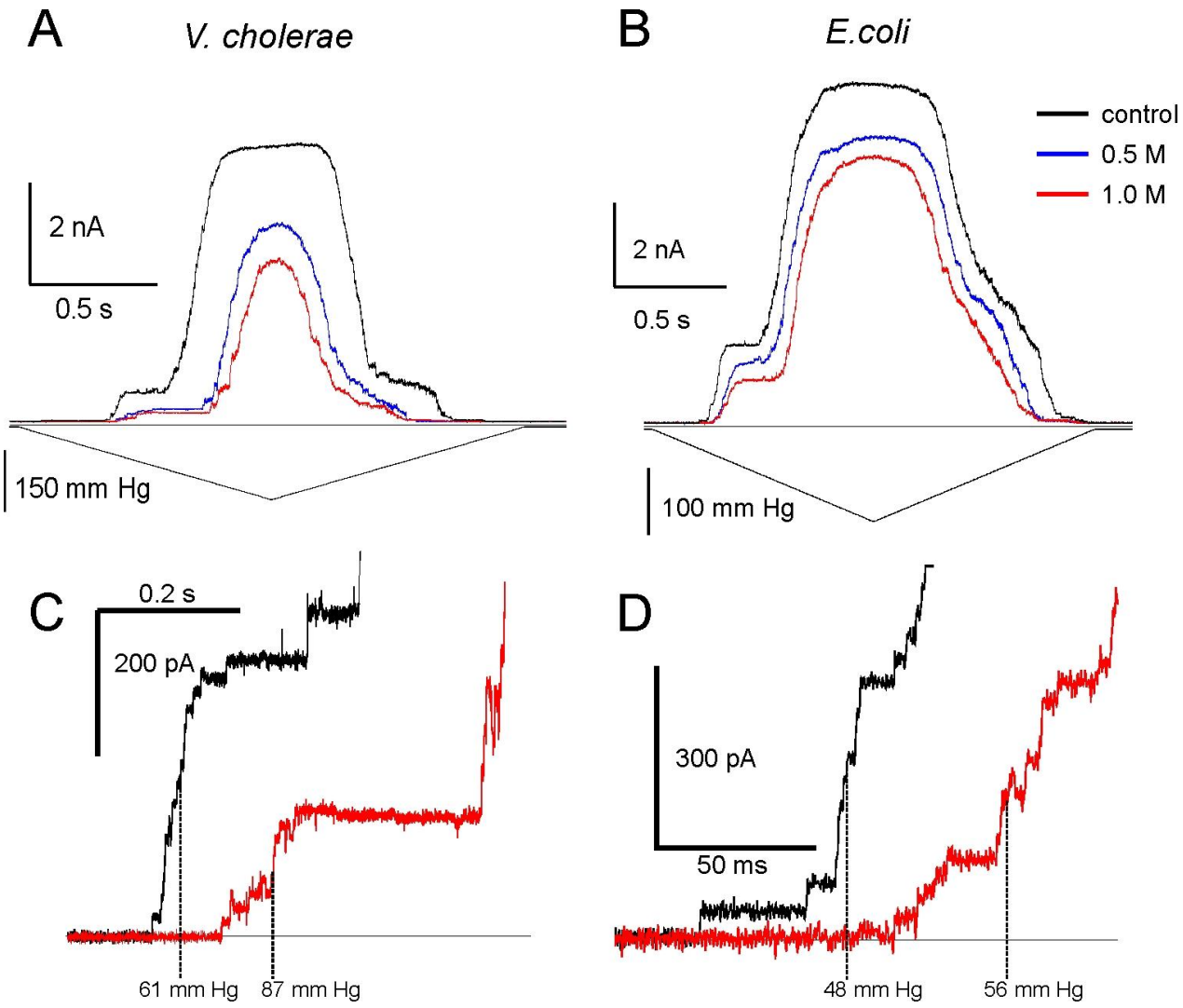

Figure 4.6. Effects of trehalose on MscS-like and MscL-like channel activation. Trehalose induces substantial left shift of activation curves, which is more pronounced for MscL in *V. cholerae* (A) than in *E. coli* (B). The three curves represent trehalose concentrations of 0 (black), 0.5 (blue) and 1.0 M (red). Magnified early responses in *V. cholerae* (C) and *E. coli* (D) specifically show the left shift of the MscS curve as well as reduced single channel conductance in response to 1 M trehalose.

Current-to-voltage relationships were analyzed for the two dominant channel activities in the absence and presence of trehalose on the cytoplasmic side of the patch. Fig. 4.7 shows these changes upon the addition of 1 M trehalose. Data (Fig. 4.7 and Table 4.1) was treated using the macroscopic conductance equation [155], which accounts for pore resistance (*Rp*) and access resistances from each side of the channel

(Rs_1 and Rs_2) (see Methods and Fig. 4.7C). Previously, it was shown that the unitary conductances of both MscL and MscS scales linearly with specific conductivity of the recording buffer suggesting bulk-like conditions for ion transport through wide water-filled pores [101, 105]. Conductivity measurements indicated that specific resistance of the recording buffer increased three times, from 33 Ωcm to 98 Ωcm in the presence of 1 M trehalose. We presumed, if trehalose freely partitioned into the channel pore, we would observe a proportional decrease in pore conductance. Values of conductance determined from the data (G_{exp}) match closely with those calculated via the macroscopic conductance equation (G_{calc}); variation of only Rs_1 (the cytoplasmic side of the membrane patch) proportional to changes of bulk specific resistance (ρ) due to trehalose sufficiently explains the observed change in unitary currents. This suggests that the resistance of the pore itself (Rp) does not visibly change upon osmolyte addition and thus, trehalose does not freely partition from the cytoplasm or accumulate in MscS- or MscL-like pores. Pre-filters on the cytoplasmic side of each channel formed by C-terminal domains [40, 41, 161] may impede partitioning, whereas the exit toward the periplasm is likely to be unimpeded. The presented data does not exclude trehalose permeation through MscL or MscS pores, it simply shows that the steady-state pore occupancy with the osmolyte is low, possibly due to a slower (pre-filter limited) entry rate from the cytoplasmic side and a higher rate of exit on the periplasmic side.

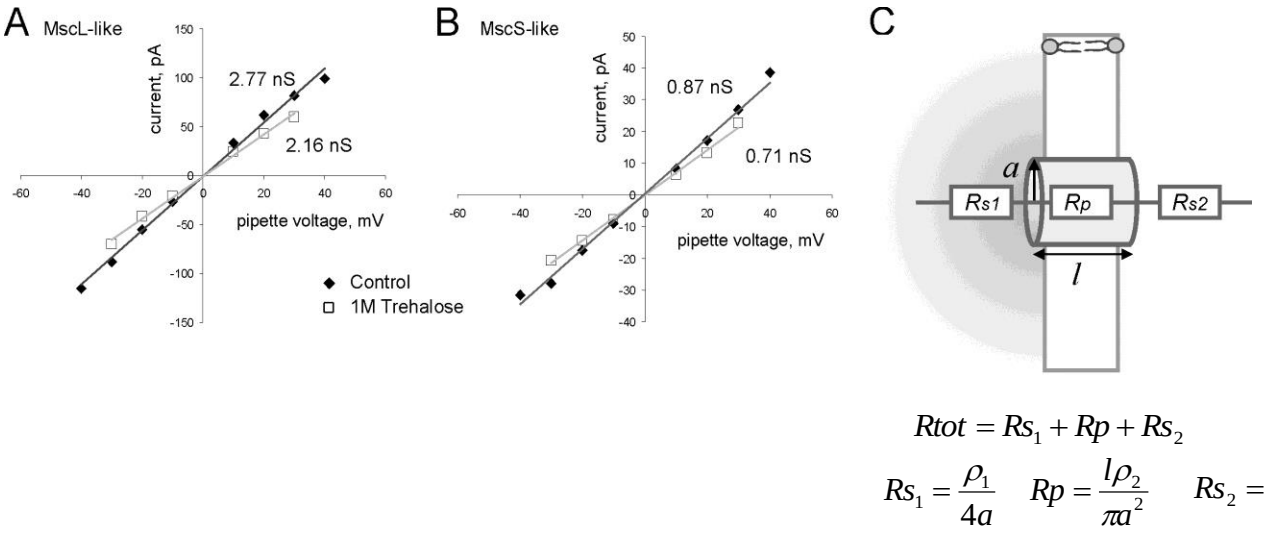

$$Rtot = Rs_1 + Rp + Rs_2$$

$$Rs_1 = \frac{\rho_1}{4a} \quad Rp = \frac{l\rho_2}{\pi a^2} \quad Rs_2 = \frac{\rho_2}{4a}$$

Figure 4.7. (A, B) Current-to-voltage relationships for single-channel currents recorded in control and in the presence of 1 M trehalose on the cytoplasmic side for MscL- and MscS-like channels in *V. cholerae*. Each plot presents the data of one typical experiment with all I-V curves obtained on the same patch. Based on four independent experiments, unilateral addition of trehalose decreased the slope conductance by a factor of 0.78±0.03 for MscL-like and by a factor of 0.80±0.06 for MscS-like channels (mean ± std, n=4). (C) Model of a channel, depicting how the total series resistance (R*tot*) is determined by the pore itself (*Rp*) as well as the access resistance on either side of the membrane (Rs_1, Rs_2). The values are dependent on channel radius (*a*), length (*l*), and the conductivity of the solution (ρ), which can be found in Table 2. Shaded area on the left represents the compartment with trehalose.

DISCUSSION

Vibrio cholerae readily produces filamentous forms and giant spheroplasts under experimental conditions similar to what was developed for *E. coli*. This enables direct patch-clamp characterization of the *V. cholerae* cytoplasmic membrane and the individual components involved in osmotolerance. The first electrophysiological survey of *V. cholerae* revealed a robust tension-stimulated conductance response mediated by two dominant types of MS channel activities, similar to what was observed in *E. coli*: the MscS-like (0.8-1 nS) and MscL-like (2.6-3 nS) channels. The N16961 *Vibrio cholerae* genome (Heidelberg et al., 2000) harbors one clear ortholog of *E. coli* MscL (NP_233001, 136 aa, 65% identity) and a likely ortholog of *E. coli* MscS (NP_230134.1,

287 aa, 48% overall identity with a 84% conserved TM3-beta domain region). A more distant MscS ortholog is coded by NP_232581.1 (291 aa, 21% identity). An additional ORF predicts a longer 569 aa protein with an N-terminal extension (NP_231387.2, 37% identity of the homologous C-terminal part to *E. coli* MscS). A putative ortholog of *E. coli* MscM (YbdG) [87] is also present in the N16961 *V. cholerae* genome (NP_229921.1, 412 aa, 54% identity), but there is no obvious ortholog of MscK (KefA) [88]. Because these channel species have not been characterized individually, we presume that MscS-like activities can potentially be generated by a mixed channel population.

Based on the densities of active channels in excised patches (Table 4.1), the numbers of channels per cell (5-8 μm^2 in surface area) can be estimated as 18-30 heptameric MscSs and 20-35 pentameric MscLs in AW405 *E. coli*. *V. cholerae*, respectively, should have 6-10 MscS-like and 50-90 functional MscL-like channels per cell. Our estimation of the number of *E. coli* MscL channels is about 2-3 times lower than previously determined in fluorescent microscopy experiments [162] which estimated 300-400 MscL subunits per cell grown in MLB medium. It is possible that not all synthesized subunits form functional pentamers.

The notable difference in mechanoelectrical responses of the two dominant species is that the density of MscL-like channels is approximately three times higher while the density of MscS-like channels is about three times lower in *V. cholerae* compared to *E. coli*. Not only is the proportion of MscL to MscS activities different, but the pressure midpoint ratio $p_{0.5}$MscS/$p_{0.5}$MscL for the two dominant channel types in *Vibrio* is lower, at 0.48 ± 0.05 versus 0.60 ± 0.05 for *E. coli.* If we take the MscL-like

activation midpoint as a reference, the *Vibrio* MscS-like channel activates earlier than its *E. coli* counterpart. In addition, the *Vibrio* MscS-like wave shows no hysteresis during a 1 s triangular ramp, signifying a faster closing rate than that in *E. coli*. MscS-like channels of *Vibrio* exhibit similar rectifying conductance and tension-dependent inactivating behavior as *E. coli* MscS. *Vibrio* MscS-like channels recover from inactivation as fast as *E. coli* MscS does [50, 90], with a characteristic time of 1.5 s.

Despite *Vibrio cholerae* N16691 having a three times larger overall density of mechanosensitive channels, it is less tolerant to strong down-shocks (1000-1200 mOsM) compared to *Escherichia coli* AW405. *Vibrio alginolyticus,* for instance, a strictly marine representative of this genus lacking the *mscL* gene, is extremely sensitive to osmotic downshifts, but expression of *E. coli* MscL in this microorganism was shown to dramatically increase its shock tolerance [163]. High density of MscL channels in *V. cholerae* might compensate for some other traits that make it osmotically vulnerable. The data above allows us to infer the traits to be considered.

In the event of abrupt osmotic shock, the bacterial osmolyte release system will be able to rescue the cell by releasing excess osmolytes faster than hydrostatic pressure inside the cell reaches the lytic level. In the beginning, osmotic influx of water will stretch the elastic cell wall and the outer membrane. Tension in the inner membrane during osmotic swelling will begin to develop as the membrane unfolds. The kinetics of tension buildup will be defined by the magnitude of the osmotic gradient, elasticity of the cell wall, and the membrane excess area which requires a certain degree of cell wall distension. Once the threshold tension that activates MS channels is reached, the rate of osmolyte release should be high enough to negate the osmotic water influx before critical

rupturing tension develops. The observed lower tolerance of *V. cholerae* to abrupt osmotic down-shocks compared to *E. coli*, despite a higher density of MscL, points to the necessity of better understanding the following factors:

1) Distribution of cell sizes in the population. According to the law of Laplace, tension in the membrane is proportional to the pressure gradient multiplied by the radius of curvature and thus larger cells must be more vulnerable. It has been well documented that stress conditions lead to the decrease of average size in microbial populations [148, 164]. In exponential cultures, *V. cholerae* cells appear to be slightly larger than *E. coli*. The lower tail of size distributions in both populations may constitute the most shock-tolerant cells. In addition to outward cell geometry, the excess amount of membrane, and the mechanical strength of the retaining cell wall (peptidoglycan layer) might vary between the two species.

2) Water permeability and relative densities of MscS and MscL. Under hydrostatic pressure of water flooding the cytoplasm through the membrane and aquaporins, MscS is predicted to open first and dissipate osmotic gradients. If MscS's osmolyte permeability is insufficient, building up tension will open MscL, a true emergency valve which activates near the lytic tension. Earlier activation of MscS would mediate a more gradual permeability response with tension, which might be beneficial. The density of MscS-like channels in *V. cholerae* under the specific conditions of this study is lower than in *E. coli*, thus the first line of defense is not as strong. In *E. coli*, expression of both channels is under the control of stress-activated factor RpoS, and overexpression of one partially represses the other. The physiological role of densities of aquaporins, MscS, and MscL channels in both species needs to be better understood. It

was proposed that a high density of MscL may increase effective elasticity of the membrane and thus dampen tension due to protein expansion [165]. In addition, the clustering and distribution of channels between the cylindrical part of the rod-shaped cell and the poles [166], where curvatures and tensions are different may influence the hydrostatic pressure at which threshold tension is reached.

3) The nature of internal osmolytes and channel permeability. The relatively large size of permeation pores in MscS and MscL may ensure that the release kinetics are comparable with the millisecond kinetics of osmotic swelling [91]. For this reason, efficiency of compatible osmolyte release might be an important factor defining the speed of cellular escape from osmotic rupture. However, permeabilities of MscS or MscL for organic osmolytes have not been studied in detail. Also, the composition of preferred compatible osmolytes used by each of the bacterial species might be different [34, 167]. In this investigation we were able to observe modulating effects of the common compatible osmolyte trehalose on the behavior of both MscS-like and MscL-like channels. Right shifts of activation curves were accompanied with substantial inactivation of MscS-like channels. Our single-channel recordings suggest that trehalose present in the cytoplasmic compartment does not freely partition into the pore, yet these conductance measurements do not exclude permeation.

In conclusion, the establishment of *V. cholerae* as a system for electrophysiological analysis opens new perspectives for studies of mechanically-activated osmolyte release system and electrogenic transport in this pathogen. The first patch-clamp survey has shown that *V. cholerae* has lower density of MscS-like channels, but higher density of MscL-like channels compared to *E. coli*. Both *V. cholerae* channels

have gating and conductive properties comparable to their *E. coli* counterparts. This is the first report on WT *Vibrio cholerae,* which shows that compatible osmolytes, especially trehalose, strongly modulate the mechanoelectrical response, shifting activation curves to the right. Trehalose does not seem to partition freely into the open MscL channel, bringing into question the actual exit path of this abundant osmolyte. The comparison of *E. coli* and *V. cholerae*'s sensitivities to osmotic down-shock strongly suggests that there must be other factors that contribute to the environmental fitness of this bacterium other than just the density of mechanosensitive channels in its membrane.

Acknowledgement

The authors thank Claire Costenoble-Caherty for expert technical assistance with bacterial cultures, BLAST searches and alignments. This work was partially supported by the NIH RO1 A1039129-11A2 and the NSF 0813066 grants to A.H. and NIH R21 AI105655-01 to SS and AH

Chapter 5: General conclusions and future directions

Conclusion 1

The key feature of MscS adaptive behavior is tension-driven inactivation from the resting state, the process which competes with opening. This inactivation is strongly promoted by crowding agents on the cytoplasmic side. Both transitions (close-open and close-inactivation) were believed to occur mostly through conformational changes in the transmembrane domain. Recent genetic screen experiments and modeling suggested that the cytoplasmic cage domain must be involved. In the work described here, I've shown that the association between the N-terminus of the pore lining transmembrane helix (TM3b) and the beta domain of the cage plays a critical role in channel gating and inactivation. Stabilization of this contact with mutations impedes opening and causes massive silent inactivation; disruption of these interactions stabilizes the open state, reduces inactivation, and removes sensitivity to crowding agents and voltage. Molecular simulations indicated that the inactivated state of the channel has a higher degree of lateral in-plane expansion in response to axial compression in comparison to the resting state. The ability of the inactivated state to expand in the membrane confers this ability to respond to synergistic action of crowding pressure and tension. This possibly allows for a feedback system between efflux of water and osmolytes through mechanosensitive channels and the elastic recoil of the peptidolglycan sacculus in order to maintain a constant turgor pressure.

Physical compaction of the cytoplasmic domain of MscS

I propose that the compressibility of the cage be further investigated. Can the portals be closed by axial pressure (as shown in Fig. 5.1) and can this allow the cage to act as a second gate? EMP simulations suggest that such a flattening of the cytoplasmic cage is attainable, but is it realistic?

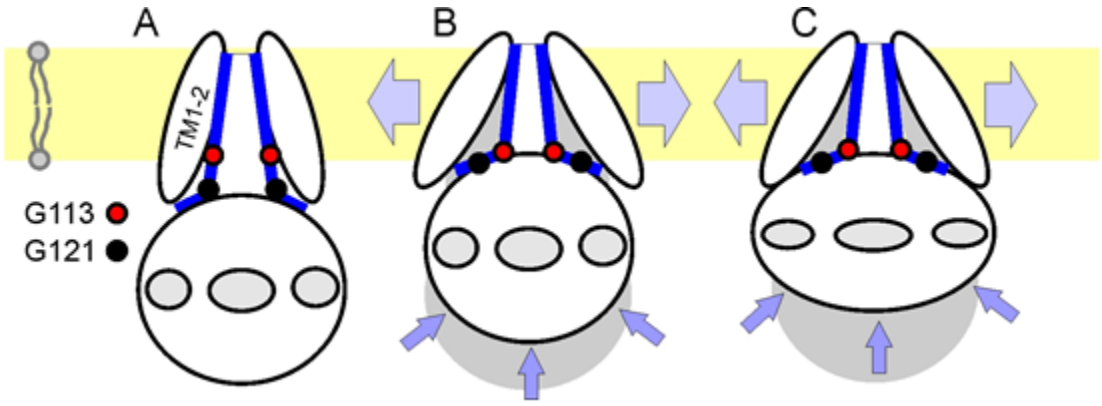

Figure 5.1. The mechanism of crowding sensing by MscS. (A) The resting state; (B) the predicted mechanism of inactivation associated with kinking at G113 involving concerted axial compression of the molecule by crowding pressure and simultaneous in-plane expansion under lateral tension; (C) a hypothetical conformation with flattened cage with diminished conductance of side portals.

I have completed a few initial experiments which examined cysteine cross-linking of the cage. Fig. 5.2 shows the approximate locations of residues G140 and A230 on the upper and lower hemispheres of the cage in the crystallographic, partially compacted, and flattened conformations. To attempt to capture these states, cysteine mutants were introduced and a G140C/A230C mutants was created and the single channel conductance was measured in reducing conditions (1 mM DTT) and with an oxidizer (10 mM H_2O_2). The overall results show an increase in opening events characterized by a lower current

amplitude; this decrease in single channel currents indicates that upon cross-linking, the cage enters a more compact state and is thus less permeable.

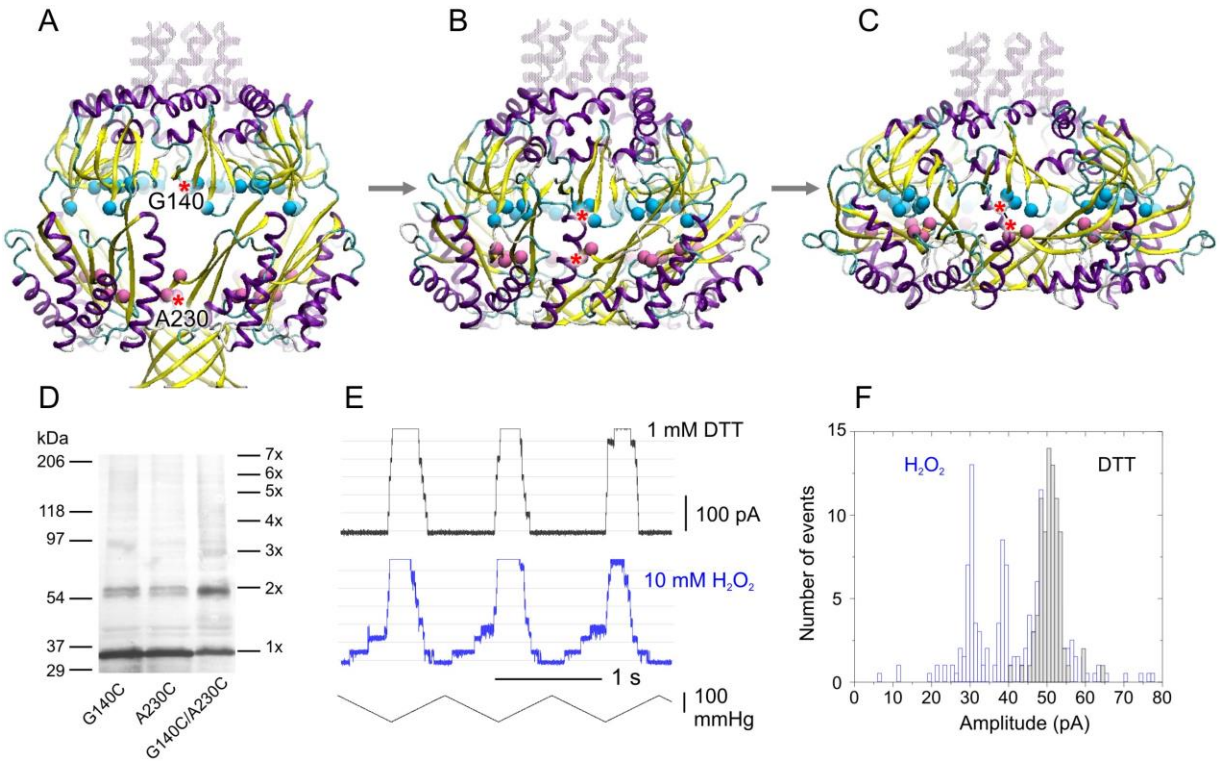

Figure 5.2. Compressibility of the cytoplasmic domain of MscS. Three EMP-generated conformations of the cage: crystal (A), compact (B) and collapsed flat (C) are shown above. Asterisks show □ carbon locations of residues G140 and A230, two residues on opposite ends of the windows in the cage. A Western Blot illustrating the probability of G140C-A230C cross-linking (in comparison to each single mutant) under 10 mM H2O2 is shown in (D). Upon addition of 10 mM H2O2, the single channel conductance is diminished in comparison to its activity under reduced conditions (1 mM DTT, +50 mV pipette) (E). Histograms of single-channel currents from the traces (F).

To test the second gate hypothesis, MscS A106C was reacted with 1 mM MTSET(+) (methanethiosulfonate-ethyltrimethylammonium). This positively-charged molecule locks the channel in the open state by reacting with the cysteine and stabilizing the hydrated state of the pore (Fig. 5.3A). Upon the addition of ~15% Ficoll 400, the channel activity remains unchanged, implying that the crowding was unable to force the channel to close (Fig. 5.3B). This suggests that either the channel has only one gate or

that crowding is unable to collapse the cage. Interestingly, the overall conductance of the patch does not change in the presence of the crowders; the results of the G140C/A230C crosslinking experiment did imply that compressing the cage would in fact reduce the conductance of individual channels. It is possible that crowder-induced inactivation of MscS occurs through a much more subtle change of volume of the cytoplasmic cage than what is simulated in the cross-linking experiment. Another interesting result to note is that while the channel is locked in the open state by MTSET, it still retains some negative voltage sensitivity; the initial opening of the full channel population (shown by the initial negative current spike) is quickly followed by closure of about half of the channels.

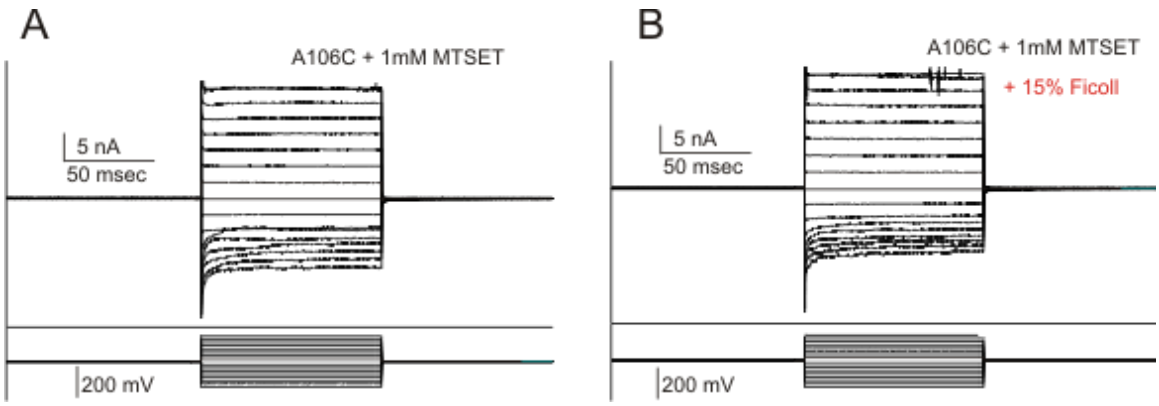

Figure 5.3. Chemical activation of A106C MscS with MTSET. After activation by tension in the presence of 1 mM MTSET, patches of A106C MscS spheroplasts remains open with no tension. The figure above shows several traces of the same patch under various voltages. The conductance of the open population is the same both before (A) and after (B) the addition of 15% Ficoll 400.

Further experiments need to be conducted to determine the true nature of compaction of the cage via crosslinking. The inactivation and closing rate of the G140C/A230C mutant in oxidizing conditions should provide a glimpse into the role of actual cage compaction in those processes. The A106C + MTSET experiment should also

be performed for a longer period of time under negative voltage to see how it compares to the same phenomenon in WT MscS, which requires approximately 2 sec to completely inactivate, as seen in Fig. 2.6 from Chapter 2.

Molecular size effects crowding sensitivity of MscS

The interior of an E. coli cell is extremely crowded, with protein concentrations likely exceeding 0.3 g/mL. In my work I have shown that macromolecular crowding is effective at increasing the activation threshold as well as the closing and inactivation rate of MscS. This crowding was simulated by the addition of 5 wt/vol% Ficoll 400 to the cytoplasmic side of an excised patch of *E. coli*. The application of 1 M trehalose (~24% wt/vol) showed a similar modulation of MscS opening and closing but did not affect inactivation (Fig. 5.4). Trehalose is small, with a mass of less than 0.4 kDa, while Ficoll 400 is a thousand times more massive (400 kDa); thus it can be inferred that the size of crowding molecules effects the exerted crowding pressure on the cytoplasmic cage of MscS.

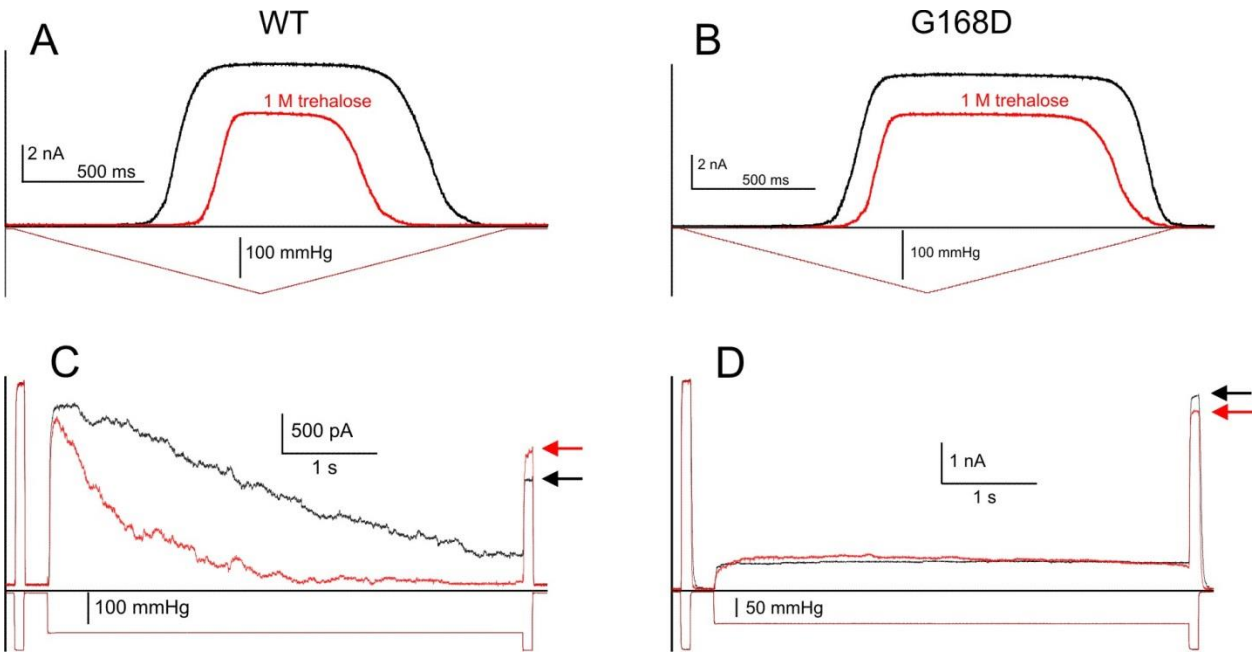

Figure 5.4. The crowding effect of 1M (24 vol%) trehalose on WT and G168D MscS opening, closing and inactivation. Under symmetric ramps of pressure, both the opening and closing of WT (A) and G168D (B) MscS are modulated by the presence of 1M trehalose (red traces). The shift toward higher tensions required to open and close the channel is comparable to that which occurred during identical protocols in the presence of 5% Ficoll (Fig. 2.4A). The notable difference is the more pronounced drop in maximum current due to the higher resistance of a 1M trehalose solution. Pulse-step-pulse protocols were then used to investigate the tension-driven inactivation of WT (C) and G168D (D) before (black traces) and after (red traces) exposure to 1M trehalose in a similar manner as was done with 5% Ficoll (Fig 2.5A and B). Differences in amplitude of pulses in the beginning and end of the traces indicate the degree of inactivation (arrows). While trehalose, possibly permeable through the cage portals, is able to alter channel opening and closing in the same manner as cage-impermeable Ficoll 400, it has minimal effect on inactivation. Under similar tension, Ficoll drives the entire population of WT MscS into the inactivated state (Fig 2.5).

Since the molecular mass of many protein complexes in the cell are of comparable size to Ficoll 400, our crowding induced via 5-10% Ficoll 400 is not an overestimate of crowding but instead a moderate attempt to mimic the intracellular environment. Knowing this, I propose that the size requirement for gating and inactivation changes due to crowding be investigated. A simple way to do this would be to examine at what concentration do compatible osmolytes and crowding agents of different sizes begin to alter the opening threshold of MscS (which was seen for 1 M trehalose) and what combination of size/concentration characteristics is required to

actually induce inactivation. This could perhaps discern what physiological conditions in the cell are considered optimal for channel gating and therefore in which conditions a bacteria has the best chance for surviving osmotic downshock.

Conclusion 2

The ability to permeate the cell membrane is a necessary for any antibiotic agent to perform its designated task. As an amphipathic agent intercalates into a membrane, it alters the lateral pressure profile. Since MscS gates via tension in the membrane, it can be affected by changes in the lateral pressure profile of the bilayer. I have shown that our lab has made strides toward utilizing MscS as a reporter of this increase in lateral pressure in a native bacterial membrane. We have compared two different methods of estimating membrane partitioning, surface activity and lipid monolayer affinity, with alterations of the activation midpoint of MscS. These methods were used to investigate partitioning capabilities of the antibacterial agent platensimycin and three analogs generated in Dr. Sintim's lab. The intercalation of these substances into the native membrane (gauged by activation curve shifts) generally correlated with their affinity for phospholipid monolayers. We attribute the discrepancies between the partitioning coefficients derived from monolayer experiments (K_{lip}) and patch clamp (K_{mem}) to differing properties of the phospholipids in each case, namely the difficulty of large, bulky sidechains to intercalate into a bacterial membrane in the same manner as in an expanded monolayer.

Further monitoring of intercalation into the bacterial membrane and other special cases

Upon amphipath addition to the cytoplasmic side of a membrane patch, there is a sudden increase in the activation midpoint. For some of the tested substances, namely QD-11, this is followed by a gradual return to the original midpoint value which can take over 30 minutes. We interpret this activity as a redistribution of the amphipath to the outer leaflet of the membrane, which reduces the asymmetric pressure on the gate of MscS. Once the agent occupies the outer leaflet, it can potentially redistribute into the bulk solution on the pipette side of the patch. This would mimic successful internalization of an antibiotic agent.

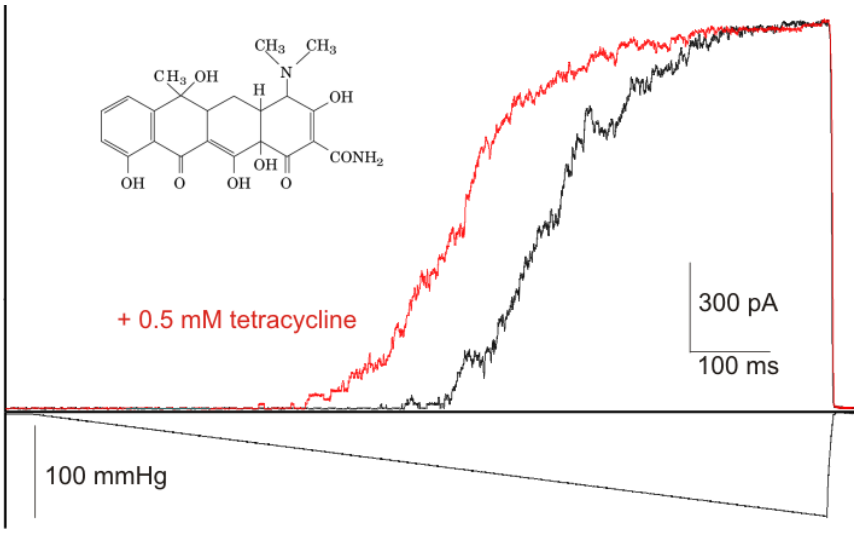

Figure 5.5. Tetracycline lowers the gating threshold of MscS. Upon exposure to 0.5 mM of the polycyclic antibiotic tetracycline (inset), the activation curve of A98S MscS experiences a left shift (red trace). This transient alteration of the activation curve is usually followed by a shift back toward its original position.

We found different results when we tested tetracycline, a triakylamine polycyclic antibiotic, for its ability to partition into the membrane; the activation curve of MscS actually shifts to the left upon its addition, implicating that the lateral pressure on the gate has been reduced and the channel now opens at lower tensions (Fig. 5.5). This led us to

infer that the plane of adsorption for tetracycline may be different from those of amphipaths we examined previously. MD simulations of tetracycline intercalation into the membrane differ from those of a known 'right-shifting' agent, butyl paraben. Instead of partitioning into the acyl chain region of the simulated bilayer like paraben, tetracycline adheres peripherally to the membrane by interacting mostly with the polar head region (Fig. 5.6). Comparison of computed lateral pressure profiles for both butyl paraben and tetracycline shows that the increase of the lateral pressure peak in the head group region of the tetracycline simulation is compensated by a decrease of lateral pressure in the acyl chain region. This reduction of hydrocarbon packing pressure may be responsible for the lower gating threshold observed. Therefore, MscS senses not only the presence of intercalating substances but also their plane of adsorption to the membrane.

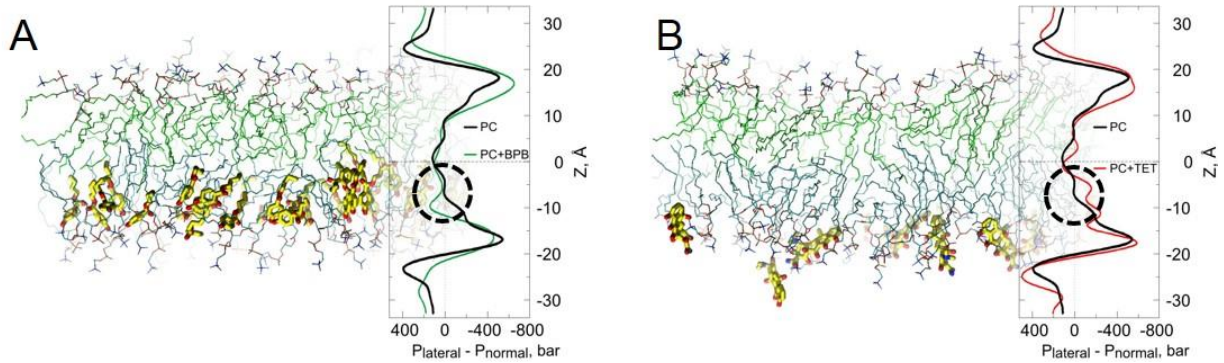

Figure 5.6. Polycyclic aromatic compounds interact with the polar head groups in a simulated bilayer. Above depicts an MD simulated phosphatidylcholine (PC) bilayer and its associated lateral pressure profile both before (black curves) and after (red curves) the addition of (A) butyl paraben and (B) tetracycline. The butyl paraben molecules intercalate into the acyl chain region in (A) while tetracycline interacts with the head groups in (B). As a result, the lateral pressure in the acyl chain increases in (A) while the pressure in that position decreases in (B) (dashed circles).

Further testing of such polycyclic aromatic compounds should be done to understand these effects. Compounds which induce MS channel gating at low tensions

could be useful antimicrobial agents since gain-of-function mutations of both MscS and MscL reduce colony growth.

Conclusion 3

The ability of a facultative pathogen, such as *Vibrio cholerae*, to withstand the osmotic shock associated with it enteric-to-freshwater transmission cycle is essential to its survival. Our group has developed a successful protocol for spheroplast generation of *V. cholerae,* which is the first step in mechanoelectrical examination of a bacterial membrane. Patch-clamp experiments revealed that the MS channels in *V. cholerae* operate similarly to those in *E. coli*, with one opening a ~1 nS pore at moderate tensions (termed MscS-like) and another which gates at higher tensions with a ~3 nS pore (MscL-like). Inactivation of the MscS-like channel was very similar to its counterpart in *E.coli* and the voltage sensitivity was also the same in both species. Shifting of the activation curve MS channels in the presence of the compatible osmolyte trehalose occurred in both species as well; notably, trehalose did not appear to freely partition into the channel pore in *V. cholerae*. The activation midpoint ratio of the channels was a bit lower in *V. cholerae* (0.48 versus 0.6) and the MS channel density appeared to be higher in *V. cholerae* than in *E. coli* even though *E. coli* is more tolerant to osmotic shock, indicating that osmotic shock survival depends on more than simply the number of release valves present.

Investigation of osmolyte permeability through mechanosensitive channels

It has been long held that MS channels release osmolytes upon osmotic shock. Current-to-voltage relationships were analyzed for the activities of the MscS-like and MscL-like channels in *V. cholerae* in the absence and presence of trehalose on the cytoplasmic side of an excised patch. The macroscopic conductance of the channels were analyzed by taking into account the resistance of the pore, the resistance associated with approaching the pore from either side (access resistance), and the resistance of the recording buffer either with or without trehalose. The moderate decrease in channel conductivity upon trehalose addition indicated that the resistance of the pore itself does not visibly change and thus trehalose does not freely partition or accumulate in the MscS-like and MscL-like channels.

The above description of channel conductance change doesn't dismiss the role of MS channels as osmolyte release valves, it just suggests that they do not occupy the channel for a substantial amount of time. This could be due to a difference in entrance and exit rates of the osmolyte; if the cage slows the entry to the pore but exit from the pore is very rapid, the presence of the osmolyte could be difficult to detect. To further examine the osmolyte permeability, different osmolytes (glycine betaine or proline) should be tested and the osmolyte location should be flipped, with the pipette being backfilled with osmolytes, such that they can now enter from the extracellular side. If the cytoplasmic cage does indeed act as a filter and slows down permeation from the intracellular side of the patch, then the conductance of the patch should decrease to a larger magnitude than the previous experiment.

The mechanosensitive channels in the facultative pathogen Pseudomonas aeruginosa

P. aeruginosa occupies both soil and water and causes fatal sepsis in damaged tissues or individuals with compromised immune systems. By readily forming biofilms on medical equipment, *P. aeruginosa* has become a serious problem associated with catheter infection. The medical relevance each of these bacteria present make them optimal choices for spheroplast development. We have developed such a protocol and I performed a few initial electrophysiological examinations of the mechanosensitive channels present.

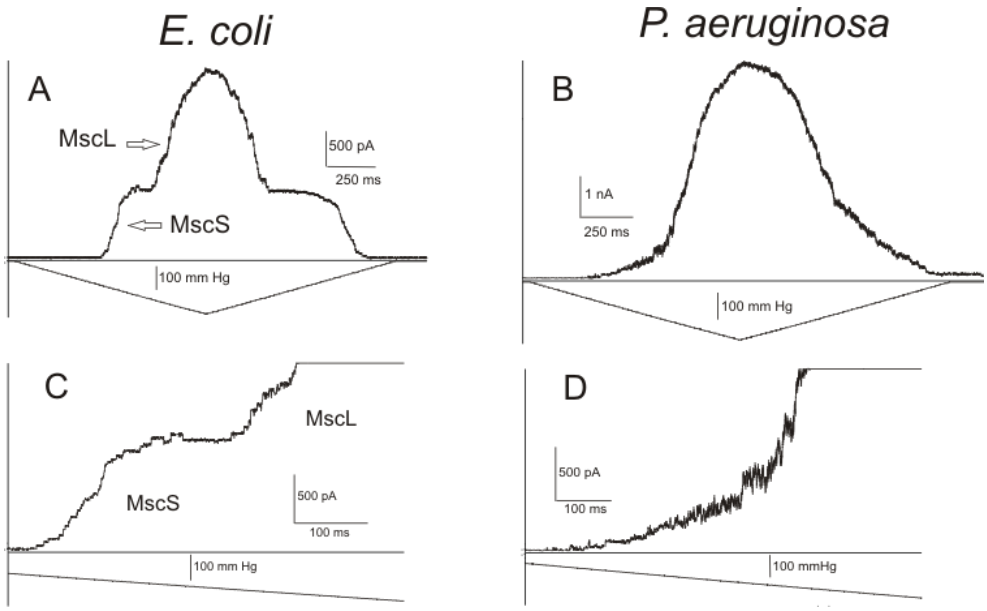

Figure 5.7. Mechanoelectrical responses of E. coli and P. aeruginosa. Above are the typical responses of both E. coli (A) and P. aeruginosa (B) to a 1s ramp of increasing pressure. The two-wave response in E. coli is due to the presence of two different channel populations (MscS and MscL, labelled with arrows) which each activate at different tension threshold. P. aeruginosa (B) does not exhibit clear channel population transitions, but rather displays a gradual increase in current. (C) shows the clear transition between MscS and MscL channels, while (D) shows that there is no obvious delineation.

Unlike the typical two-wave response of E. coli during a 1 s ramp of increasing pressure in patch-clamp experiments, *P. aeruginosa* shows a gradual increase in conductance without an obvious distinction between channel populations (Fig. 5.7). This could possibly indicate that there is a smaller distance between the two activation midpoints than there is in E. coli. The obvious instability and subconducting states in the smaller MscS-like channel(s) in *P. aeruginosa* may also be responsible for the lack of a clear delineation between channel populations. Initial osmotic survivability experiments indicate that this bacteria is also less tolerant of osmotic shock than E. coli (Fig. 5.8).

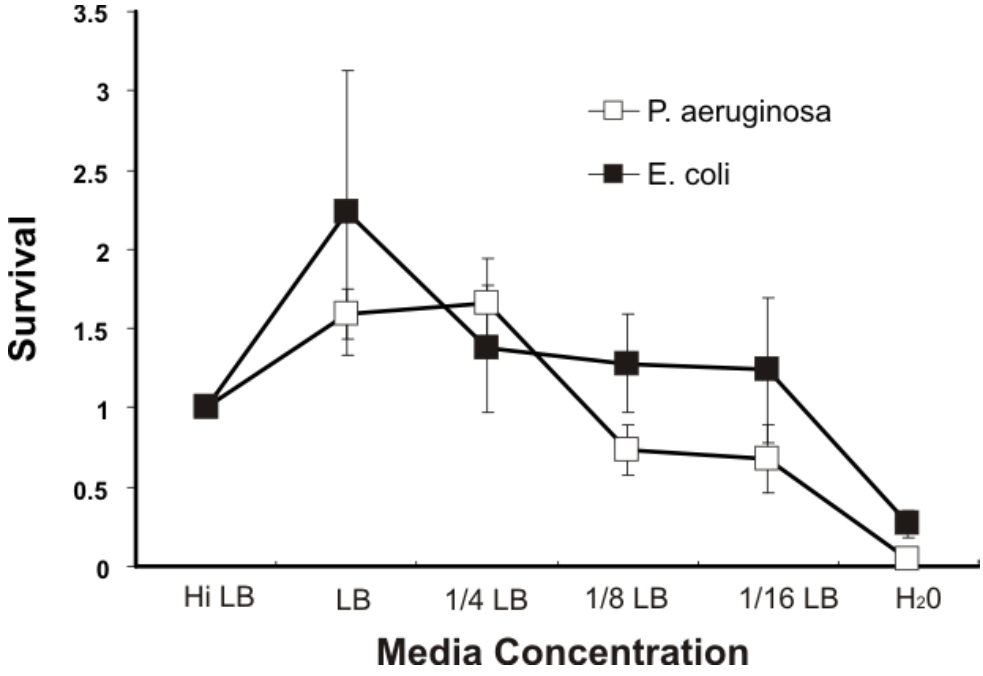

Figure 5.8. Survival of *P. aeruginosa* and *E. coli* in response to abrupt osmotic downshock. Above is the survival reported for each species after a 15 minute shock in the stated dilutions. Data obtained by Christina Mayhew.

To continue to examine *P. aeruginosa*, as well as *V. cholerae*, our lab is currently working on isolating the genes associated with the MscS and MscL homologs in both species. Once this has been done we hope to transform each into *E. coli* MJF465 (*mscS*-,

mscK-, *mscL*-) on its own to elucidate gating via patch-clamp. We will also determine the ability of each of these channels to rescue MJF465 from osmotic shock. This will give us the first detailed description of the osmotic survival of these two facultative pathogens.

The detection of the V. cholerae autoinducer CAI-1 partitioning into the P. aeruginosa membrane

As bacteria generate resistances to known antibiotic methods, it becomes essential to discover new ways to stop infections. Recently, quorum sensing has been suggested as an interesting system that can be harnessed to reduce pathogenesis [168]. Specifically, *V. cholerae* uses the amphipathic autoinducer CAI-1 to coordinate gene expression of neighboring cells: when cell density is minimal and CAI-1 concentration is low, *V. cholerae* is virulent and forms biofilms. As the cell density increases, CAI-1 concentration also increases and the bacteria becomes nonvirulent and biofilm formation halts, possibly leading to an increase in transmission. CAI-1 has been shown to enable genetic competence in *V. cholerae* and facilitate transformation of species and non-species specific DNA into the cell [169]. Also, CAI-1 has been found to reduce cell growth and native quorum sensing in other bacteria species, namely *P. aeruginosa* [170]. The mode of action for this competitive inhibition is not yet detailed, however initial studies suggest that CAI-1 may permeate and perturb the membrane of *P. aeruginosa* enough to compromise the integrity of the cell.

I have been provided a stock of CAI-1 from the lab of Dr. Sintim and performed some initial investigations on the effect of CAI-1 on the MS channel response in *P. aeruginosa*. The results suggest that ~10-100 uM CAI-1 does indeed alter the MS

activation curve in *P. aeruginosa* and *V. cholerae* excised membrane patches in the same manner as other amphipaths we've studied (Fig. 5.9). Further experimentation will be needed to determine the magnitude of this effect and whether it falls within the concentration range of CAI-1 antimicrobial activity against *P. aeruginosa*.

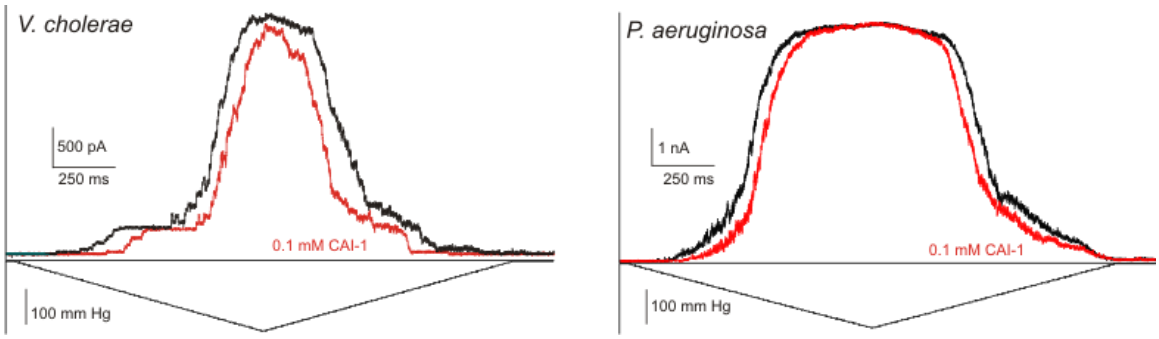

Figure 5.9. Effect of 0.1 mM CAI-1 on *V.cholerae* and *P. aeruginosa*. Upon exposure to the *V. Cholerae* autoinducer CAI-1, the activation midpoint of both species is shifted toward higher tension.

Closing remarks

Since its isolation 20 years ago, MscS has become the most thoroughly studied mechanosensitive channel in science. The large catalogue of data available and the established protocols for the manipulation of MscS make it an attractive molecule for *in vivo*, *in vitro* and, increasingly, *in silico* analysis of ion channel gating. I am confident that future studies will lead to the further utilization of MscS as both a molecular tool and target.

Supplemental Methods, Figures and Tables

Taken from:

> **Ian Rowe**, Andriy Anishkin, Kishore Kamaraju, Kenjiro Yoshimura and Sergei Sukharev. "The cytoplasmic cage domain of the mechanosensitive channel MscS is a sensor of macromolecular crowding." *Journal of General Physiology* 2014 (*in press*)

Modeling and simulations

The extrapolated motion protocol (EMP), which allowed us to generate the library of 86000 models and briefly described previously [48-50] will be presented in detail in a separate paper (Anishkin et al, in preparation).

The criteria for automated model selection based on experimentally determined spatial proximities are given in the main text. Here we only present the details and parameters of equilibrium and steered MD simulations used in this work.

Candidate models of the resting and inactivated states satisfying the constraints were equilibrated and refined in MD simulations with explicit medium. To ensure better equilibration of the lipid bilayer and adjustment to the channel, we used POPC membrane from the previously equilibrated model of the resting MscS embedded in the membrane [49] and replaced the protein structure by one of the two conformations selected from EMP exploration results as described above. Slightly overlapping lipids were displaced towards the bulk of the membrane. Simulation cell setup and all the molecular modifications (protein embedding, overlapping lipid displacement etc.) was done using

VMD[98]. The final simulation cell contained ~170000 atoms in total, including ~30000 protein atoms (1960 residues), 220 POPC molecules, ~37000 TIP3P waters, 65 potassium and 72 chloride ions (corresponding to a 200 mM salt solution). The whole system was energy minimized with a restrained protein backbone for 10000 steps using the conjugate energy gradient algorithm. The minimized system was simulated for 3 ns with the protein backbone harmonically restrained near the modeled positions with a spring constant of 1 kcal/mol/Å for 3 ns. A flexible hexagonal cell was simulated with periodic boundary conditions under 1 bar of pressure and a lateral tension of 40 dyne/cm. All simulations were performed using NAMD2 with the CHARMM27 force field, the particle-mesh Ewald method for long-range electrostatics estimation, a 10 Å cutoff for short-range electrostatic and Van der Waals forces, and a Langevin thermostat set at 310 K. The equilibration of models in explicit lipid bilayer included 20 ns unrestrained simulation for each of the structures, followed by a refinement using 5 ns symmetry-driven simulated annealing as described previously[99].

To explore the structural changes in MscS under increased crowding in the cytoplasm we have approximated the pressure of the large macromolecules by a force acting on the C-terminal half of the cytoplasmic cage (residues 183-280). To speed up the simulation, the force was applied only to non-hydrogen backbone atoms of that region (393 atoms per monomer, 2751 per whole channel). The force was always acting in the same direction – towards the midplane of the bilayer. The magnitude of force was set for slow exponential growth from 0.001 to 0.1 kcal/mol/Å/atom over the course of 20 ns simulations. To prevent the net displacement of the protein and membrane under the force, we have restrained the center of mass of non-hydrogen backbone atoms of TM1-

TM2 helices at the level of lipid bilayer (residues 12 to 54 and 70 to 89) in the direction normal to the membrane midplane. Note that only the average position of the center of mass of this region was restrained, while any relative motions within (e.g. helices tilting or kinking) were not affected. All the simulation conditions and settings were the same as in the relaxation simulations described above. The starting conformations of the protein (resting and inactivated) were taken from the final step of the symmetry-annealing of the relaxed structures.

Visualization of the channel structures was performed using the Visual Molecular Dynamics (VMD) package[98]. All the structural analysis (relative position of the protein domains, in-plane area of the channel in the membrane, and estimation of the cytoplasmic cage volume) was done using custom-written Tcl scripts for VMD.

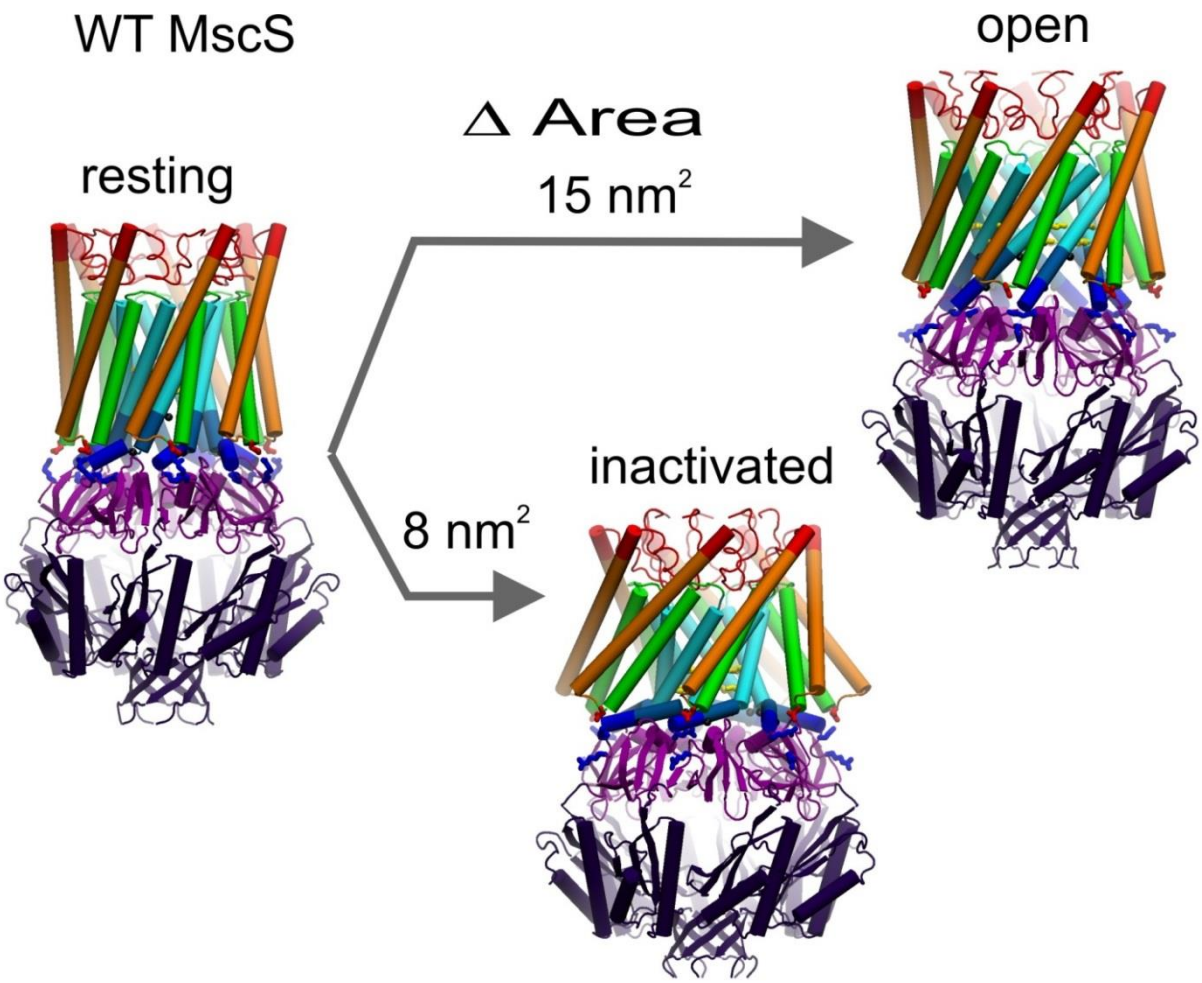

Figure S1. The scheme representing the functional cycle of WT MscS. The compact resting state is occupied at low sub-threshold tensions. It is characterized by the upright positions of peripheral (TM1-TM2) helices forming the buried contact with the pore-forming TM3s. This state is stabilized by D62-R131 salt bridges between the TM1-TM2 loops and the upper hemisphere of the cage. The application of super-threshold tension drives the population of resting channels in two different paths. The first is opening, which leads to hydration of the hydrophobic gate associated with a larger (~15 nm^2) in-plane expansion of the TM domain[50] and likely preserves TM2-TM3 contacts. The second inactivation pathway, trigged by tension of a similar threshold, leads to the detachment of the peripheral helices from the central TM3 core, accompanied by a kinking of TM3 helices at G113 which is stabilized by an association between the beta domains of the cage (purple) and the TM3b segments. Inactivation is associated with a smaller in-plane expansion of the TM domain[90]. The return to the resting state is predicted to include straightening if G113 kinks, detachment of beta domains from the TM3b segments and re-formation of D62-R131 bridges. This transition is predicted to result in a ~12 Å displacement of the gate upward, toward the midplane of the membrane.

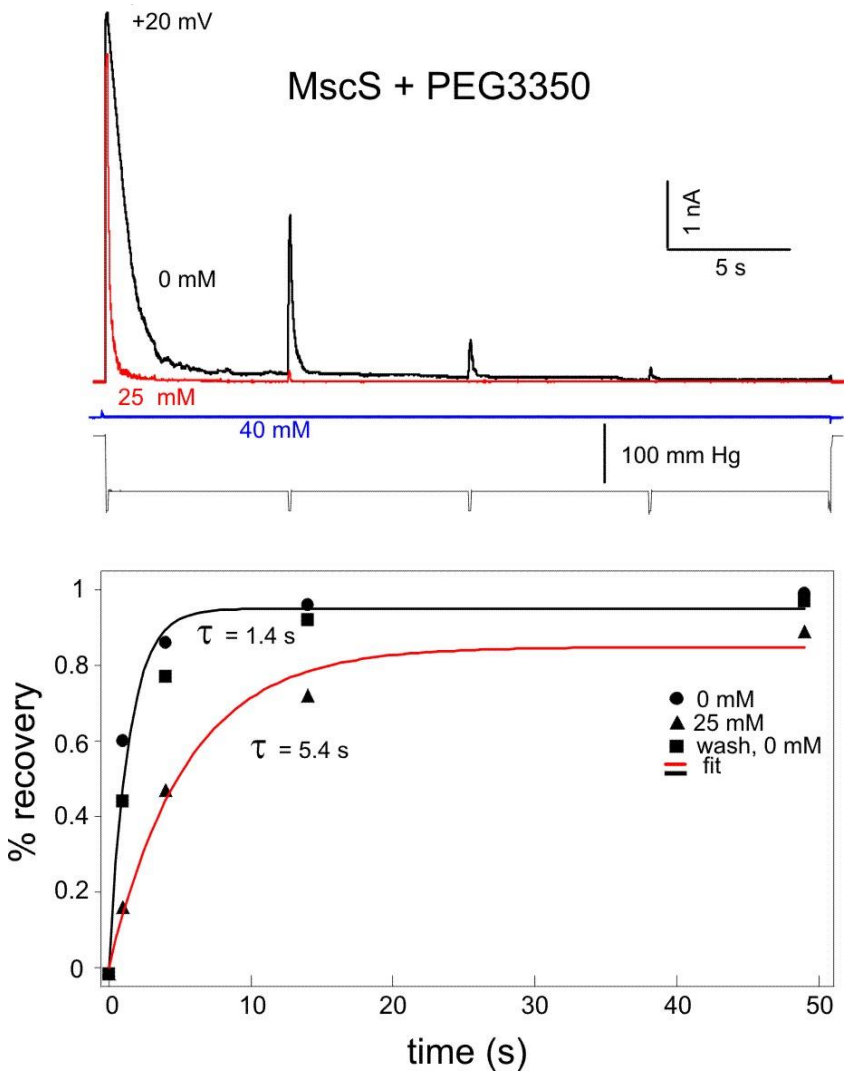

Figure S2. The change in MscS inactivation and recovery rates in control and in the presence of 25 mM (7.5 vol%) and 40 mM (12 vol%) of PEG 3350 on the cytoplasmic side of the excised patch. The 'comb' pressure protocol incudes a prolonged (30s) conditioning step of pressure, typically chosen at the midpoint of activation (p1/2), and a train of interspersed saturation pulses indicating fraction of active channels. In control, MscS shows decaying activation to four of the pulses 6 s apart. 25 mM PEG makes the channel open only once. 40 mM PEG activates only about 3% of the population, which immediately inactivates. The rate of recovery is visibly decreased by 25 mM of PEG. This experiment allows us separate the previously described processes of crowder-promoted adaptation[62] from tension- and crowder-dependent inactivation.

Mutant	pMscS/pMscL	Midpoint (mN/m)	Open state stability	Ramp Response	Inactivation	Recovery	τ of recovery (sec)
WT	0.6	7.8	WT-like	WT-like	WT-like	WT-like	1.3 ± 0.6
A98S	0.45	5.8	Unstable	WT-like	Less than WT	-	-
G113A	0.6	7.8	Very Stable	WT-like	Less than WT	-	-
N117A	1	13	WT-like	WT-like	WT-like	Fast	-
N117V	1	13	Unstable	Minimal	WT-like	Fast	0.5 ± 0.02
G121A	0.6	7.8	Very Stable	WT-like	Less than WT	Slow	229 ± 8.4
F151R	0.6	7.8	Very Stable	Reduced	WT-like	Slow	3.4 ± 1.9
F151D	0.6	7.8	Very Stable	WT-like	Less than WT	-	-
N167D	1	13	Unstable	WT-like	WT-like	Fast	1.9 ± 0.6
N167V	1	13	Unstable	None	More than WT	Fast	0.6 ± 0.2
G168D	0.6	7.8	Very Stable	WT-like	Less than WT	-	-
N117V/N167V	1	13	Unstable	None	More than WT	Fast	-
F151R/N167D	1	13	Unstable	None	WT-like	Slow	13.2 ± 5.8

Table S1. Summary gating phenotypes for several mutants with altered contact region between the C-terminal segment (TM3b) of the gate-forming TM3 helix and the beta domain of the MscS cage. The above mutants were generated and scrutinized via patch clamp to investigate the deviations from WT MscS they produced. The given midpoint and recovery values are based on a minimum of three independent measurements where possible. Omissions in recovery information are due to either a lack of adaptation, thus prohibiting inactivation measurements (A98S, G113A, F151D, and G168D), or extreme gating tensions which destabilize the patch (N117A, N117V/N167V).

Reference List

1. Bayer, M.E., *Response of Cell Walls of Escherichia coli to a Sudden Reduction of the Environmental Osmotic Pressure.* J.Bacteriol., 1967. **93**(3): p. 1104-1112.

2. Cai, S., et al., *Regulation of cytoskeletal mechanics and cell growth by myosin light chain phosphorylation.* Am.J.Physiol, 1998. **275**(5 Pt 1): p. C1349-C1356.

3. Cornet, M., I.H. Lambert, and E.K. Hoffmann, *Relation between cytoskeleton, hypo-osmotic treatment and volume regulation in Ehrlich ascites tumor cells.* J.Membr.Biol., 1993. **131**(1): p. 55-66.

4. Ben-Shahar, Y., *Sensory functions for degenerin/epithelial sodium channels (DEG/ENaC).* Adv Genet, 2011. **76**: p. 1-26.

5. Zhou, X.L., et al., *The transient receptor potential channel on the yeast vacuole is mechanosensitive.* Proc Natl Acad Sci U S A, 2003. **100**(12): p. 7105-10.

6. Eijkelkamp, N., K. Quick, and J.N. Wood, *Transient receptor potential channels and mechanosensation.* Annu Rev Neurosci, 2013. **36**: p. 519-46.

7. Honore, E., *The neuronal background K2P channels: focus on TREK1.* Nat Rev Neurosci, 2007. **8**(4): p. 251-61.

8. Coste, B., et al., *Piezo1 and Piezo2 are essential components of distinct mechanically activated cation channels.* Science, 2010. **330**(6000): p. 55-60.

9. Prole, D.L. and C.W. Taylor, *Identification and analysis of putative homologues of mechanosensitive channels in pathogenic protozoa.* PLoS One, 2013. **8**(6): p. e66068.

10. Haswell, E.S. and E.M. Meyerowitz, *MscS-like proteins control plastid size and shape in Arabidopsis thaliana.* Curr.Biol., 2006. **16**(1): p. 1-11.

11. Vogel, V. and M. Sheetz, *Local force and geometry sensing regulate cell functions.* Nat.Rev.Mol.Cell Biol., 2006. **7**(4): p. 265-275.

12. Hoffmann, E.K. and S.F. Pedersen, *Sensors and signal transduction in the activation of cell volume regulatory ion transport systems.* Contrib.Nephrol., 1998. **123**: p. 50-78.

13. Moore, S.W., P. Roca-Cusachs, and M.P. Sheetz, *Stretchy proteins on stretchy substrates: the important elements of integrin-mediated rigidity sensing.* Dev.Cell, 2010. **19**(2): p. 194-206.

14. Pellegrino, M., et al., *Mechanosensitive Cation Channels of Leech Neurons*, in *Mechanosensitivity in Cells and Tissues*, A. Kamkin and I. Kiseleva, Editors. 2005: Moscow.

15. Katz, B., *Depolarization of sensory terminals and the initiation of impulses in the muscle spindle.* J.Physiol, 1950. **111**(3-4): p. 261-282.

16. Wolbarsht, M.L., *Electrical characteristics of insectmechanoreceptors.* J.Gen.Physiol, 1960. **44**: p. 105-122.

17. Corey, D.P. and A.J. Hudspeth, *Response latency of vertebrate hair cells.* Biophys J, 1979. **26**(3): p. 499-506.

18. Neher, E. and B. Sakmann, *Single-channel currents recorded from membrane of denervated frog muscle fibres.* Nature, 1976. **260**(5554): p. 799-802.

19. Guharay, F. and F. Sachs, *Stretch-activated single ion channel currents in tissue-cultured embryonic chick skeletal muscle.* J Physiol, 1984. **352**: p. 685-701.

20. Morris, C.E. and R. Horn, *Failure to elicit neuronal macroscopic mechanosensitive currents anticipated by single-channel studies.* Science, 1991. **251**(4998): p. 1246-1249.

21. Sukharev, S.I., et al., *A large-conductance mechanosensitive channel in E. coli encoded by mscL alone.* Nature, 1994. **368**(6468): p. 265-268.

22. Strange, K., *Cellular and Molecular Physiology of Cell Volume Regulation*. 1994, Boca Raton, Florida: CRC Press.

23. Brahm, J., *Diffusional water permeability of human erythrocytes and their ghosts.* J.Gen.Physiol, 1982. **79**(5): p. 791-819.

24. Brown, A.D. and J.R. Simpson, *Water relations of sugar-tolerant yeasts: the role of intracellular polyols.* J.Gen.Microbiol., 1972. **72**(3): p. 589-591.

25. Epstein, W. and S.G. Schultz, *Cation Transport in Escherichia coli: V. Regulation of cation content.* J.Gen.Physiol, 1965. **49**(2): p. 221-234.

26. Ballal, A., B. Basu, and S.K. Apte, *The Kdp-ATPase system and its regulation.* J.Biosci., 2007. **32**(3): p. 559-568.

27. Malli, R. and W. Epstein, *Expression of the Kdp ATPase is consistent with regulation by turgor pressure.* J.Bacteriol., 1998. **180**(19): p. 5102-5108.

28. Laimins, L.A., D.B. Rhoads, and W. Epstein, *Osmotic control of kdp operon expression in Escherichia coli.* Proc.Natl.Acad.Sci.U.S.A, 1981. **78**(1): p. 464-468.

29. Douglas, R.M., et al., *The distribution of homologues of the Escherichia coli KefC K(+)-efflux system in other bacterial species.* J.Gen.Microbiol., 1991. **137**(8): p. 1999-2005.

30. Wood, J.M., *Bacterial osmoregulation: a paradigm for the study of cellular homeostasis.* Annu.Rev.Microbiol., 2011. **65**: p. 215-238.

31. Arakawa, T. and S.N. Timasheff, *The stabilization of proteins by osmolytes.* Biophys.J., 1985. **47**(3): p. 411-414.

32. Dinnbier, U., et al., *Transient accumulation of potassium glutamate and its replacement by trehalose during adaptation of growing cells of Escherichia coli K-12 to elevated sodium chloride concentrations.* Arch.Microbiol., 1988. **150**(4): p. 348-357.

33. Lucht, J.M. and E. Bremer, *Adaptation of Escherichia coli to high osmolarity environments: osmoregulation of the high-affinity glycine betaine transport system proU.* FEMS Microbiol.Rev., 1994. **14**(1): p. 3-20.

34. Schleyer, M., R. Schmid, and E.P. Bakker, *Transient, specific and extremely rapid release of osmolytes from growing cells of Escherichia coli K-12 exposed to hypoosmotic shock.* Arch.Microbiol., 1993. **160**(6): p. 424-431.

35. Ruthe, H.J. and J. Adler, *Fusion of bacterial spheroplasts by electric fields.* Biochim.Biophys.Acta, 1985. **819**(1): p. 105-113.

36. Martinac, B., et al., *Pressure-sensitive ion channel in Escherichia coli.* Proc.Natl.Acad.Sci.U.S.A, 1987. **84**(8): p. 2297-2301.

37. Sukharev, S.I., et al., *Two types of mechanosensitive channels in the Escherichia coli cell envelope: solubilization and functional reconstitution.* Biophys.J., 1993. **65**(1): p. 177-183.

38. Levina, N., et al., *Protection of Escherichia coli cells against extreme turgor by activation of MscS and MscL mechanosensitive channels: identification of genes required for MscS activity.* EMBO J., 1999. **18**(7): p. 1730-1737.

39. Cui, C. and J. Adler, *Effect of mutation of potassium-efflux system, KefA, on mechanosensitive channels in the cytoplasmic membrane of Escherichia coli.* J.Membr.Biol., 1996. **150**(2): p. 143-152.

40. Chang, G., et al., *Structure of the MscL homolog from Mycobacterium tuberculosis: a gated mechanosensitive ion channel.* Science, 1998. **282**(5397): p. 2220-2226.

41. Steinbacher, S., et al., *Structures of the prokaryotic mechanosensitive channels MscL and MscS.* Mechanosensitive Ion Channels, Part A, 2007. **58**: p. 1-24.

42. Bass, R.B., et al., *Crystal structure of Escherichia coli MscS, a voltage-modulated and mechanosensitive channel.* Science, 2002. **298**(5598): p. 1582-1587.

43. Anishkin, A. and S. Sukharev, *Water dynamics and dewetting transitions in the small mechanosensitive channel MscS.* Biophys.J., 2004. **86**(5): p. 2883-2895.

44. Belyy, V., et al., *The tension-transmitting 'clutch' in the mechanosensitive channel MscS.* Nat.Struct.Mol.Biol., 2010. **17**(4): p. 451-458.

45. Spronk, S.A., D.E. Elmore, and D.A. Dougherty, *Voltage-dependent hydration and conduction properties of the hydrophobic pore of the mechanosensitive channel of small conductance.* Biophys.J., 2006. **90**(10): p. 3555-3569.

46. Wang, W., et al., *The structure of an open form of an E. coli mechanosensitive channel at 3.45 A resolution.* Science, 2008. **321**(5893): p. 1179-1183.

47. Gandhi, C.S. and D.C. Rees, *Biochemistry. Opening the molecular floodgates.* Science, 2008. **321**(5893): p. 1166-1167.

48. Anishkin, A., K. Kamaraju, and S. Sukharev, *Mechanosensitive channel MscS in the open state: modeling of the transition, explicit simulations, and experimental measurements of conductance.* J Gen Physiol, 2008. **132**(1): p. 67-83.

49. Anishkin, A., B. Akitake, and S. Sukharev, *Characterization of the resting MscS: modeling and analysis of the closed bacterial mechanosensitive channel of small conductance.* Biophys J, 2008. **94**(4): p. 1252-1266.

50. Akitake, B., et al., *Straightening and sequential buckling of the pore-lining helices define the gating cycle of MscS.* Nat Struct Mol Biol, 2007. **14**(12): p. 1141-1149.

51. Akitake, B., A. Anishkin, and S. Sukharev, *The "dashpot" mechanism of stretch-dependent gating in MscS.* J.Gen.Physiol, 2005. **125**(2): p. 143-154.

52. Sotomayor, M. and K. Schulten, *Molecular dynamics study of gating in the mechanosensitive channel of small conductance MscS.* Biophys.J., 2004. **87**(5): p. 3050-3065.

53. Kubitschek, H.E., *Cell volume increase in Escherichia coli after shifts to richer media.* J.Bacteriol., 1990. **172**(1): p. 94-101.

54. Zimmerman, S.B. and S.O. Trach, *Estimation of macromolecule concentrations and excluded volume effects for the cytoplasm of Escherichia coli.* J.Mol.Biol., 1991. **222**(3): p. 599-620.

55. Minton, A.P., *Models for excluded volume interaction between an unfolded protein and rigid macromolecular cosolutes: macromolecular crowding and protein stability revisited.* Biophys.J., 2005. **88**(2): p. 971-985.

56. Zimmerman, S.B. and B. Harrison, *Macromolecular crowding increases binding of DNA polymerase to DNA: an adaptive effect.* Proc.Natl.Acad.Sci.U.S.A, 1987. **84**(7): p. 1871-1875.

57. Grajkowski, W., A. Kubalski, and P. Koprowski, *Surface changes of the mechanosensitive channel MscS upon its activation, inactivation, and closing.* Biophys.J, 2005. **88**(4): p. 3050-3059.

58. Zimmerberg, J. and V.A. Parsegian, *Polymer inaccessible volume changes during opening and closing of a voltage-dependent ionic channel.* Nature, 1986. **323**(6083): p. 36-39.

59. Timasheff, S.N., *In disperse solution, "osmotic stress" is a restricted case of preferential interactions.* Proc.Natl.Acad.Sci.U.S.A, 1998. **95**(13): p. 7363-7367.

60. Jiang, X., et al., *C-type inactivation involves a significant decrease in the intracellular aqueous pore volume of Kv1.4 K+ channels expressed in Xenopus oocytes.* J.Physiol, 2003. **549**(Pt 3): p. 683-695.

61. Edwards, M.D., W. Bartlett, and I.R. Booth, *Pore mutations of the Escherichia coli MscS channel affect desensitization but not ionic preference.* Biophys.J, 2008. **94**(8): p. 3003-3013.

62. Grajkowski, W., A. Kubalski, and P. Koprowski, *Surface changes of the mechanosensitive channel MscS upon its activation, inactivation, and closing.* Biophys.J., 2005. **88**(4): p. 3050-3059.

63. Koprowski, P., et al., *Genetic screen for potassium leaky small mechanosensitive channels (MscS) in Escherichia coli: recognition of cytoplasmic beta domain as a new gating element.* J Biol.Chem., 2011. **286**(1): p. 877-888.

64. Gullingsrud, J. and K. Schulten, *Lipid bilayer pressure profiles and mechanosensitive channel gating.* Biophys.J., 2004. **86**(6): p. 3496-3509.

65. Laan, v.d.B.-v.d., et al., *Stability of KcsA tetramer depends on membrane lateral pressure.* Biochemistry, 2004. **43**(14): p. 4240-4250.

66. Cantor, R.S., *The lateral pressure profile in membranes: a physical mechanism of general anesthesia.* Toxicol.Lett., 1998. **100-101**: p. 451-458.

67. Cantor, R.S., *Receptor desensitization by neurotransmitters in membranes: are neurotransmitters the endogenous anesthetics?* Biochemistry, 2003. **42**(41): p. 11891-11897.

68. Markin, V.S. and B. Martinac, *Mechanosensitive ion channels as reporters of bilayer expansion. A theoretical model.* Biophys.J., 1991. **60**(5): p. 1120-1127.

69. Akitake, B., et al., *2,2,2-Trifluoroethanol changes the transition kinetics and subunit interactions in the small bacterial mechanosensitive channel MscS.* Biophys J, 2007. **92**(8): p. 2771-2784.

70. Kamaraju, K. and S. Sukharev, *The membrane lateral pressure-perturbing capacity of parabens and their effects on the mechanosensitive channel directly correlate with hydrophobicity.* Biochemistry, 2008. **47**(40): p. 10540-10550.

71. Kamaraju, K., et al., *Effects on membrane lateral pressure suggest permeation mechanisms for bacterial quorum signaling molecules.* Biochemistry, 2011. **50**(32): p. 6983-6993.

72. WHO. *Cholera Fact Sheet*. 2013 [cited 2013 October 1]; Available from: http://www.who.int/mediacentre/factsheets/fs107/en/.

73. Cayley, S., et al., *Characterization of the cytoplasm of Escherichia coli K-12 as a function of external osmolarity. Implications for protein-DNA interactions in vivo.* J Mol Biol, 1991. **222**(2): p. 281-300.

74. Minton, A.P., *Molecular crowding: analysis of effects of high concentrations of inert cosolutes on biochemical equilibria and rates in terms of volume exclusion.* Methods Enzymol., 1998. **295**: p. 127-149.

75. van den Berg, B., R.J. Ellis, and C.M. Dobson, *Effects of macromolecular crowding on protein folding and aggregation.* EMBO J, 1999. **18**(24): p. 6927-33.

76. Ellis, R.J., *Macromolecular crowding: obvious but underappreciated.* Trends Biochem.Sci., 2001. **26**(10): p. 597-604.

77. Zhou, H.X., G. Rivas, and A.P. Minton, *Macromolecular crowding and confinement: biochemical, biophysical, and potential physiological consequences.* Annu Rev Biophys, 2008. **37**: p. 375-97.

78. Record, M.T., Jr., et al., *Responses of E. coli to osmotic stress: large changes in amounts of cytoplasmic solutes and water.* Trends Biochem Sci, 1998. **23**(4): p. 143-8.

79. Wood, J.M., *Osmosensing by bacteria: signals and membrane-based sensors.* Microbiol.Mol.Biol.Rev., 1999. **63**(1): p. 230-262.

80. Reiser, V., D.C. Raitt, and H. Saito, *Yeast osmosensor Sln1 and plant cytokinin receptor Cre1 respond to changes in turgor pressure.* J Cell Biol., 2003. **161**(6): p. 1035-1040.

81. Liedtke, W., *TRPV4 as osmosensor: a transgenic approach.* Pflugers Arch., 2005. **451**(1): p. 176-180.

82. Wood, J.M., *Bacterial osmosensing transporters.* Methods Enzymol., 2007. **428**: p. 77-107.

83. Csonka, L.N. and A.D. Hanson, *Prokaryotic osmoregulation: genetics and physiology.* Annu.Rev.Microbiol., 1991. **45**: p. 569-606.

84. Wood, J.M., et al., *Osmosensing and osmoregulatory compatible solute accumulation by bacteria.* Comp Biochem.Physiol A Mol.Integr.Physiol, 2001. **130**(3): p. 437-460.

85. Cayley, S. and M.T. Record, Jr., *Roles of cytoplasmic osmolytes, water, and crowding in the response of Escherichia coli to osmotic stress: biophysical basis of osmoprotection by glycine betaine.* Biochemistry, 2003. **42**(43): p. 12596-609.

86. Cayley, D.S., H.J. Guttman, and M.T. Record, Jr., *Biophysical characterization of changes in amounts and activity of Escherichia coli cell and compartment water and turgor pressure in response to osmotic stress.* Biophys J, 2000. **78**(4): p. 1748-64.

87. Schumann, U., et al., *YbdG in Escherichia coli is a threshold-setting mechanosensitive channel with MscM activity.* Proc.Natl.Acad.Sci.U.S A, 2010. **107**(28): p. 12664-12669.

88. Li, Y., et al., *Ionic regulation of MscK, a mechanosensitive channel from Escherichia coli.* EMBO J., 2002. **21**(20): p. 5323-5330.

89. Edwards, M.D., et al., *Characterization of three novel mechanosensitive channel activities in Escherichia coli.* Channels (Austin), 2012. **6**(4): p. 272-81.

90. Kamaraju, K., et al., *The pathway and spatial scale for MscS inactivation.* Journal of General Physiology, 2011. **138**: p. 49-57.

91. Boer, M., A. Anishkin, and S. Sukharev, *Adaptive MscS gating in the osmotic permeability response in E. coli: the question of time.* Biochemistry, 2011. **50**(19): p. 4087-4096.

92. Sukharev, S., B. Akitake, and A. Anishkin, *The bacterial mechanosensitive channel MscS: Emerging principles of gating and modulation.* Mechanosensitive Ion Channels, Part A, 2007. **58**: p. 235-267.

93. Lai, J.Y., et al., *Open and shut: crystal structures of the dodecylmaltoside solubilized mechanosensitive channel of small conductance from Escherichia coli and Helicobacter pylori at 4.4 A and 4.1 A resolutions.* Protein Sci, 2013. **22**(4): p. 502-9.

94. Vasquez, V., et al., *Three-dimensional architecture of membrane-embedded MscS in the closed conformation.* J Mol Biol, 2008. **378**(1): p. 55-70.

95. Koprowski, P., W. Grajkowski, and A. Kubalski, *The MscS cytoplasmic domain and its conformational changes on the channel gating.* Mechanosensitive Ion Channels, Part A, 2007. **58**: p. 295-309.

96. Nomura, T., M. Sokabe, and K. Yoshimura, *Interaction between the cytoplasmic and transmembrane domains of the mechanosensitive channel MscS.* Biophys J, 2008. **94**(5): p. 1638-1645.

97. Machiyama, H., H. Tatsumi, and M. Sokabe, *Structural Changes in the Cytoplasmic Domain of the Mechanosensitive Channel MscS During Opening.* Biophysical Journal, 2009. **97**(4): p. 1048-1057.

98. Humphrey, W., A. Dalke, and K. Schulten, *VMD: visual molecular dynamics.* J.Mol.Graph., 1996. **14**(1): p. 33-38.

99. Anishkin, A., et al., *Hydration properties of mechanosensitive channel pores define the energetics of gating.* Journal of Physics-Condensed Matter, 2010. **22**(45).

100. Yoshimura, K., A. Batiza, and C. Kung, *Chemically charging the pore constriction opens the mechanosensitive channel MscL.* Biophys J, 2001. **80**(5): p. 2198-206.

101. Sukharev, S., *Purification of the small mechanosensitive channel of Escherichia coli (MscS): the subunit structure, conduction, and gating characteristics in liposomes.* Biophys.J., 2002. **83**(1): p. 290-298.

102. Belyy, V., et al., *Adaptive behavior of bacterial mechanosensitive channels is coupled to membrane mechanics.* J Gen Physiol, 2010. **135**(6): p. 641-652.

103. Moe, P. and P. Blount, *Assessment of Potential Stimuli for Mechano-Dependent Gating of MscL: Effects of Pressure, Tension, and Lipid Headgroups.* Biochemistry, 2005. **44**(36): p. 12239-12244.

104. Zhang, X., et al., *Structure and molecular mechanism of an anion-selective mechanosensitive channel of small conductance.* Proc Natl Acad Sci U S A, 2012. **109**(44): p. 18180-5.

105. Sukharev, S.I., et al., *Energetic and spatial parameters for gating of the bacterial large conductance mechanosensitive channel, MscL.* J.Gen.Physiol, 1999. **113**(4): p. 525-540.

106. Cox, C.D., et al., *Selectivity mechanism of the mechanosensitive channel MscS revealed by probing channel subconducting states.* Nat Commun, 2013. **4**: p. 2137.

107. Koch, A.L. and S. Woeste, *Elasticity of the sacculus of Escherichia coli.* J.Bacteriol., 1992. **174**(14): p. 4811-4819.

108. Yao, X., et al., *Thickness and elasticity of gram-negative murein sacculi measured by atomic force microscopy.* J Bacteriol, 1999. **181**(22): p. 6865-75.

109. Pivetti, C.D., et al., *Two families of mechanosensitive channel proteins.* Microbiol.Mol.Biol.Rev., 2003. **67**(1): p. 66-85, table.

110. Balleza, D. and F. Gomez-Lagunas, *Conserved motifs in mechanosensitive channels MscL and MscS.* Eur.Biophys J, 2009.

111. Vollmer, W. and J.V. Holtje, *Morphogenesis of Escherichia coli.* Curr Opin Microbiol, 2001. **4**(6): p. 625-33.

112. Vasquez, V. and E. Perozo, *Voltage dependent gating in MscS.* Biophysical Journal, 2004. **86**(1): p. 545A-545A.

113. Nakayama, Y., K. Yoshimura, and H. Iida, *Electrophysiological characterization of the mechanosensitive channel MscCG in Corynebacterium glutamicum.* Biophys J, 2013. **105**(6): p. 1366-75.

114. Petrov, E., et al., *Patch-clamp characterization of the MscS-like mechanosensitive channel from Silicibacter pomeroyi.* Biophys J, 2013. **104**(7): p. 1426-34.

115. Naismith, J.H. and I.R. Booth, *Bacterial Mechanosensitive Channels-MscS: Evolution's Solution to Creating Sensitivity in Function.* Annu.Rev.Biophys., 2012. **41**: p. 157-177.

116. Sikkema, J., J.A. de Bont, and B. Poolman, *Interactions of cyclic hydrocarbons with biological membranes.* J Biol Chem, 1994. **269**(11): p. 8022-8.

117. Gulyaeva, N., et al., *Relative hydrophobicity and lipophilicity of drugs measured by aqueous two-phase partitioning, octanol-buffer partitioning and HPLC. A simple model for predicting blood-brain distribution.* Eur J Med Chem, 2003. **38**(4): p. 391-6.

118. Ambroggio, E.E., et al., *Surface behaviour and peptide-lipid interactions of the antibiotic peptides, Maculatin and Citropin.* Biochim Biophys Acta, 2004. **1664**(1): p. 31-7.

119. Suomalainen, P., et al., *Surface activity profiling of drugs applied to the prediction of blood-brain barrier permeability.* J Med Chem, 2004. **47**(7): p. 1783-8.

120. Di, L., et al., *High throughput artificial membrane permeability assay for blood-brain barrier.* Eur J Med Chem, 2003. **38**(3): p. 223-32.

121. Steinkopf, S., et al., *Interaction of local anaesthetic articaine enantiomers with brain lipids: a Langmuir monolayer study.* Eur J Pharm Sci, 2012. **47**(2): p. 394-401.

122. Hansen, A.H., et al., *Propofol modulates the lipid phase transition and localizes near the headgroup of membranes.* Chem Phys Lipids, 2013. **175-176**: p. 84-91.

123. Sheetz, M.P. and S.J. Singer, *Biological membranes as bilayer couples. A molecular mechanism of drug-erythrocyte interactions.* Proc.Natl.Acad.Sci.U.S.A, 1974. **71**(11): p. 4457-4461.

124. Martinac, B., J. Adler, and C. Kung, *Mechanosensitive ion channels of E. coli activated by amphipaths.* Nature, 1990. **348**(6298): p. 261-3.

125. Markin, V.S. and B. Martinac, *Mechanosensitive ion channels as reporters of bilayer expansion. A theoretical model.* Biophys J, 1991. **60**(5): p. 1120-7.

126. Wang, J., et al., *Platensimycin is a selective FabF inhibitor with potent antibiotic properties.* Nature, 2006. **441**(7091): p. 358-361.

127. Brown, A.K., et al., *Platensimycin activity against mycobacterial beta-ketoacyl-ACP synthases.* PLoS One, 2009. **4**(7): p. e6306.

128. Wright, H.T. and K.A. Reynolds, *Antibacterial targets in fatty acid biosynthesis.* Curr Opin Microbiol, 2007. **10**(5): p. 447-53.

129. Wang, J. and H.O. Sintim, *Dialkylamino-2,4-dihydroxybenzoic acids as easily synthesized analogues of platensimycin and platencin with comparable antibacterial properties.* Chemistry, 2011. **17**(12): p. 3352-3357.

130. Wang, J., V. Lee, and H.O. Sintim, *Efforts towards the identification of simpler platensimycin analogues--the total synthesis of oxazinidinyl platensimycin.* Chemistry, 2009. **15**(12): p. 2747-2750.

131. M. J. Frisch, G.W.T., H. B. Schlegel, G. E. Scuseria, M. A. Robb, J. R. Cheeseman, G. Scalmani, V. Barone, , et al., *Gaussian 09, Revision A.02*. 2009, Gaussian, Inc.: Wallingford, CT.

132. Suomalainen, P., et al., *Surface activity profiling of drugs applied to the prediction of blood-brain barrier permeability.* J.Med.Chem., 2004. **47**(7): p. 1783-1788.

133. Gerebtzoff, G., et al., *Halogenation of drugs enhances membrane binding and permeation.* Chembiochem, 2004. **5**(5): p. 676-84.

134. Kamaraju, K., et al., *The pathway and spatial scale for MscS inactivation.* J.Gen.Physiol, 2011. **138**(1): p. 49-57.

135. Seelig, A., *Local anesthetics and pressure: a comparison of dibucaine binding to lipid monolayers and bilayers.* Biochim.Biophys.Acta, 1987. **899**(2): p. 196-204.

136. Seelig, A., *The use of monolayers for simple and quantitative analysis of lipid-drug interactions exemplified with dibucaine and substance P.* Cell Biol.Int.Rep., 1990. **14**(4): p. 369-380.

137. Seelig, A., *Interaction of a substance P agonist and of substance P antagonists with lipid membranes. A thermodynamic analysis.* Biochemistry, 1992. **31**(11): p. 2897-904.

138. Thuren, T., J.A. Virtanen, and P.K. Kinnunen, *Estimation of the equilibrium lateral pressure in 1-palmitoyl-2-[6(pyren-1-yl)]hexanoyl-glycerophospholipid liposomes.* Chem Phys Lipids, 1986. **41**(3-4): p. 329-34.

139. Chandler, D., *Interfaces and the driving force of hydrophobic assembly.* Nature, 2005. **437**(7059): p. 640-7.

140. BRITTEN, R.J. and F.T. McCLURE, *The amino acid pool in Escherichia coli.* Bacteriol.Rev., 1962. **26**: p. 292-335.

141. Berrier, C., et al., *Multiple mechanosensitive ion channels from Escherichia coli, activated at different thresholds of applied pressure.* J.Membr.Biol., 1996. **151**(2): p. 175-187.

142. Stokes, N.R., et al., *A role for mechanosensitive channels in survival of stationary phase: regulation of channel expression by RpoS.* Proc Natl Acad Sci U S A, 2003. **100**(26): p. 15959-15964.

143. Perozo, E., *Gating prokaryotic mechanosensitive channels.* Nature Reviews Molecular Cell Biology, 2006. **7**(2): p. 109-119.

144. Gullingsrud, J. and K. Schulten, *Gating of MscL studied by steered molecular dynamics.* Biophys.J., 2003. **85**(4): p. 2087-2099.

145. Pruzzo, C. and A. Huq, *Pathogenic Vibrio species in marine and estuarine environment.*, R.C. Belkin, Editor. 2005, Kluwer Academic/Plenum. p. 217-252.

146. Huq, A. and C.J. Grim, *Aquatic Realm and Cholera. Epidemiological and Molecular Aspects on Cholera (Infectious Disease).* T. Ramamurthy and S.K. Bhattachrya, Editors. 2011, Springer: New York Dordrecht Heidelberg London. p. 311-340.

147. Grim, C.J., et al., *Genome sequence of hybrid Vibrio cholerae O1 MJ-1236, B-33, and CIRS101 and comparative genomics with V. cholerae.* J Bacteriol., 2010. **192**(13): p. 3524-3533.

148. Barcina, I., *Survival strategies of enteric bacteria in aquatic systems.* Microbiologia, 1995. **11**(3): p. 389-392.

149. Keymer, D.P., et al., *Genomic and phenotypic diversity of coastal Vibrio cholerae strains is linked to environmental factors.* Appl.Environ.Microbiol., 2007. **73**(11): p. 3705-3714.

150. Naughton, L.M., et al., *Osmoadaptation among Vibrio species and unique genomic features and physiological responses of Vibrio parahaemolyticus.* Appl.Environ.Microbiol., 2009. **75**(9): p. 2802-2810.

151. Duret, G., V. Simonet, and A.H. Delcour, *Modulation of Vibrio cholerae porin function by acidic pH.* Channels (Austin.), 2007. **1**(2): p. 70-79.

152. Duret, G. and A.H. Delcour, *Deoxycholic acid blocks vibrio cholerae OmpT but not OmpU porin.* J Biol.Chem., 2006. **281**(29): p. 19899-19905.

153. Pagel, M. and A.H. Delcour, *Effects of conjugated and unconjugated bile acids on the activity of the Vibrio cholerae porin OmpT.* Mol.Membr.Biol., 2011. **28**(1): p. 69-78.

154. Hall, J.E., *Access resistance of a small circular pore.* The Journal of General Physiology, 1975. **66**(4): p. 531-532.

155. Hille, B., *Ionic channels of excitable membranes*. 3d ed. 2001: Sinauer Asssociates Inc. Sunderland, MA.

156. Moe, P.C., P. Blount, and C. Kung, *Functional and structural conservation in the mechanosensitive channel MscL implicates elements crucial for mechanosensation.* Mol Microbiol, 1998. **28**(3): p. 583-92.

157. Chiang, C.S., A. Anishkin, and S. Sukharev, *Gating of the large mechanosensitive channel in situ: estimation of the spatial scale of the transition from channel population responses.* Biophys.J., 2004. **86**(5): p. 2846-2861.

158. Rudolph, A.S., J.H. Crowe, and L.M. Crowe, *Effects of three stabilizing agents--proline, betaine, and trehalose--on membrane phospholipids.* Arch.Biochem.Biophys., 1986. **245**(1): p. 134-143.

159. Luzardo, M.C., et al., *Effect of trehalose and sucrose on the hydration and dipole potential of lipid bilayers.* Biophys.J, 2000. **78**(5): p. 2452-2458.

160. Villarreal, M.A., et al., *Molecular dynamics simulation study of the interaction of trehalose with lipid membranes.* Langmuir, 2004. **20**(18): p. 7844-7851.

161. Anishkin, A., et al., *On the Conformation of the COOH-terminal Domain of the Large Mechanosensitive Channel MscL.* J.Gen.Physiol, 2003. **121**(3): p. 227-244.

162. Bialecka-Fornal, M., et al., *Single-cell census of mechanosensitive channels in living bacteria.* PLoS One., 2012. **7**(3): p. e33077.

163. Nakamaru, Y., et al., *Mechanosensitive channel functions to alleviate the cell lysis of marine bacterium, Vibrio alginolyticus, by osmotic downshock.* FEBS Lett., 1999. **444**(2-3): p. 170-172.

164. Chaiyanan, S., et al., *Viability of the nonculturable Vibrio cholerae O1 and O139.* Syst Appl Microbiol, 2001. **24**(3): p. 331-41.

165. Boucher, P.A., C.E. Morris, and B. Joos, *Mechanosensitive closed-closed transitions in large membrane proteins: osmoprotection and tension damping.* Biophys.J., 2009. **97**(10): p. 2761-2770.

166. Romantsov, T., et al., *Protein localization in Escherichia coli cells: comparison of the cytoplasmic membrane proteins ProP, LacY, ProW, AqpZ, MscS, and MscL.* J Bacteriol., 2010. **192**(4): p. 912-924.

167. Pflughoeft, K.J., K. Kierek, and P.I. Watnick, *Role of ectoine in Vibrio cholerae osmoadaptation.* Appl.Environ.Microbiol., 2003. **69**(10): p. 5919-5927.

168. de Kievit, T.R. and B.H. Iglewski, *Bacterial quorum sensing in pathogenic relationships.* Infect Immun, 2000. **68**(9): p. 4839-49.

169. Suckow, G., P. Seitz, and M. Blokesch, *Quorum sensing contributes to natural transformation of Vibrio cholerae in a species-specific manner.* J Bacteriol, 2011. **193**(18): p. 4914-24.

170. Ganin, H., et al., *Vibrio cholerae autoinducer CAI-1 interferes with Pseudomonas aeruginosa quorum sensing and inhibits its growth.* ACS Chem Biol, 2012. **7**(4): p. 659-65.